CHARACTERIZATION OF PUNCHING SHEAR CAPACITY OF THIN UHPC PLATES

by

Devin K. Harris

Thesis submitted to the faculty of the

Virginia Polytechnic Institute and State University

in partial fulfillment of the requirements for the degree of

MASTER OF SCIENCE

IN

CIVIL ENGINEERING

APPROVED:

Carin Roberts-Wollmann

Thomas E. Cousins

Raymond H. Plaut

December 2004

Blacksburg, Virginia

Keywords: UHPC, Punching shear, Fiber reinforced concrete, Ductal®

CHARACTERIZATION OF PUNCHING SHEAR CAPACITY OF THIN UHPC PLATES

by

Devin K. Harris

ABSTRACT

UHPC (ultra-high performance concrete) is a relatively new type of concrete that exhibits mechanical properties that are far superior to those of conventional concrete and in some cases rival those of steel. The main characteristics that distinguish UHPC from conventional reinforced concrete are the improved compressive strength, the tensile strength, the addition of steel fibers, and the resistance to corrosion and degradation. The mechanical properties of UHPC allow for smaller, thinner, lighter sections to be designed while strength is maintained or improved. The use of UHPC has been limited to a few structural applications due to the high cost of the materials and the lack of established design guidelines.

A proposed material model based on material and finite element models has served as the foundation of this research effort. The model was used to minimize the dimension of an optimum section in order to limit the material usage and maximize the performance. In the model, the top flange served as the riding surface and contained no reinforcing steel to resist shear. The lack of steel reinforcement allowed for the possibility of a punching shear failure to occur from the application of a point load such as a wheel tire patch load. The model and optimized section served as the foundation for this research, the characterization of punching shear capacity of thin UHPC plates.

A total of 12 UHPC slabs were tested to failure to determine the boundary between a flexural failure and a punching shear failure. The variables considered were the slab thickness and loading plate dimensions. The results of the testing were compared to

existing models for punching shears and other failure modes, with varying success. The test results aided in the development of a design equation for the prediction of punching shear in UHPC slabs. After evaluation of the test results, recommendations are made as to which model predicts the punching shear capacity of UHPC slabs and the minimum slab thickness required to prevent a punching shear failure.

ACKNOWLEDGEMENTS

I would first like to express my sincere appreciation to the faculty members at Virginia Polytechnic Institute and State University for their support during my graduate studies at the MS level. More specifically, I would like to express my appreciation for Dr. Carin Roberts-Wollmann for her guidance and support during my research efforts and course work. I would also like to thank Dr. Thomas Cousins for his guidance in the classroom and for also serving on my committee. I would like to thank Dr. Raymond Plaut for his guidance inside and outside the classroom. Dr. Plaut was instrumental in my attending Virginia Tech and has served as an excellent motivator for me during my MS studies. Thanks also go out to the Federal Highway Administration for sponsoring my research project, and Lafarge North America for providing the materials.

My research project would not have been possible without the help and support of the structures laboratory crew, specifically Dennis Huffman and Brett Farmer. A great deal of appreciation is given to David Martin, Chuck Newhouse, Sean Sullivan and Stephen Blumenbaum for their assistance in the lab throughout my testing.

Most importantly I would like to thank my wife Arlene for her continual support. Without it I would have never returned to school and never succeeded.

TABLE OF CONTENTS

ABSTRACT i
ACKNOWLEDGEMENTS iv
TABLE OF CONTENTS v
LIST OF FIGURES ix
LIST OF TABLES xiv
Chapter 1 - Introduction 1
1.1 Bridge Market for UHPC 1
1.2 Project Overview and Scope 2
1.3 Thesis Organization 3
Chapter 2 - Literature Review 5
2.1 Summary of Literature Review 5
2.2 Ultra High-Performance Concrete (UHPC) 5
2.2.1 History of UHPC 5
2.2.2 General Composition 6
2.2.3 Material Physical Properties 7
2.2.3.1 Compressive Strength 7
2.2.3.2 Tensile Strength / Flexural Strength 8
2.2.3.3 Other Physical Properties 9
2.2.4 Advantages 9
2.2.5 Disadvantages 10
2.3 Model-Based Optimization of UHPC 12
2.3.1 UHPC Model and Model Validation 12
2.3.2 UHPC Section Design Formula, Strategy, and Criteria 13
2.3.3 UHPC Simulation 14
2.4 ACI Punching Shear 15
2.4.1 Brief History of ACI Punching Shear 15
2.4.2 General Mechanism of Failure 16
2.4.3 Current ACI Punching Shear Guidelines 17
2.5 Existing Models for Punching Shear 19
2.5.1 Yankelevsky and Leibowitz Model 20

2.5.2 Walraven, Pat, and Markov 20
2.5.3 Shaaban and Gesund Model 21
2.5.4 Narayanan and Darwish Model 21
2.5.5 ACI Concrete Breakout Strength Model 22
2.6 Summary of Literature Review 23
Chapter 3 - Preliminary Analysis 24
3.1 Summary of preliminary analysis procedures and assumptions 24
3.2 Failure Mechanisms 24
3.2.1 Flexural Failure Mechanism 25
3.2.1.1 Yield Line Analysis 25
3.2.1.2 Flexural Capacity (Ultimate) 27
3.2.1.3 Yield Line Analysis Results for UHPC 29
3.2.2 Punching Shear Failure Mechanism 31
3.2.2.1 Tensile Strength of Ductal® 31
3.2.2.2 ACI Approximation 32
3.2.3 RISA 3-D Model 34
3.3 Specimen Sizing and Selection 35
3.4 Review of Preliminary Analysis 35
Chapter 4 - Materials and Testing 37
4.1 Overview 37
4.2 Specimen Fabrication 37
4.3 Experimental Setup 38
4.3.1 Frame 39
4.3.2 Instrumentation 41
4.4 Test Matrix 45
4.4.1 Trial Specimens 45
4.4.2 Test Parameters and Series Details 45
4.4.2.1 Series 1 45
4.4.2.2 Series 2 46
4.4.2.3 Series 3 46
4.5 Test Procedures 47

4.5.1 Loading 47
4.5.2 Testing 47
Chapter 5 - Presentation of Results and Analysis 48
5.1 Overview 48
5.2 Failure Mechanisms 48
5.3 Testing Results 54
5.3.1 Series 1 Results 54
5.3.2 Series 2 Results 59
5.3.3 Series 3 Results 63
5.4 Comparison of Results to Other Models 68
5.4.1 Narayanan and Darwish Equation 68
5.4.2 Shaaban and Gesund Equation 70
5.4.3 Modified ACI Equation for Concrete Breakout Strength 71
5.4.4 ACI Curve – Fit Equations 73
5.4.5 Comparison of Results to Model Equations 76
5.4.5.1 Preliminary Analysis 76
5.4.5.2 ACI Punching Shear Design Equation 77
5.4.5.3 Narayanan and Darwish Equation 78
5.4.5.4 Shaaban and Gesund Equation 78
5.4.5.5 ACI Concrete Breakout Equation 80
5.4.5.6 ACI Curve-Fit Equation 80
5.4.5.7 Comparison of Prediction Equations 81
5.5 Proposed Slab Thickness 83
5.6 Flexural Failures 84
5.7 Summary of Results 86
Chapter 6 - Summary, Conclusions, Recommendations 87
6.1 Summary 87
6.2 Conclusions 89
6.3 Recommendations for Future Research 90
References 91
APPENDIX A 94

Edge Condition: Four Edges Pinned 94
Edge Condition: Three Edges Pinned / One Edge Fixed 96
Edge Condition: Two Edges Pinned / Two Edges Fixed 97
Edge Condition: One Edge Pinned / Three Edges Fixed 98
Edge Condition: Four Edges Fixed 99
Edge Condition: Radial Pattern 99
APPENDIX B 100
Summary of Results 100
Series 1 101
Series 2 109
Series 3 119
VITA 132

LIST OF FIGURES

Figure 2-1 - Representation of Modified Compact Grading 6
Figure 2-2 - Representation of Fiber Contribution 7
Figure 2-3 - 1 in. thick 6 ft x 10 ft slab supporting 2,000 lb car 8
Figure 2-4 - Comparison of material section weights for equivalent flexural strength 10
Figure 2-5- Comparison of Life Cycle Cost of UHPC vs. Conventional Concrete 11
Figure 2-6 - Equivalent Stress vs. Deflection of Ductal® and conventional HPC 12
Figure 2-7 – Comparison of Optimized UHPC Bridge Girder to AASHTO girder 14
Figure 2-8 – Misconception of Punching Shear Failure 16
Figure 2-9– Correct Representation of Punching Shear Failure 17
Figure 2-10– Illustration of d 18
Figure 2-11– Critical perimeter 19
Figure 2-12 – Concrete Breakout Failure Surface 22
Figure 2-13 – Unreinforced Concrete (or Ductal®) Punching Shear Failure Surface 23
Figure 3-1 – Generic Failure Mechanism for SS Slab with Uniformly Distributed Load 25
Figure 3-2 – Typical Moment-Curvature Relationship for Reinforced Concrete Slab 26
Figure 3-3– Stress vs. Strain Relationship for UHPC 27
Figure 3-4– Section model for UHPC Slab 28
Figure 3-5– Moment-Curvature Relationship for UHPC 29
Figure 3-6– Generic Yield Line Analysis Configuration 31
Figure 3-7– Risa 3-D Model of UHPC slab (restrained on two sides) 35
Figure 4-1 – 45 in. x 45 in. Slab layout with block-outs 38
Figure 4-2 – Elevation 1 of Frame (all dimensions in inches) 39
Figure 4-3 – Elevation 2 of Frame (all dimensions in inches) 40
Figure 4-4 – Photo of Actual Frame 40
Figure 4-5 – Detail of Frame Restraint System 41
Figure 4-6 – Fully Restrained Yield Line Pattern 42
Figure 4-7 – Strain Placement Configurations 43
Figure 4-8 – Ram/Load Cell Combination 43
Figure 4-9 – Wire Pot Displacement Transducer 44
Figure 4-10 – Linear Variable Displacement Transducer 44

Figure 5-1– Typical Punching Shear Failure for Ductal® 49
Figure 5-2 - Fiber Orientation vs. Crack Pattern 50
Figure 5-3 - Typical Crack Pattern for Punching Shear Failure 50
Figure 5-4 – Typical Flexural Failure for Ductal® 52
Figure 5-5 – Typical Load vs. Displacement Curve for Series 1 - Slab #1 55
Figure 5-6 – *Typical Load vs. Strain (Diagonal) for Series 1 – Slab #2 (Tensile Face)* .. 56
Figure 5-7– Load vs. Strain (Orthogonal) for Series 1 – Slab #2 (Tensile Face) 58
Figure 5-8 – Typical Load vs. Strain for Series 1 – Slab #2 (Loading Face) 58
Figure 5-9 – Typical Load vs. Displacement Curve for Series 2 – Slab #1 (Punching Shear Failure) 60
Figure 5-10– Typical Load vs. Displacement Curve for Series 2 – Slab #2 (Flexural Failure) 61
Figure 5-11 – Typical Load vs. Strain (Diagonal) for Series 2 – Slab #2 (Tensile Face) 61
Figure 5-12 – Typical Load vs. Strain (Orthogonal) for Series 2 – Slab #2 (Tensile Face) 62
Figure 5-13 – Typical Load vs. Strain (Loading Face) for Series 2 – Slab #1 62
Figure 5-14 – Typical Load vs. Displacement Curve for Series 3 – Slab #3 (Punching Shear Failure) 65
Figure 5-15– Typical Load vs. Displacement Curve for Series 3 – Slab #5 (Flexural Failure) 65
Figure 5-16 – Typical Load vs. Strain (Diagonal) for Series 3 – Slab #3 66
Figure 5-17 – Typical Load vs. Strain (Orthogonal) for Series 3 - Slab #2 66
Figure 5-18 – Typical Load vs. Strain (Loading Face) for Series 3 - Slab #5 67
Figure 5-19 – Concrete Breakout Failure Surface 72
Figure 5-20 – Ductal® Breakout (Punching Shear) Failure Surface 72
Figure 5-21 – Preliminary Analysis Prediction for Punching Shear Capacity vs. Actual 77
Figure 5-22 – ACI 318-02 Prediction for Punching Shear Capacity vs. Actual 78
Figure 5-23– Narayanan & Darwish Prediction for Punching Shear Capacity vs. Actual 79
Figure 5-24– Shaaban & Gesund Prediction for Punching Shear Capacity vs. Actual 79
Figure 5-25 – Modified ACI Prediction for Concrete Breakout (Punching) Capacity vs. Actual 80

Figure 5-26 – Curve-Fit Prediction for Punching Shear Capacity vs. Actual 81
Figure 5-27 – Yield Line Analysis Prediction for Flexural Capacity vs. Actual..... 85
Figure A-1 - Case A 94
Figure A-2 - Case B 94
Figure A-3 - Case C 95
Figure A-4 - Case D 96
Figure A-5 - Case E 96
Figure A-6 - Case F 97
Figure A-7 - Case G 97
Figure A-8 - Case H 97
Figure A-9 - Case I 98
Figure A-10 - Case J 98
Figure A-11 - Case K 99
Figure A-12 - Case L 99
Figure B-13 – Failure Surface (2.0 in. slab - 1.5 in. plate) 101
Figure B-14 - Load vs. Displacement (2.0 in. slab - 1.5 in. plate)..... 101
Figure B-15 – Load vs. Diagonal Strain (2.0 in. slab - 1.5 in. plate)..... 102
Figure B-16 - Load vs. Orthogonal Strain (2.0 in. slab - 1.5 in. plate)..... 102
Figure B-17 - Load vs. Bottom Strain (2.0 in. slab - 1.5 in. plate) 103
Figure B-18 – Failure Surface (2.0 in. slab – 2.0 in. plate) 103
Figure B-19 - Load vs. Displacement (2.0 in. slab – 2.0 in. plate)..... 104
Figure B-20 - Load vs. Diagonal Strain (2.0 in. slab – 2.0 in. plate)..... 104
Figure B-21 - Load vs. Orthogonal Strain (2.0 in. slab – 2.0 in. plate) 105
Figure B-22 - Load vs. Bottom Strain (2.0 in. slab – 2.0 in. plate) 105
Figure B-23 – Failure Surface (2.0 in. slab – 1.0 in. plate) 106
Figure B-24 - Load vs. Displacement (2.0 in. slab – 1.0 in. plate)..... 106
Figure B-25 - Load vs. Diagonal Strain (2.0 in. slab – 1.0 in. plate)..... 107
Figure B-26 - Load vs. Orthogonal Strain (2.0 in. slab – 1.0 in. plate) 107
Figure B-27 - Load vs. Bottom Strain (2.0 in. slab – 2.0 in. plate) 108
Figure B-28 – Failure Surface (2.5 in. slab – 2.0 in. plate) 109
Figure B-29 - Load vs. Displacement (2.5 in. slab – 2.0 in. plate)..... 109

Figure B-30 - Load vs. Diagonal Strain (2.5 in. slab – 2.0 in. plate)..... 110
Figure B-31 - Load vs. Orthogonal Strain (2.5 in. slab – 2.0 in. plate)..... 110
Figure B-32 - Load vs. Bottom Strain (2.5 in. slab – 2.0 in. plate)..... 111
Figure B-33 – Failure Surface (2.5 in. slab – 3.0 in. plate)..... 111
Figure B-34 - Load vs. Displacement (2.5 in. slab – 3.0 in. plate)..... 112
Figure B-35- Load vs. Diagonal Strain (2.5 in. slab – 3.0 in. plate)..... 112
Figure B-36 - Load vs. Orthogonal Strain (2.5 in. slab – 3.0 in. plate)..... 113
Figure B-37 - Load vs. Bottom Strain (2.5 in. slab – 3.0 in. plate)..... 113
Figure B-38 – Failure Surface (2.5 in. slab – 1.5 in. plate)..... 114
Figure B-39 - Load vs. Displacement (2.5 in. slab – 1.5 in. plate)..... 114
Figure B-40 - Load vs. Diagonal Strain (2.5 in. slab – 1.5 in. plate)..... 115
Figure B-41 - Load vs. Orthogonal Strain (2.5 in. slab – 1.5 in. plate)..... 115
Figure B-42 - Load vs. Bottom Strain (2.5 in. slab – 1.5 in. plate)..... 116
Figure B-43 – Failure Surface (2.5 in. slab – 2.5 in. plate)..... 116
Figure B-44 - Load vs. Displacement (2.5 in. slab – 2.5 in. plate)..... 117
Figure B-45 - Load vs. Diagonal Strain (2.5 in. slab – 2.5 in. plate)..... 117
Figure B-46 - Load vs. Orthogonal Strain (2.5 in. slab – 2.5 in. plate)..... 118
Figure B-47 - Load vs. Bottom Strain (2.5 in. slab – 2.5 in. plate)..... 118
Figure B-48 – Failure Surface (3.0 in. slab – 2.5 in. plate)..... 119
Figure B-49 - Load vs. Displacement (3.0 in. slab – 2.5 in. plate)..... 119
Figure B-50 - Load vs. Diagonal Strain (3.0 in. slab – 2.5 in. plate)..... 120
Figure B-51 - Load vs. Orthogonal Strain (3.0 in. slab – 2.5 in. plate)..... 120
Figure B-52 - Load vs. Bottom Strain (3.0 in. slab – 2.5 in. plate)..... 121
Figure B-53 – Failure Surface (3.0 in. slab – 1.5 in. plate)..... 121
Figure B-54 - Load vs. Displacement (3.0 in. slab – 1.5 in. plate)..... 122
Figure B-55 - Load vs. Diagonal Strain (3.0 in. slab – 1.5 in. plate)..... 122
Figure B-56 - Load vs. Orthogonal Strain (3.0 in. slab – 1.5 in. plate)..... 123
Figure B-57 - Load vs. Bottom Strain (3.0 in. slab – 1.5 in. plate)..... 123
Figure B-58 – Failure Surface (3.0 in. slab – 1.0 in. plate)..... 124
Figure B-59 - Load vs. Displacement (3.0 in. slab – 1.0 in. plate)..... 124
Figure B-60 - Load vs. Diagonal Strain (3.0 in. slab – 1.0 in. plate)..... 125

Figure B-61 - Load vs. Orthogonal Strain (3.0 in. slab – 1.0 in. plate) 125
Figure B-62 - Load vs. Bottom Strain (3.0 in. slab – 1.0 in. plate) 126
Figure B-63 – Failure Surface (3.0 in. slab – 2.0 in. plate) 126
Figure B-64 - Load vs. Displacement (3.0 in. slab – 2.0 in. plate)..... 127
Figure B-65 - Load vs. Diagonal Strain (3.0 in. slab – 2.0 in. plate)..... 127
Figure B-66 - Load vs. Orthogonal Strain (3.0 in. slab – 2.0 in. plate) 128
Figure B-67 - Load vs. Bottom Strain (3.0 in. slab – 2.0 in. plate) 128
Figure B-68 – Failure Surface (3.0 in. slab – 1.75 in. plate) 129
Figure B-69 - Load vs. Displacement (3.0 in. slab – 1.75 in. plate)..... 129
Figure B-70 - Load vs. Diagonal Strain (3.0 in. slab – 1.75 in. plate)..... 130
Figure B-71 - Load vs. Orthogonal Strain (3.0 in. slab – 1.75 in. plate) 130
Figure B-72 - Load vs. Bottom Strain (3.0 in. slab – 1.75 in. plate) 131

LIST OF TABLES

Table 2-1 - Comparison of UHPC Composition to HPC 6
Table 3-1 – Flexural Capacity (M_u) of UHPC Slabs 28
Table 3-2 – Matrix of Restraint Configuration for Yield Line Analysis 30
Table 3-3 – Punching Shear Capacity of UHPC vs. 10,000 psi Conventional Mix 34
Table 4-1 – Series 1 Matrix (2.0 in. slabs) 46
Table 4-2 – Series 2 Matrix (2.5 in. slabs) 46
Table 4-3 – Series 3 Matrix (3.0 in. slabs) 47
Table 5-1 – Series 1 Test Results 54
Table 5-2 – Series 1 Comparison of Predicted vs. Actual 59
Table 5-3 – Series 2 Test Results 59
Table 5-4 – Series 2 Comparison of Predicted vs. Actual 63
Table 5-5 – Series 3 Test Results 64
Table 5-6 – Series 3 Comparison of Predicted vs. Actual 68
Table 5-7 – Statistical Results 82
Table 5-8 – Summary of Flexural Failure Results 85
Table B-1 -Summary of Results 100
Table B-2 – Summary of Material Properties 100

Chapter 1 - Introduction

1.1 Bridge Market for UHPC

In the ever growing market of bridge construction, the demand for new bridge structures is outpacing the supply. Some of this backlog stems from the need to rehabilitate and/or replace existing bridge structures that have deteriorated. Some of these deteriorating bridges have exceeded their service life and need replacement, while others are no longer capable of fulfilling the requirements of increased traffic loads. Many of the bridges built in the past were designed and built with many of the same materials that are in use today, steel and reinforced concrete. These materials have been proven to be very effective over the years, and improvements in material properties have allowed for changes to be made in the design of bridge structures. The improved material properties allow bridge structures to be lighter, have smaller cross sections, span further distances, and require less maintenance.

A relatively new material on the market, ultra-high performance concrete (UHPC), relies on the same principles as conventional concrete, but provides improved mechanical properties resulting from changes in the blend composition. The compressive strength, the property most often associated with concrete, of UHPC can exceed the compressive strength of conventional reinforced concrete by an order of magnitude. Additionally, UHPC exhibits a tensile strength unheard of in conventional concrete, allowing for the possibility of eliminating steel reinforcement in some applications. The use of UHPC allows for section dimensions to be minimized, taking advantage of the improved material properties while minimizing material usage and cost. In addition to the improved strength properties, UHPC maintains a very low permeability, making the material resistant to the corrosion and deterioration often associated with reinforced concrete and steel structures. This resistance directly correlates to a longer service life that can be achieved with the use of UHPC, making it an ideal material for a number of structural applications, particularly bridge structures.

The benefits of UHPC are quite substantial, but are offset by the high cost of the material. With the material being relatively new, there have only been a limited number of structural applications and the costs have remained high because the material is still considered to be a specialty product. The expectation is that as design with UHPC becomes a more common practice, the costs will decrease as the industry becomes more familiar and comfortable with it.

1.2 Project Overview and Scope

With UHPC being a relatively new material to the industry, only a limited amount of research has been performed, leaving a number of opportunities for the characterization of the material's behavior. The Federal Highway Administration (FHWA) and Virginia Department of Transportation (VDOT) have spearheaded the research conducted on UHPC in the United States by testing the response of UHPC in bridge structure applications. The purpose of their efforts is to determine the feasibility of using UHPC in bridge structures in the United States. Park *et al.* (2003) have developed a material model for UHPC and optimized a section for use as a bridge girder with an integrated riding surface; the model developed was validated with results from testing performed by the FHWA. The optimized section minimized the material usage and eliminated the use of shear reinforcement based on the comparison of the global model to the test results. However, no test results were available for comparison of the local effects in the slab/riding surface. With all of the section dimensions minimized, the resulting section has a thin top flange that also serves as the riding surface. The possibility exists that a punching shear failure could occur with a tire patch load applied to the surface.

This project's main objective was to develop a model for the prediction of the punching shear capacity of UHPC slabs and present a design equation for the prediction of punching shear capacity. Another objective was to determine the minimum slab thickness that could be used as a riding surface to prevent a punching shear failure from

occurring. The final goal was to minimize the material used due to the high cost of the material; this would require that test specimens be designed as small as possible and still be capable of failing in punching shear. Initially a generic model was developed, based on the ACI 318-02 design equations for punching shear, to predict the punching shear capacity of UHPC. The predicted response was compared to a prediction of the flexural capacity determined from yield line analysis to determine which configurations would cause punching shear failures and which would cause flexural failures. To accomplish these objectives, a total of 12 – 45 in. x 45 in. (36 in. x 36 in. unsupported area) slabs were tested to failure to determine the boundary between a ductile flexural failure and a brittle punching shear failure. The factors that were varied in the testing were the slab thickness and loading plate area. The results of the testing were then compared to the prediction models and other proposed models for punching shear, and recommendations were made as to the best predictor of punching shear strength of UHPC slabs.

1.3 Thesis Organization

The thesis organization follows the path of the progression of the research project. The second chapter provides a more thorough introduction to UHPC and highlights the material properties, advantages and disadvantages. More detail is provided on the optimized model developed at MIT which serves as the foundation for this research. A brief introduction to the mechanisms of punching shear is also provided, along with the history and background of the ACI design equations for punching shear. The third chapter highlights the mechanisms of failure of a two-way slab system and illustrates the methodology for the development of the preliminary prediction equations. Chapter four presents the material testing phase of the project and provides insight into the fabrication, testing, and instrumentation of the slab specimens. The fifth chapter presents the testing results and provides comparisons to the model developed in the preliminary analysis phase. This chapter also presents additional models not used in the preliminary analysis phase and makes comparisons; the best model for the prediction of punching shear

capacity is also determined. The final chapter summarizes the research, and provides conclusions and recommendations for future research.

Chapter 2 - Literature Review

2.1 Summary of Literature Review

Limited research has been conducted on the mechanical properties of UHPC, with none specifically devoted to the punching shear capacity of UHPC slabs. The following literature review discusses the history, properties, and capabilities of UHPC. In addition, a brief summary of the modeling optimization study for UHPC conducted at MIT is provided, as it serves as a cornerstone of this research effort. Some background and history of the current ACI guidelines, ACI 318-02, for punching shear is included for comparative purposes. Finally, other models for punching shear are presented.

2.2 Ultra High-Performance Concrete (UHPC)

2.2.1 History of UHPC

Ultra-high performance concrete (UHPC) is a relatively new type of concrete that provides significant improvements in strength, ductility, workability, and durability when compared to reinforced concrete or conventional high-performance concrete (HPC). The distinguishing factor between UHPC and HPC is that these improved characteristics are inherent to UHPC, whereas with HPC the mix is designed to meet special combinations of performance and uniformity requirements (Semioli 2001).

The recent development of UHPC has been primarily spearheaded by two independent French constructors, Bouygues Construction and Eiffage Group (EGI), with the aid of construction materials companies, Lafarge Corporation and Sika Corporation, respectively. The independent efforts of both companies created the products, Ductal®, brand name for Bouygues and BSI (Béton Special Industriel), brand name for EGI, with similar characteristics. While both materials exhibit similar qualities, the focus of this research effort is centered on Ductal® as a result of the scope of the research proposal.

2.2.2 General Composition

UHPC, specifically Ductal®, contains many of the same constituent materials as conventional concrete mix designs, but the proportions are varied (Graybeal and Hartmann 2003). The UHPC composition provided in Table 2-1 is derived from testing conducted by Graybeal and Hartmann (2003) and is used primarily for comparative purposes.

Table 2-1 - Comparison of UHPC Composition to HPC

Material	UHPC Amount (lb/yd^3)	HPC* Amount (lb/yd^3)
Portland Cement	1200	752
Coarse Aggregate	0	1671
Fine Sand	1720	1350
Silica Fume	390	75
Ground Quartz	355	0
Super Plasticizer	51.8	0
Steel Fibers	263	0
Accelerator	50.5	0
Water Reducer	0	207 fl oz.
Air Entrainment	0	6.6 fl oz.
Retarder	0	25-30 fl oz.
Water	184	235

**Mix design from Virginia Avenue Bridge over Clinch River-Richlands, VA (TFHRC)*

The most distinguishing characteristics of the composition of UHPC are the lack of coarse aggregate, the use of steel fibers, high proportion of cement/cementitious materials, and low volume of water. The use of only fine sand aggregate creates a dense cement matrix with minimal voids (Fig. 2-1), which results in a significant increase in strength.

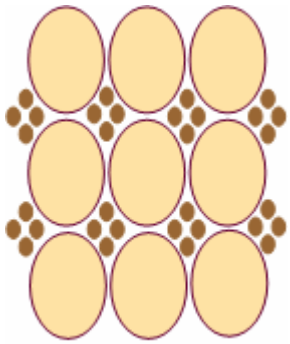

(Perry Presentation)

Figure 2-1 - Representation of Modified Compact Grading

The steel fibers in the cement matrix are designed to provide a bond at the micro level and minimize micro-cracking (Fig. 2-2). In turn they act as micro-reinforcement similar to mild steel reinforcement in conventional reinforced concrete on the macro level (Perry – Material History Presentation).

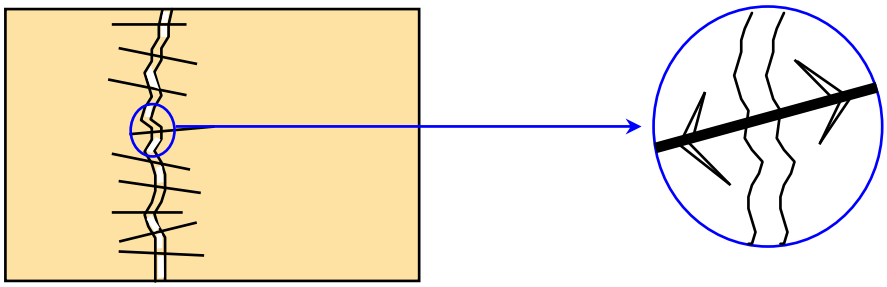

(Perry Presentation)

Figure 2-2 - Representation of Fiber Contribution

2.2.3 Material Physical Properties

The majority of the improvements in material properties can be attributed to the finely graded and tightly packed materials and steel fibers that aid in holding the cement matrix together after cracking has occurred (Graybeal and Hartmann 2003).

2.2.3.1 Compressive Strength

One of the most significant assets of UHPC is the improvement in compressive strength; UHPC has been demonstrated to achieve compressive strengths ranging from 23-33 ksi (Perry and Zakariasen 2003). This improvement in compressive strength has far exceeded the results achieved with conventional concretes and may allow for the possibility of UHPC to be more competitive in markets that have been typically dominated by steel construction.

In tests conducted by Graybeal and Hartmann (2003) at the FWHA laboratory, the curing method applied yielded significant variations in compressive strength, up to a 65% difference between steam curing and ambient air curing. While various curing methods

can be applied in field applications, the quality control on curing methods makes UHPC more suitable for precast operations.

2.2.3.2 Tensile Strength / Flexural Strength

The significant improvements in compressive strength are complimented by the fact that UHPC also exhibits tensile strength that has not been demonstrated in conventional concretes. This tensile strength allows the material to support both pre-cracking and post-cracking loads without experiencing the brittle failure that would be common in a conventional concrete. UHPC has demonstrated tensile strengths ranging from 0.9-1.7 ksi with various curing regimes and standard ASTM testing methods (Graybeal and Hartmann 2003). These tensile strengths were achieved as a result of the interaction of the steel fibers on the microscopic level and their ability to sustain load after the onset of cracking.

In addition to the improvements in tensile strength, UHPC can also achieve flexural strengths ranging from 5,000 – 7,200 psi (Perry and Zakariasen 2003). This combination of the tensile and flexural strength makes UHPC an extremely ductile material, capable of supporting significant loads beyond cracking. An example of UHPC's ductility can be observed in Fig. 2-3 (Perry – Material History Presentation).

(imagineductal website)

Figure 2-3 - 1 in. thick 6 ft x 10 ft slab supporting 2,000 lb car

This combination of the unique physical properties of UHPC allows designers to create thinner sections, longer spans, and taller structures (Perry and Zakariasen 2003).

2.2.3.3 Other Physical Properties

In addition to improved strength and ductility, UHPC exhibits some characteristics that make it very attractive for use in a number of applications. Due to the dense cementitious matrix and small and disconnected pore structure, UHPC maintains a very low permeability - roughly 1/10 the size of granite (Lafarge). UHPC allows for negligible carbonation or penetration of chlorides/sulfates and also maintains a high resistance to acid attack (Perry and Zakariasen 2003). UHPC's excellent resistance to freeze-thaw cycles also develops from the dense matrix, making it ideal for virtually any climate condition.

UHPC also exhibits very low creep and shrinkage when compared to conventional concretes, making the material suitable for precast/prestressed structures (Perry and Zakariasen 2003). The material can also be classified as a self-forming (self-consolidating) concrete due to the ease of flow of the material, which can be poured or pumped into place with limited or no vibration.

2.2.4 Advantages

With the significantly improved physical properties of UHPC, there are a number of advantages when compared to conventional concretes and even steel for structural applications. The high strength of UHPC allows the designer to use smaller sections, resulting in the use of less material, to yield the same capacity as illustrated in Fig. 2-4. The properties of UHPC can be optimized when used in conjunction with prestressing, which maximizes the use of the inherent tensile capabilities.

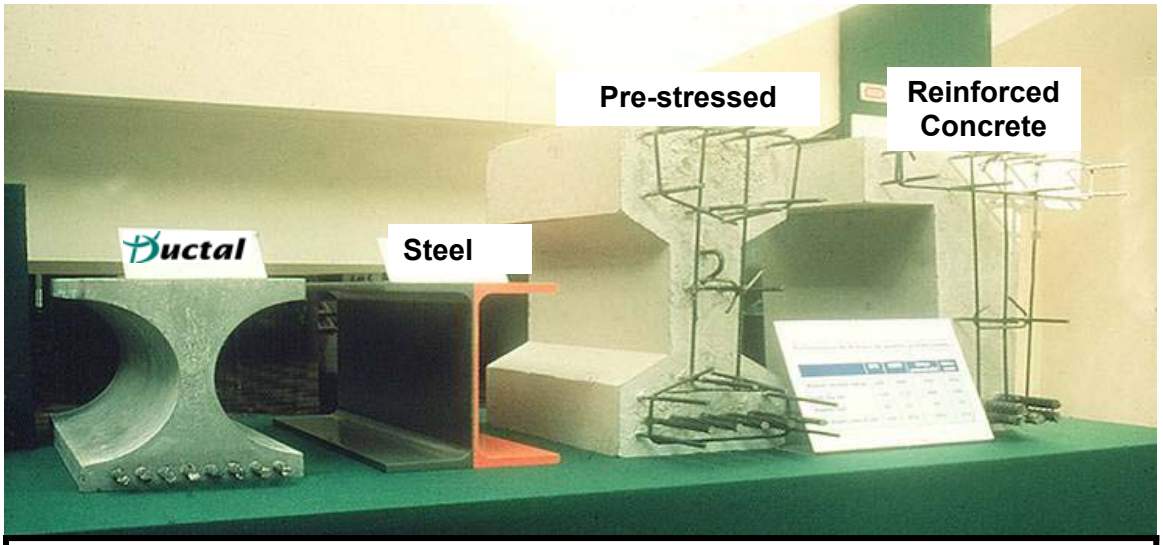

MASS (WEIGHT) OF BEAMS				
	Ductal	Steel	Pre-stressed	Reinforced
kg/m	140	112	467	530
lbs/ft	94	75	313	355

(Perry Presentation)

Figure 2-4 - Comparison of material section weights for equivalent flexural strength

The presence of the steel fiber reinforcement and interaction of the matrix allow for the elimination of flexural and shear mild reinforcement in a number of cases. This topic will be discussed further in Chapter 3.

Due to the durability and low permeability, UHPC structures are expected to have a longer service life than conventional reinforced concrete structures. UHPC is designed to be able to resist the effects of damaging environments and save money over the life of a project (Fig. 2-5).

2.2.5 Disadvantages

The biggest disadvantage of using UHPC in today's market is the initial cost. With UHPC being relatively new to the industry, there have been only a limited number of

applications. The design and use of the material has not yet been optimized or streamlined and as a result, the cost is still significantly higher than that of conventional concrete. The producers expect that as UHPC becomes more common in practice, the cost of use will decrease and they suggest that savings will be achieved over the life cycle when compared to conventional solutions as illustrated in Fig. 2-5.

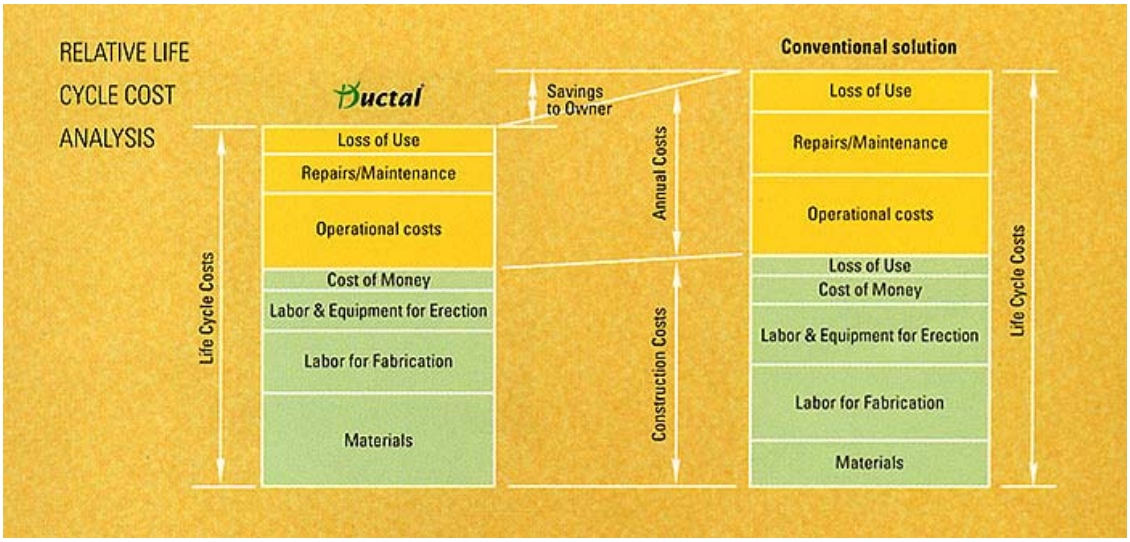

(Lafarge website)

Figure 2-5- Comparison of Life Cycle Cost of UHPC vs. Conventional Concrete

While the strength of UHPC allows for minimization of section properties, design with UHPC must still meet the stiffness requirements for serviceability. There is a limit as to how thin or small a member can be and still meet deflection and vibration requirements.

Another difficulty with the use of UHPC in design is that it is more suited for use in a precasting facility rather than an onsite application. UHPC in standard formwork does not allow for use of the material to its full potential; however, standard sections can be minimized (shorter sections, thinner flanges/webs, etc.) to make better use of the material properties.

2.3 Model-Based Optimization of UHPC

2.3.1 UHPC Model and Model Validation

Park *et al.* (2003) concluded that UHPC can be characterized as a material with two phases, the high strength cementitious matrix and the high strength fiber reinforcement, with distinct kinematics and possible mechanical interaction. UHPC is capable of supporting load until the point of cracking of the cementitious matrix and then can continue to support additional load after a minimal drop in stress (Fig. 2-6).

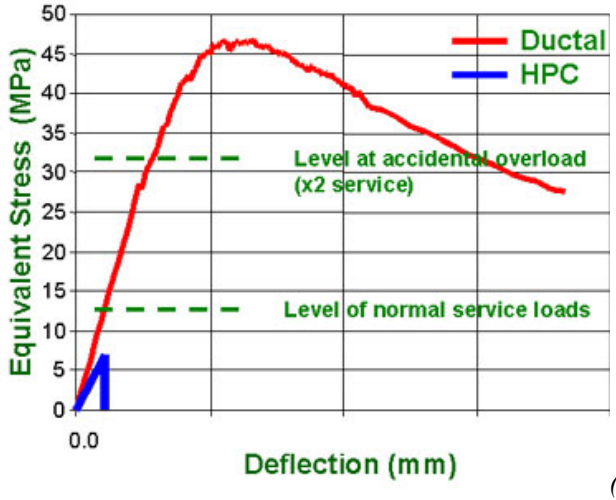

(Perry Presentation)

Figure 2-6 - Equivalent Stress vs. Deflection of Ductal® and conventional HPC

A two-phase constitutive model was developed for the material based on this relationship. The model developed attributes this overall composite behavior to the interaction of the brittle plastic matrix phase and the elastoplastic fiber phase.

The results of the model were input into a finite element program and compared to experimental test results from the Federal Highway Administration flexure and shear tests of UHPC specimens. During these tests, conventional reinforced concrete was replaced with unreinforced UHPC in standard AASHTO Type II girders and loaded to failure. The model was modified to take into consideration the effects of prestressing

steel on strength, stiffness, and crack pattern, and produced very accurate results when compared with the experimental data on both the global and local scale.

A maximum crack opening criterion for design purposes was introduced based on the UHPC design guidelines issued by the French Association of Civil Engineering (AFGC 2002) and were further expanded into a limiting strain criterion.

Limiting crack criterion

ω_{lim} = 0.3 mm = 0.012 in — for unreinforced UHPC sections

$\omega_{lim} = \min (L_f/4; h/100)$ — for reinforced UHPC sections

Limiting strain criterion

$\varepsilon_{lim} \leq \omega_{lim} / l_c = 1.5\ \omega_{lim} / h$ — for unreinforced sections

$\varepsilon_{lim} \leq \omega_{lim} / l_c = \min (3\ L_f / 8h; 3/200)$ — for reinforced UHPC sections

where:

ω_{lim} = maximum admissible crack opening

L_f = fiber length

ε_{lim} = maximum admissible strain

l_c = characteristic length = 2/3h

h = height of structure

The limiting crack and strain criteria can be used to determine a lower bound on the limiting load for a member when coupled with the proposed model and also prevent excessive deformation in UHPC members.

2.3.2 UHPC Section Design Formula, Strategy, and Criteria

The design strength of UHPC for flexure mimics that of conventional reinforced concrete, but ties in the effective composite strength of the lower (tensile) flange material. In conventional reinforced concrete, the tensile contribution is excluded from nominal strength because concrete exhibits a very low contribution before cracking and none beyond cracking. Also differing from conventional reinforced concrete design, UHPC

employs a limiting crack criterion which may reduce the nominal strength in certain instances.

The strategy adopted for the design of UHPC follows that of AASHTO LRFD in that there are two limit states, service limit state (SLS) and ultimate strength limit state (ULS), that need to be satisfied. The SLS design requirement adopted limits the design member to no cracking, while the ULS follows the UHPC guidelines developed by the AFGC previously shown. Using this strategy, an optimized section was developed by allowing variation in the section height and fixing the other variables to known or suitable quantities.

2.3.3 UHPC Simulation

The final phase of the model-based optimization process was the implementation into a real life simulation. The model was applied to a medium span, simply supported, prestressed bridge girder and optimized using a combination of the material model, previously developed 3-D optimization techniques, and the crack limitation criterion. Applying UHPC to a conventional bridge application yielded a smaller section than conventional bridge girders that integrated the riding surface into the girder (see Fig. 2-7).

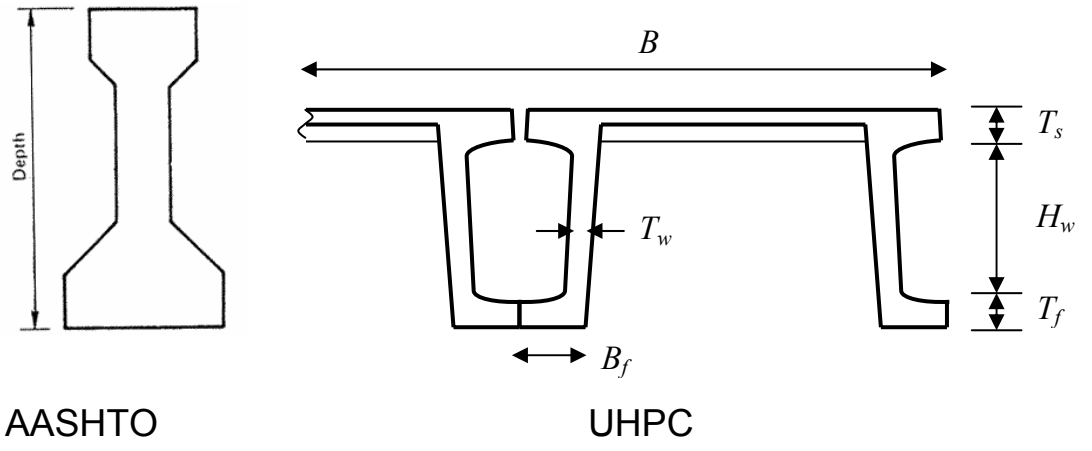

(Ulm Presentation)

Figure 2-7 – Comparison of Optimized UHPC Bridge Girder to AASHTO girder

Limitations on the minimum thickness of the slab section were developed as a result of the service limit state 'no cracking' criterion; the section was capable of meeting the flexural strength requirements with thin slabs (2 in.), but was unable to satisfy the SLS requirements with slabs thinner than 4 in. While the limitation to 4 in. slab thickness is conservative, it serves as a safe lower bound in the absence of experimental data to support thinner slabs, which will be the focus of this research effort.

2.4 ACI Punching Shear

2.4.1 Brief History of ACI Punching Shear

Shear failure of a member results from a combination of shearing forces and bending moment and in some cases the addition of axial load and/or torsion (ASCE-ACI Task Committee 1973). A good understanding of the shear strength of concrete members was not achieved until the early 1970's. During the early 1970's the basic philosophy of the ACI Building Code changed; the use of stirrup reinforcement to restrain growth of inclined cracking and provide increased ductility was included in the ACI Building Code (ASCE-ACI Task Committee 1973). This basic philosophy is more applicable to beam or flexural members, as conventional stirrups are not frequently used in slab systems. Due to their multi-dimensional geometry, slab systems are highly redundant structural systems and are able to achieve a higher degree of ductility than concrete beams (ASCE-ACI Task Committee 1974). Slab systems are subject to serviceability failures, excessive deflection and deformation, as a result of this ductility and are also prone to shear failures at overloads. The serviceability failures are not catastrophic, but shear failures can lead to the collapse of a floor system and even progressive failure of floor systems below. With slab systems being capable of developing a considerably larger nominal shear stress in the presence of principal moments, when compared to beams, the proper design for punching shear is critical.

The general method of analysis used by ACI for shear strength of slabs is considered to be applicable to the transfer of forces from slabs to columns, transfer of forces from columns to footings, and the strength of a slab - e.g., a bridge deck supporting a concentrated or moving load (ASCE-ACI Task Committee 1974). The design procedures put forth by ACI are based primarily on test data for the development of empirical formulas with little emphasis placed on the development of a model to characterize the true failure mechanism (ASCE-ACI Task Committee 1974). This method has proven effective over the years, but leaves designers without a true understanding of the punching shear phenomenon. In addition, there are limitations to the design equations of ACI such as improvement in punching shear capacity as a result of improved compressive and/or tensile strength.

2.4.2 General Mechanism of Failure

Conventional wisdom does not apply when considering the mechanism of a punching shear failure; in a slab system with a concentrated load or at a slab column connection, the loaded area is not actually pushed through the slab as shown in Fig. 2-8. Punching shear failures arise from the formation of diagonal tension cracks around the loaded area, which result in a conical failure surface as illustrated in Fig. 2-9.

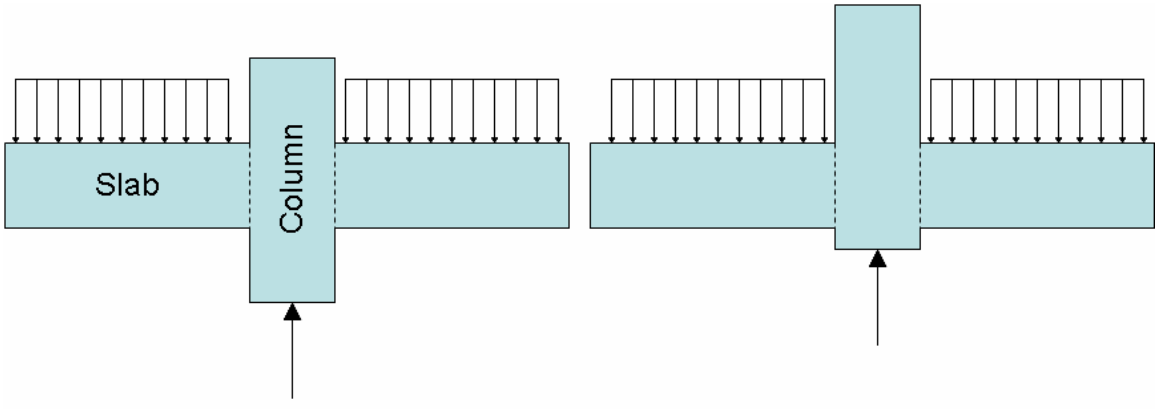

Figure 2-8 – Misconception of Punching Shear Failure

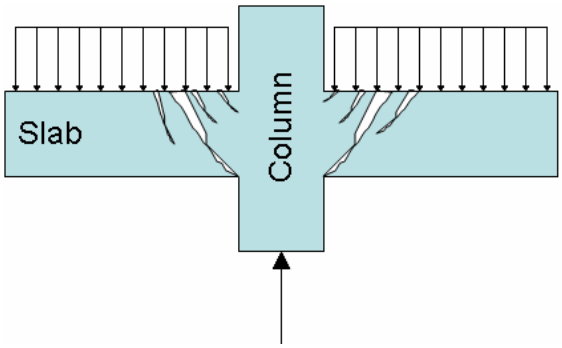

Figure 2-9– Correct Representation of Punching Shear Failure

A typical punching failure in reinforced concrete begins with the formation of flexural hinges (yield lines) around the perimeter of the loaded area. These hinges develop as a result of the moment caused in the slab by the applied load. This moment then begins to produce radial cracks that extend outward from the area of loading to the perimeter of the slab (Park and Gamble 2000). Failure of the slab occurs when the diagonal tension cracks intersect the radial cracks and produce a cone of failure.

2.4.3 Current ACI Punching Shear Guidelines

The current ACI Code (Building Code Requirements 2002) requires slab systems, without shear reinforcement, to resist punching forces resulting from applied loads.

The equations presented in ACI 318-02 are as follows:

$V_u \leq \phi V_c$

where: V_u = the factored shear force on the slab system

ϕ = the strength reduction factor for shear = 0.75

V_c = the nominal shear strength provided by concrete

V_c is the minimum of (2-1), (2-2), and (2-3)

$$V_c = (2 + \frac{4}{\beta_c})\sqrt{f'_c} b_o d$$ *Equation 2-1*

$$V_c = (\frac{\alpha_S d}{b_o} + 2)\sqrt{f'_c} b_o d$$ *Equation 2-2*

$$V_c = 4\sqrt{f'_c} b_o d$$ *Equation 2-3*

where: f'_c = compressive strength of the concrete

b_o = the perimeter of the critical section – critical perimeter (see Fig. 2-11)

d = the distance from the extreme compression fiber to the centroid of the longitudinal tension reinforcement (see Fig. 2-10)

β_c = the ratio of the long side to the short side of the concentrated load or reaction area

α_s = a factor for slab column connections based on the location of the column (interior, exterior, corner)

Figure 2-10– Illustration of d

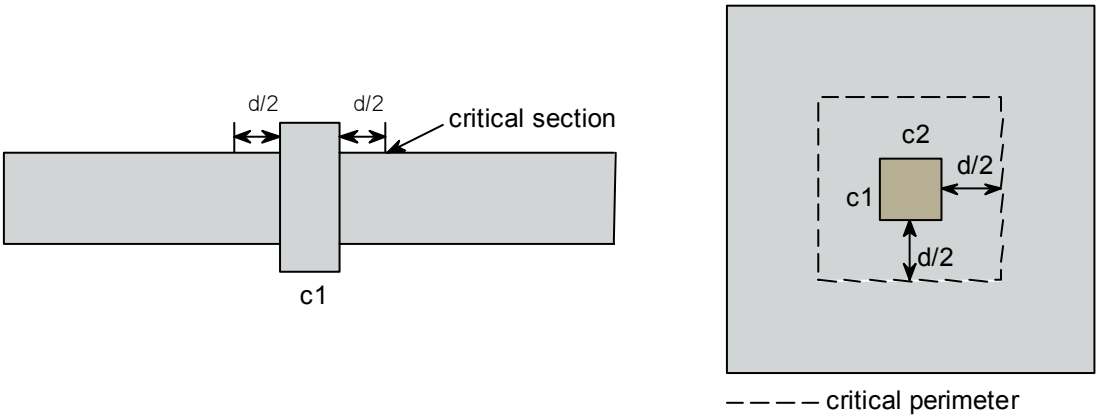

Figure 2-11– Critical perimeter

These design equations do not represent the entire design requirements for slab systems, but rather the ones applicable to the punching shear resistance of concrete slabs without shear reinforcement. As can be observed from the ACI methodology, this procedure is not directly applicable to UHPC slab systems primarily as a result of the lack of reinforcing steel for flexure, but will be used as a starting point for this research effort.

2.5 Existing Models for Punching Shear

A number of models, in addition to the ACI 318-02 design equations for punching shear, were evaluated to determine if they were applicable for predicting the punching shear capacity of UHPC. Some of the models were deemed not applicable, while others were given further consideration. This section briefly discusses the various models considered and specifies whether or not the model was evaluated further. It should be noted that a number of the models were excluded because the tensile steel reinforcement and the concrete contribution were integrated and it was not possible to distinguish the two separate components. This was the case with many of the models proposed in the initial stages (ASCE-ACI Task Committee 1974) of the development of the current ACI 318-02 design equations for punching shear. More details of the models deemed valid are presented in Chapter 5.

2.5.1 Yankelevsky and Leibowitz Model

The model proposed by Yankelevsky and Leibowitz (1999) was developed based on rigid post-fracture behavior and utilizes post fracture properties of concrete at the rough crack interfaces. The model attempts to predict the force-displacement resistance, stress distribution along the cracks, and the shape of the punched conical failure cone. The assumptions used in developing the model were:

- A single cracked surface already exists
- The cracked surface is divided into two elements, the punch wedge and outer slab
- Reinforcement is neglected
- Deformation and resistance are concentrated along cracked surface
- The failure surface is rough and aggregate interlock provides resistance

This model was not deemed applicable to UHPC for a few reasons. With UHPC not containing any coarse aggregate, the resistance from aggregate interlock would be significantly different than in conventional concrete. Additionally no consideration was given to the reinforcement, which for UHPC would eliminate the fiber contribution all together.

2.5.2 Walraven, Pat, and Markov

Walraven et al. (1987) studied the effects of fiber reinforcement on the punching shear capacity of reinforced concrete. The testing considered the effect of circular columns causing a punching shear failure in reinforced concrete slabs with additional fiber reinforcement. The research focused on determining the effect of the addition of fibers, whether they increased the strength of a cracked section or enhanced the pre-cracking strength. A new model was not developed, but empirical models for the concrete contribution were considered in conjunction with a model for the fiber contribution. The empirical models used for the concrete contribution were a function of the tensile reinforcement ratio and considered not to be applicable for UHPC.

2.5.3 Shaaban and Gesund Model

Shaaban and Gesund (1994) studied the effects of steel fiber volume on the punching shear strength of reinforced concrete slabs. In their study, thirteen slabs of varying strength and fiber volume were tested to failure to determine if the punching shear capacity could be improved through the addition of fibers. The foundation of their research was developed from earlier findings that indicated that the addition of fibers to concrete increased the tensile capacity which could be directly related to punching shear, attributed to be a principal tensile stress failure. The analysis focused on the critical punching area and how it was affected by the addition of fibers, and it was determined that there was little difference between the results and the ACI 318-89 model. An equation based on the ACI design equation that considered the fiber volume in the prediction for the punching shear capacity was proposed. This equation was deemed acceptable for comparison because it was of the same form as the ACI design equation and also considered the fiber contribution. The only significant issue regarding this model was that the fiber content in the Ductal® slabs is constant for all the tests. A more detailed discussion for this model is provided in Chapter 5.

2.5.4 Narayanan and Darwish Model

Naryanan and Darwish (1994) studied the effects of steel fiber reinforcement on the punching shear capacity of micro-concrete (concrete without coarse aggregate). The test parameters varied in their investigation were volume fraction of fibers, amount of tensile reinforcement, and concrete strength. In their study, a total of twelve slabs were tested to failure and illustrated the improvement achieved in punching shear capacity with the addition of steel fibers. They also developed an equation that was based on a semi-empirical model for the ultimate shear of fiber-reinforced concrete beams which considered the effects of concrete, steel fibers, and tensile reinforcement separately. The separate consideration of each term allowed for the punching shear capacity of UHPC slabs to be compared by neglecting the contribution of the tensile reinforcement. The results from their investigation and those of other researchers were then compared with

the prediction equation and good agreement was achieved. Additional testing by Tan and Paramasivam (1994) further validated the model. This proposed model will be discussed in more detail in Chapter 5.

2.5.5 ACI Concrete Breakout Strength Model

Based on the failure mode observed in typical punching shear failures, it was determined that the ACI 318-02 model for concrete breakout (Building Code Requirements 2002) exhibited a similar failure surface. The concrete breakout failure mechanism results from an anchor pulling out of a concrete surface is considered to be indicative of tensile capacity since reinforcement is not considered. The model was originally proposed by Fuchs *et al.* (1995) utilizing fracture mechanics concepts and test results from a large database of tests in Europe and America. The model is assumed to be similar in nature to a typical punching shear failure as seen in an unreinforced concrete slab, or in this case, UHPC (Figs. 2-12 and 2-13). This model will be discussed further in Chapter 5.

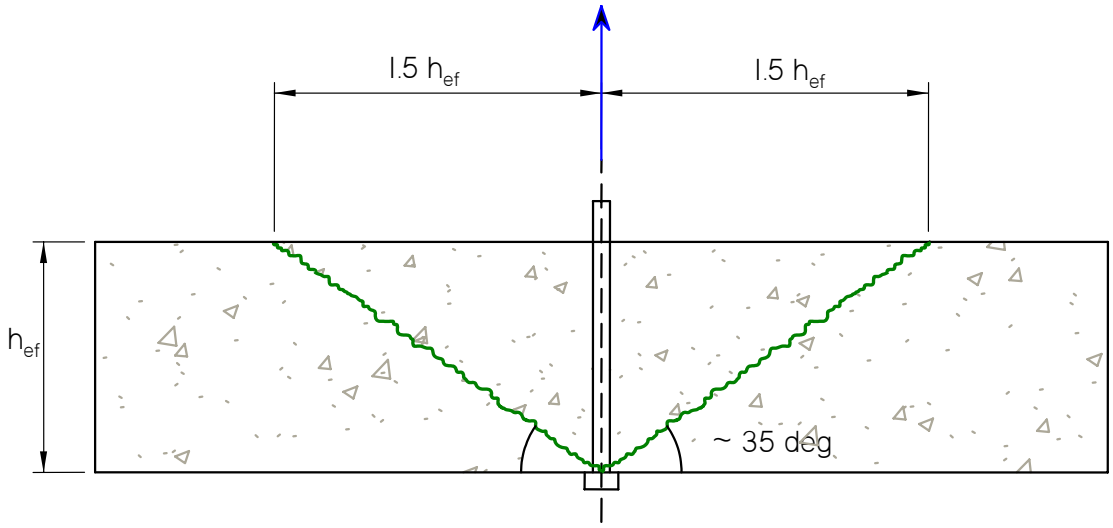

Figure 2-12 – Concrete Breakout Failure Surface

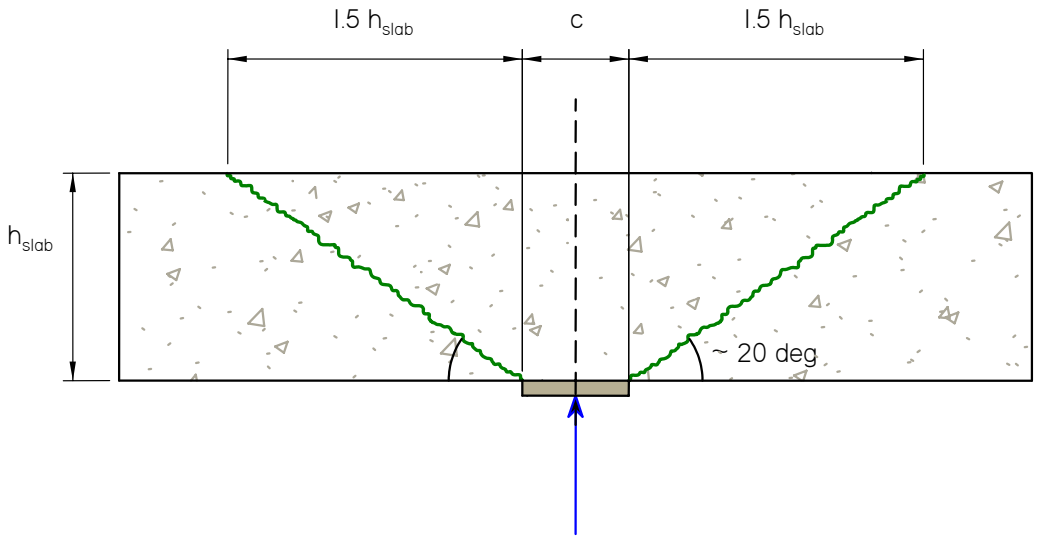

Figure 2-13 – Unreinforced Concrete (or Ductal®) Punching Shear Failure Surface

2.6 Summary of Literature Review

This chapter has presented a brief overview of UHPC and its potential impacts in structural applications. Also presented was a summary of the optimization modeling research efforts conducted at MIT and an overview of the current ACI 318-02 design requirements for punching shear as well as other models for characterizing punching shear strength. The research presented hereafter will attempt to correlate results from experimental testing with the established guidelines and develop new guidelines for UHPC slab systems.

Chapter 3 - Preliminary Analysis

3.1 Summary of preliminary analysis procedures and assumptions

Slab systems differ considerably when compared to beam members due to the multi-dimensional nature of their configuration. The geometry of a slab makes it a highly redundant system, capable of undergoing significant rotations and deflections, maintaining a plastic moment and even redistributing bending moments prior to failure. As a result of this redundancy, slabs are very complex to analyze, not adhering to simple analysis procedures that can be used on other members such as beams and columns.

The determination of punching shear capacity of slabs historically has been based on experimental data obtained from laboratory testing, but no established models exist for the determination of actual behavior at failure in a slab (ASCE-ACI Task Committee 1974). This chapter aims to establish a preliminary model for the determination of the punching shear capacity of UHPC slabs based on current ACI guidelines, modified to account for the properties of UHPC. Significant consideration is given to yield line analysis which serves as a basis for the determination of the failure mechanism, flexural failure or punching shear. This preliminary analysis was used to establish the dimensions of the specimens, the supporting system, and the loading plate sizes.

3.2 Failure Mechanisms

The goal of this research effort is to determine guidelines for the design of UHPC to resist punching shear. However, in a slab system the mechanism of failure may be either flexure or punching. In order to quantify the limits of the punching failure load, a good understanding of the flexural failure load is also required. This will allow the design of specimens which fail primarily in punching shear.

3.2.1 Flexural Failure Mechanism

3.2.1.1 Yield Line Analysis

A common method for the determination of flexural capacity of concrete slabs is yield line analysis. In yield line analysis a collapse mechanism for the slab is determined, with consideration given to the boundary conditions, and used in conjunction with the principle of virtual work to determine the ultimate load of the slab system (Park and Gamble 2000). A generic representation of a probable collapse mechanism, involving formation of plastic hinges, for a simply supported slab with a uniformly distributed load is shown in Fig. 3-1.

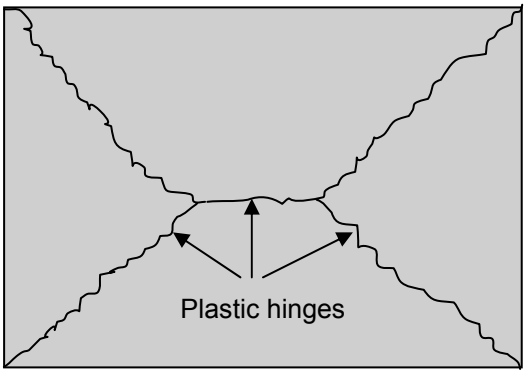

Figure 3-1 – Generic Failure Mechanism for SS Slab with Uniformly Distributed Load

The use of yield line analysis requires knowledge of the plastic flexural capacity of the slab, and the results serve as an upper bound on the ultimate load of the system. The results of yield line analysis for a given slab are either correct or too high and are highly dependent on proper selection of a failure mechanism (Park and Gamble 2000).

The critical factors that must be considered when using yield line analysis are the distribution of the slab reinforcement, the ductility of the slab, and the conditions at the ultimate load. Yield line analysis is considered applicable for use in slab systems that are reinforced uniformly, typically in orthogonal directions; it is assumed that UHPC satisfies this requirement due to the randomly distributed steel fibers in the matrix. While

conventional concrete uses rebar to provide the reinforcement, the steel fibers in UHPC serve as the micro-reinforcement in a similar manner. Slabs should also be sufficiently ductile to allow for plastic hinges to develop throughout the system; the degree of ductility or ductility factor is typically determined from the moment-curvature relationship as the ratio of the ultimate curvature (ϕ_u) to the yield curvature (ϕ_y). The moment-curvature relationship for a reinforced concrete slab can be represented by a tri-linear shape consisting of an initially elastic portion, a linear section to yielding of the reinforcement, and a nearly horizontal region until failure as illustrated in Fig. 3-2 (Park and Gamble 2000).

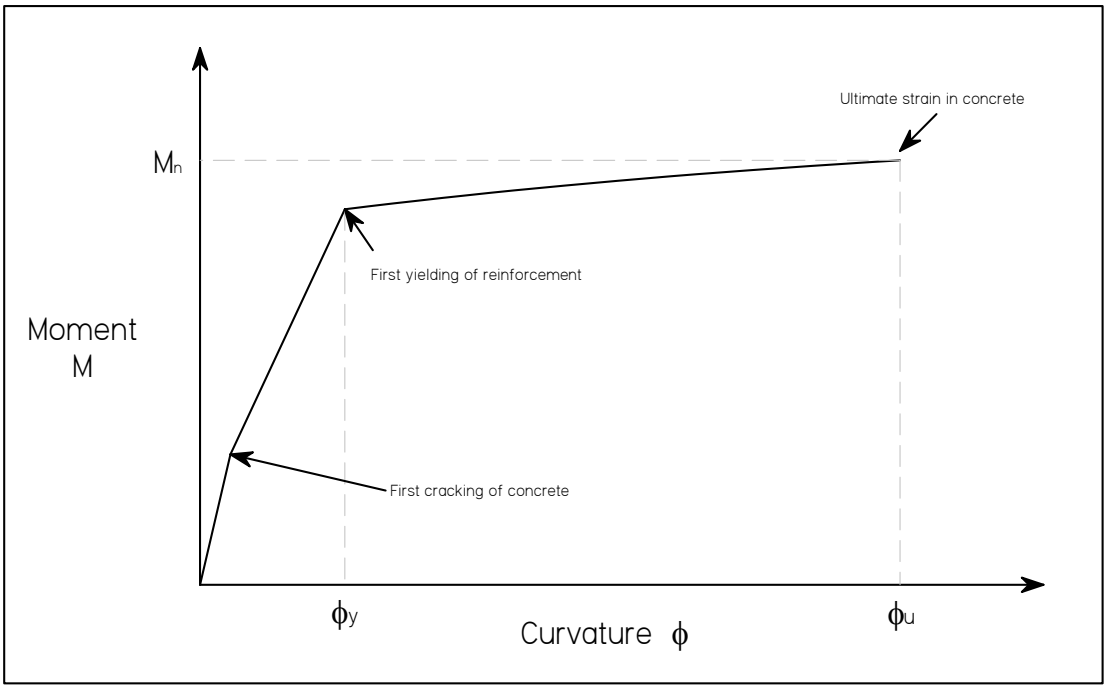

Figure 3-2 – Typical Moment-Curvature Relationship for Reinforced Concrete Slab

Due to their highly redundant nature, slabs are capable of redistributing moments after the onset of cracking. When additional load is applied to the system, a large change in curvature occurs at the locations of first yielding and plastic hinges continue to form until there are a sufficient number of sections (rigid segments between yield lines) to result in failure of the slab; at this point the slab is no longer able to support additional load (Park and Gamble 2000). Yield line analysis allows the designer to place an upper limit of the capabilities of the slab, and design accordingly.

3.2.1.2 Flexural Capacity (Ultimate)

In order to properly perform a yield line analysis for UHPC slabs, the plastic flexural capacity was required; this would serve as the resistance to rotation and deformation of the plastic hinges. The model for the stress-strain relationship of UHPC from the work of Park *et al.* (2003) is illustrated in Figure 3-3, where Ductal® is assumed to be linear elastic in the compression zone, linear elastic in the tension region up to the cracking strain, and elastic perfectly plastic to the limiting strain.

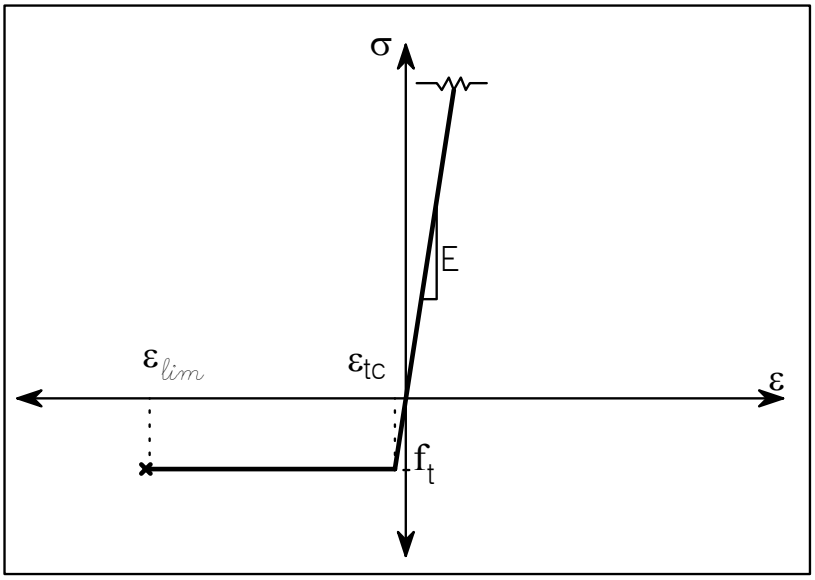

ε_{lim} = maximum admissible strain as defined by Park et al. (2003)

ε_{tc} = strain at which first cracking occurs

Figure 3-3– Stress vs. Strain Relationship for UHPC

This stress-strain relationship was used to determine the flexural capacity, M_n, for various slab thicknesses using conventional sectional analysis methods; an iterative solution to balance the forces was required to determine the depth of the compression zone (Fig. 3-4). The results of this analysis are summarized in Table 3-1.

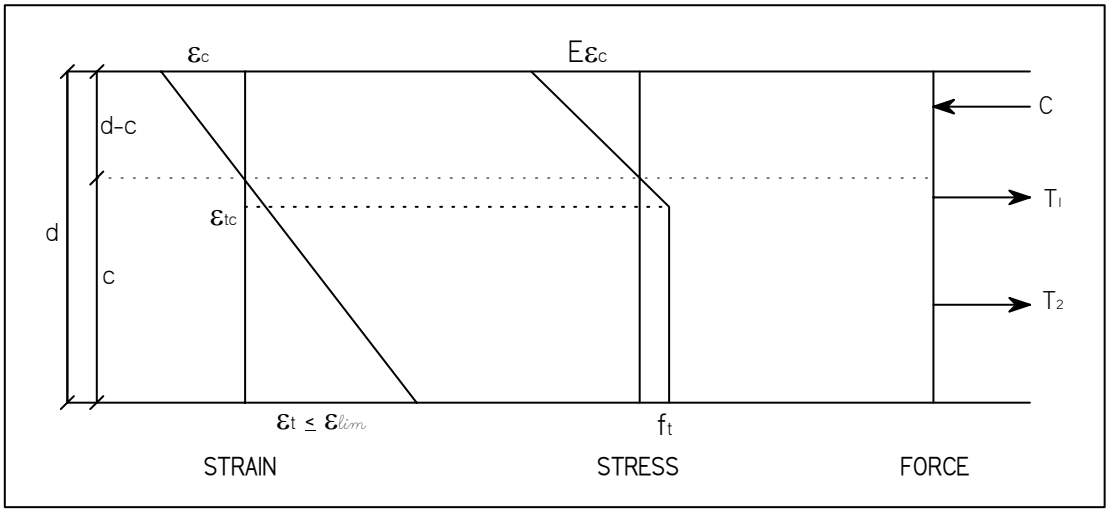

Figure 3-4– Section model for UHPC Slab

Table 3-1 – Flexural Capacity (M_u) of UHPC Slabs

d	ε_t	c	T_1	T_2	C	M_u
in	strain	in	kips	kips	kips	**kip-in/in**
2	8.86E-03	0.301	0.18	22.06	22.24	**23.5**
2.5	7.09E-03	0.414	0.27	26.99	27.27	**36.2**
3	5.91E-03	0.535	0.39	31.77	32.15	**51.6**
3.5	5.06E-03	0.664	0.52	36.40	36.92	**69.4**
4	4.43E-03	0.800	0.67	40.90	41.57	**89.7**

Assumptions: (E = 7820 ksi, f_t = 1.1 ksi, ω = 0.012 in. (0.3 mm), and b = 12 in.)

To determine if UHPC was suitable for yield line analysis, the moment curvature relationships for various plate thicknesses were developed (Fig. 3-5) and compared to the moment-curvature relationship of conventional reinforced concrete (Fig. 3-2). For UHPC, specifically Ductal®, the flexural capacity in this analysis was limited by the limiting strain, ε_{lim}, on the tensile face as proposed in the report by Park *et al.* (2003). As illustrated in Fig. 3-5, the moment-curvature relationship of UHPC can be approximately represented by a bi-linear relationship similar in shape to the tri-linear relationship of reinforced concrete. In UHPC there exists a distinct bend-over point which correlates to yielding of the reinforcing steel in conventional slabs, and the relationship also plateaus as it approaches the ultimate moment. For the 3-1/2 in. and 4 in. thick slabs, the region beyond the bend-over point does not adequately approach the horizontal plateau prior to

the ultimate moment and was not included in this research effort, as this trend is not ideal for yield line analysis.

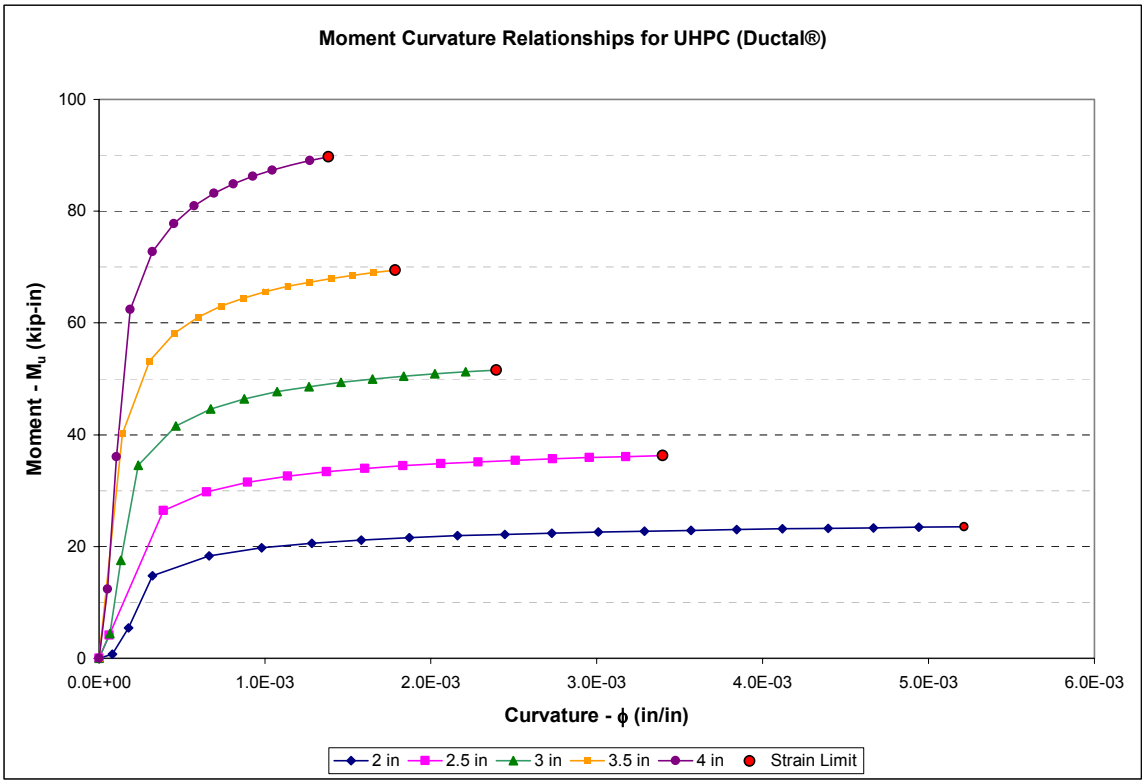

Figure 3-5– Moment-Curvature Relationship for UHPC

3.2.1.3 Yield Line Analysis Results for UHPC

Based on the moment-curvature relationships developed, yield line analyses were performed for various slab thicknesses: 2 in., 2-1/2 in., and 3 in.. The yield line analyses conducted considered a distributed load over an small area (a x b) to simulate the effect of a standard tire patch load with varying restraint conditions as summarized in Table 3-2. A generic diagram of the dimensions considered is shown in Fig. 3-6 and detailed diagrams of each configuration are further illustrated in Appendix A.

Table 3-2 – Matrix of Restraint Configuration for Yield Line Analysis

Edge Condition	North	South	East	West	Internal Work	Appendix Fig.
4 pinned						
Case A	SS	SS	SS	SS	$4M\left[\frac{2l}{w-a}+\frac{w}{l-b}\right]$	A-1
Case B	SS	SS	SS	SS	$2M\left[\frac{l}{w-a-2y}+\frac{w-a}{l}+\frac{4y}{l}+\frac{4a}{l-b}+\frac{4b}{w-a}\right]$	A-2
Case C	SS	SS	SS	SS	Not evaluated based on Case B	A-3
3 pinned/1 fixed						
Case D	SS	SS	Fixed	SS	$2M\left[\frac{2l}{w-a}+\frac{3w}{l-b}\right]$	A-4
Case E	Fixed	SS	SS	SS	$2M\left[\frac{3l}{w-a}+\frac{2w}{l-b}\right]$	A-5
2 pinned/2 fixed						
Case F	SS	SS	Fixed	Fixed	$4M\left[\frac{l}{w-a}+\frac{2w}{l-b}\right]$	A-6
Case G	Fixed	Fixed	SS	SS	$4M\left[\frac{2l}{w-a}+\frac{w}{l-b}\right]$	A-7
Case H	Fixed	SS	Fixed	SS	$6M\left[\frac{l}{w-a}+\frac{w}{l-b}\right]$	A-8
1 pinned/3 fixed						
Case I	Fixed	Fixed	Fixed	SS	$2M\left[\frac{4l}{w-a}+\frac{3w}{l-b}\right]$	A-9
Case J	SS	Fixed	Fixed	Fixed	$2M\left[\frac{3l}{w-a}+\frac{4w}{l-b}\right]$	A-10
4 fixed						
Case K	Fixed	Fixed	Fixed	Fixed	$8M\left[\frac{l}{w-a}+\frac{w}{l-b}\right]$	A-11
Radial pattern						
Case L					$2\pi\delta(m_1+m_2)$	A-12

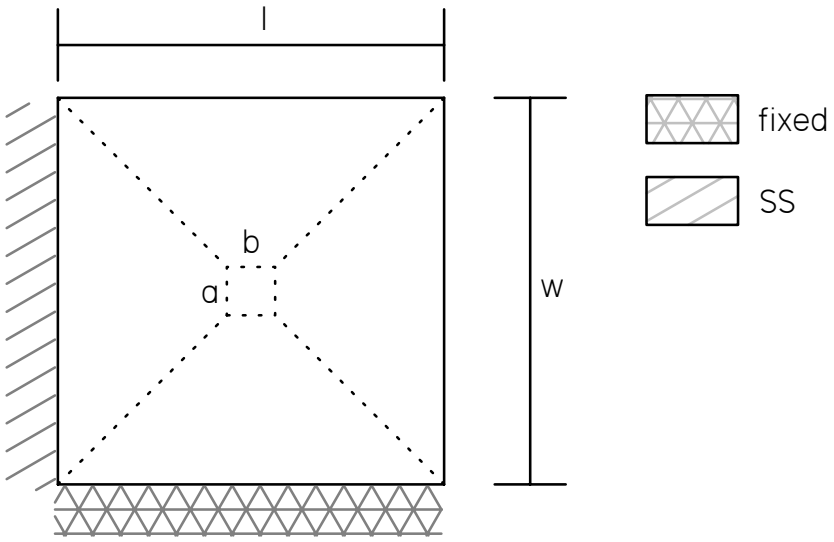

Figure 3-6– Generic Yield Line Analysis Configuration

The results of the analyses demonstrated that a configuration of four fixed edges would result in the highest load to cause a flexural failure, leaving more probability that a punching shear failure would occur for small punch sizes. It should be noted that no consideration was given to corner edge effects. The preliminary analysis for punching shear is discussed in further detail in the next section.

3.2.2 Punching Shear Failure Mechanism

3.2.2.1 Tensile Strength of Ductal®

Lack of tensile strength is one of the most distinguishing characteristics when comparing conventional concrete to UHPC. Concrete is known to have a very low tensile capacity and to be incapable of sustaining load beyond initial cracking, and for this reason additional reinforcement is required to support tensile loads. UHPC has been shown to exhibit significantly improved tensile strength, both before and after cracking (Graybeal and Hartmann 2003). This tensile strength of UHPC is achieved as a result of the interaction of the randomly oriented steel fibers acting as reinforcement on a micro level which prevents cracks from forming. After cracking has occurred, the steel fibers are capable of sustaining additional tensile loads until the fibers are pulled from the matrix

and the section severs. The tensile strength in UHPC alone is not sufficient to carry the loads for many structural applications, but does allow for the designer to reduce the amount of reinforcement needed to resist tension. The testing conducted by Graybeal and Hartmann (2003) also indicates that there can be an improvement in the tensile strength of UHPC depending on the type and time of the curing regime.

3.2.2.2 ACI Approximation

The current ACI Code (Building Code Requirements 2002) does not give significant consideration to the tensile strength in concrete in flexure and assumes it to be about 10 to 15 percent of the compressive strength. For two-way or punching shear design equations in the ACI code, the term $\sqrt{f'_c}$ (psi) is included because it serves as a measure of the concrete tensile strength, but is limited to a value of 100 psi (10,000 psi compressive strength concrete). This limit has been placed due to the limited amount of experimental test data on concrete with strengths above 10,000 psi compressive strength. Although there is limited test data for high strength concrete and UHPC does not contain reinforcement in the conventional sense, the ACI design equations presented below serve as the foundation for the preliminary prediction of the punching shear capacity of UHPC slabs.

The equations presented in ACI 318-02 are as follows:

$$V_c = (2 + \frac{4}{\beta_c})\sqrt{f'_c} b_o d \qquad \textit{Equation 3-1}$$

$$V_c = (\frac{\alpha_S d}{b_o} + 2)\sqrt{f'_c} b_o d \qquad \textit{Equation 3-2}$$

$$V_c = 4\sqrt{f'_c} b_o d \qquad \textit{Equation 3-3}$$

where: f'_c = compressive strength of the concrete

b_o = the perimeter of the critical section – critical perimeter (see Fig. 2-11)

d = the distance from extreme compression fiber to centroid of longitudinal tension reinforcement (See Fig. 2-10)

β_c = the ratio of the long side to the short side of the concentrated load or reaction area

α_s = a factor for slab column connections based on the location of the column (interior, exterior, corner)

To roughly establish the punching shear capacity of UHPC slabs, the failure surface was assumed to be the same as that previously defined by ACI for punching shear. It was also assumed that the full tensile strength of the failure surface could be developed prior to punching. By replacing the tensile contribution of conventional concrete with the tensile capacity of Ductal®, the following equation was developed:

$$V_{Ductal} = (f_t + k_m) b_o d \qquad \textit{Equation 3-4}$$

where: V_{Ductal} = Punching shear capacity of Ductal slab

f_t = Brittle tensile strength of composite matrix - Park *et al.* (2003) ~ 0.1 ksi

k_m = Post-cracking tensile strength of composite matrix - Park *et al.* (2003) ~ 1.0 ksi

b_o = Critical perimeter (defined at a distance d/2 from loading area)

d = Plate thickness (*differing from the ACI definition due to the lack of mild reinforcing steel*)

This equation was used to determine the punching shear capacity of various plate thicknesses with varying punch configurations. The results for various plate thicknesses with a standard wheel patch loading area (8 in. x 20 in.) are summarized in Table 3-3. Also included for comparison is the punching shear capacity of a 10,000 psi compressive strength concrete subjected to the same loading conditions with an assumed cover of 3/8 in., further demonstrating the improved capabilities expected from UHPC.

Table 3-3 – Punching Shear Capacity of UHPC vs. 10,000 psi Conventional Mix

d	b_o	$A = b_o d$	V_{Ductal}	$V_{10,000}$
in	in	in^2	**kips**	**kips**
2	64	128	**140.8**	**41.6**
2.5	66	165	**181.5**	**56.1**
3	68	204	**224.4**	**71.4**
3.5	70	245	**269.5**	**87.5**
4	72	288	**316.8**	**104.4**

3.2.3 RISA 3-D Model

RISA-3D was used to model the behavior of the slabs in various configurations; variations of the plate size, punch area, edge restraints, and plate thickness were all considered. The primary purpose of these models was to ensure that the stress distribution remained within the body of the slab and did not exceed the tensile capacity of the slab. For the smaller plates tested, a 45 in. square plate was sufficient to maintain the stress distribution within the slab body, while 7 ft x 12 ft slabs were required for large slabs subjected to the AASHTO wheel patch load. An example of one of the models is shown below in Fig. 3-7; the contours shown represent the principal stresses on the bottom (tensile) of a slab loaded from the top and restrained on two edges. The RISA-3D modeling proved most useful in determining the likely stress distribution that would occur with variations in the restraint conditions and verified the yield line analysis conclusion that fixed edges on all four sides would result in the largest failure load. The model also helped determine the length of plate required so the influence of the free edges would be minimized.

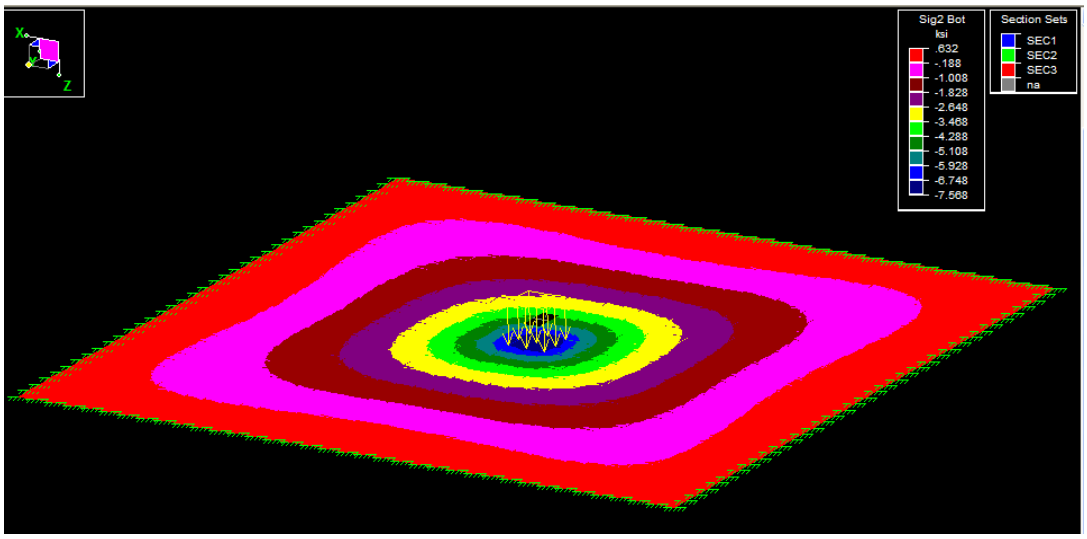

Figure 3-7– Risa 3-D Model of UHPC slab (restrained on two sides)

3.3 Specimen Sizing and Selection

Due to the high cost of Ductal®, it was prudent to minimize the material used; it was determined that 3 ft by 3 ft plates with fixed edges would provide a punching shear failure if the loading areas were sufficiently small. The expectation of the testing was that a series of plates loaded over small areas would provide sufficient insight into the punching shear capacity of UHPC which could then be scaled up to accommodate practical applications.

3.4 Review of Preliminary Analysis

The goal of this research project was to develop guidelines for the design of UHPC to resist punching shear. With slab systems there are two mechanisms of failure, flexure or punching shear, each with its own failure mode. In order to quantify the punching shear capacity of UHPC, the boundary between these two failure mechanisms must be determined.

An upper bound approach, yield line analysis, was used to determine the flexural capacity of various slab configurations. This analysis proved to be critical in that the results demonstrated that the configuration with all sides restrained would require the largest

load to cause failure, providing more opportunity to force a punching shear failure. The punching shear capacity of UHPC was estimated based on the ACI 318-02 design equations with modifications to account for the tensile capacity of UHPC. This preliminary analysis allowed for the determination of specimen sizes to be used in the experimental testing; these specimens were sized such that a punching shear failure could be achieved depending on the size of the loading area. This analysis served as the starting point for the experimental testing to be conducted. The actual test matrix will be summarized in Chapter 4 – *Materials and Testing*.

In addition to the small tests, dimensions and support conditions for larger specimens, more representative of the MIT optimized section, were also determined. The results of these tests are not presented herein.

Chapter 4 - Materials and Testing

4.1 Overview

In order to characterize the punching shear capacity of Ductal® a total of twelve 45 in. x 45 in. slabs were tested to failure. The testing was performed on three slab thicknesses, 2 in., 2-1/2 in., and 3 in., with varying punch areas. One of the objectives of the testing was to determine the boundary between punching shear and flexural failures. Due to the uncertainty of the boundary between the failure mechanisms, the determination of the punch area used was based on the results of the previous test.

4.2 Specimen Fabrication

The twelve slabs used in the testing were fabricated by Prestress Services, Inc. (PSI) in Lexington, Kentucky in October and November of 2003. The slabs were poured from the excess Ductal® concrete material used in beam segments for the Federal Highway Administration (FHWA). The formwork was designed and constructed by PSI to produce 45 in. x 45 in. slabs with block-outs as illustrated in Fig. 4-1. The forms were constructed so that they could be reused to coordinate with the Ductal® pours for the FHWA beams. The block-outs were formed with pieces of PVC in the interior and lifting eyes in the corner locations; the lifting eyes were installed to allow easy lifting and positioning of the slabs.

The slabs were poured using a trough system that was similar in width to the slab width. A mix truck was used to pour the Ductal® into the trough, which was pushed across the forms in a linear manner to fill the formwork. The slabs were covered with plastic and then subjected to an initial cure followed at a later date with a post-cure heat treatment. This curing regime was demonstrated by Graybeal and Hartmann (2003) to provide improved tensile strength.

After curing, the slabs were removed from the forms and stored in preparation for transportation to the Virginia Tech Structures Laboratory. All of the slabs exhibited a very smooth surface on all sides that were in contact with the formwork, but the surfaces in contact with the plastic tarp were rough to the touch. A number of the slabs were poured in excess of the required thickness due to the lack of precision in the trough system used, but were deemed acceptable for testing. In addition, the bolt holes on two of the slabs were not placed properly due to error in formwork fabrication and required modifications to the frame to compensate.

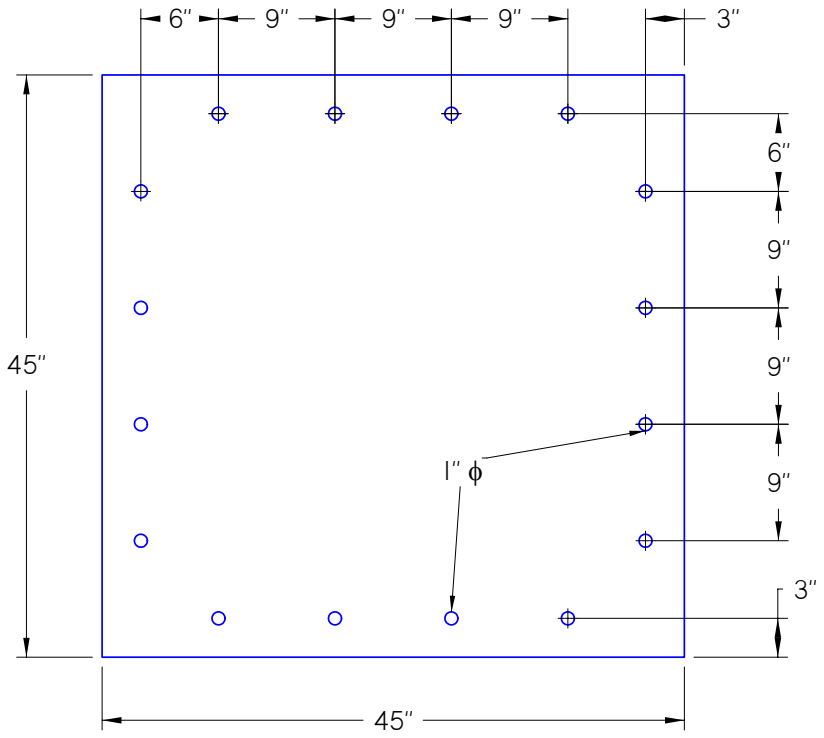

Figure 4-1 – 45 in. x 45 in. Slab layout with block-outs

4.3 Experimental Setup

Historically concrete slabs have been tested as simply supported systems loaded from above. A very limited number of experiments have been conducted on fully restrained slab systems, making the frame design challenging, but a series of tests conducted by

Keenan (1969) served as a good example of how to effectively fully restrain a slab. The effective restraint of the slab edges was crucial to the experiment because a simply supported slab would reduce the load required to cause a flexural failure; this decrease in load would lower the probability of achieving a punching shear failure. The restraint system employed in the study by Keenan (1969) utilized a system of channels and angles to prevent deflection or rotation of the edges and served as the foundation for the restraint system used in this experiment.

4.3.1 Frame

Steel and concrete frames were considered for the testing, but a steel frame was utilized due to ease of construction, placement and reconfiguration possibilities. A sketch of the final frame configuration in shown is Figs. 4-2 and 4-3, with the actual frame shown in Fig. 4-4.

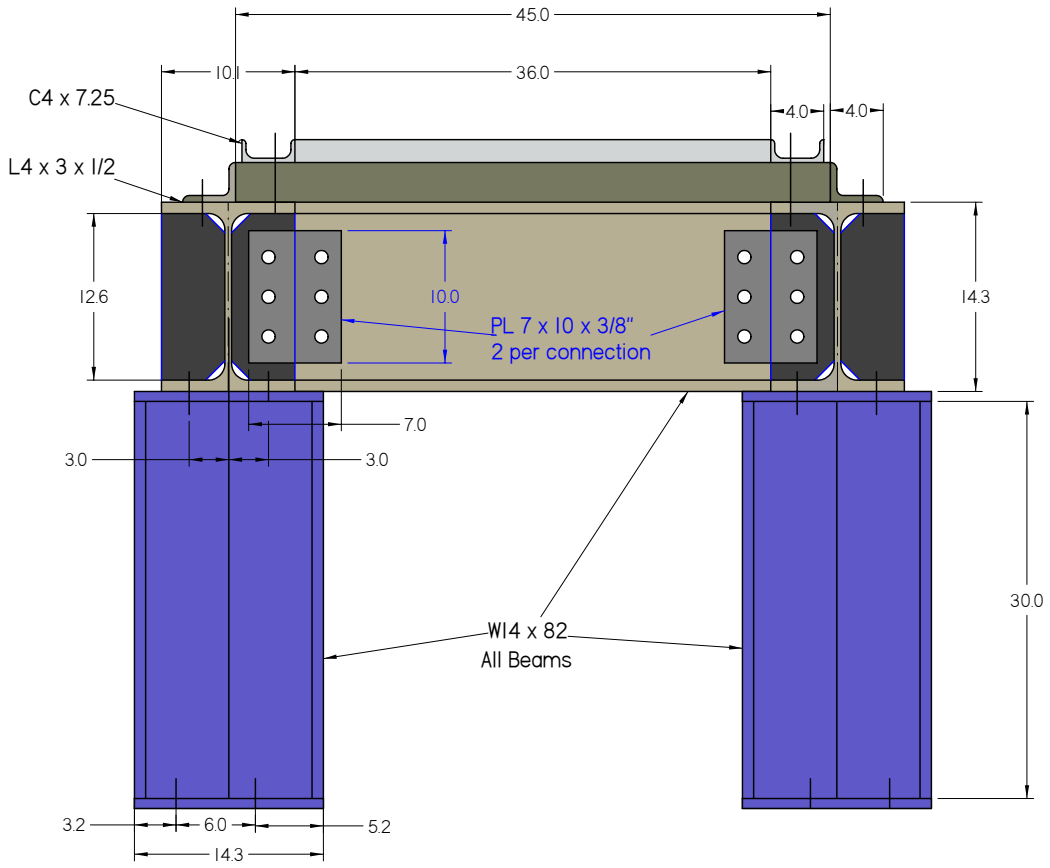

Figure 4-2 – Elevation 1 of Frame (all dimensions in inches)

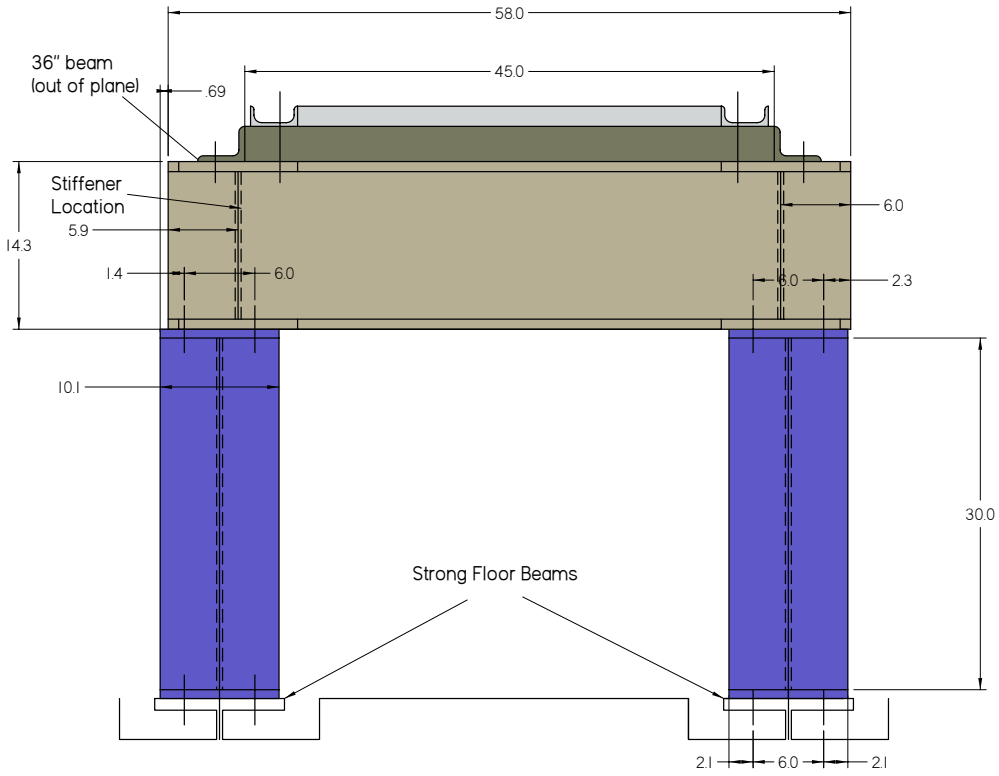

Figure 4-3 – Elevation 2 of Frame (all dimensions in inches)

Figure 4-4 – Photo of Actual Frame

The slabs were supported by W14 x 82 beams bolted to W14 x 82 columns which were bolted to the reaction floor. The rotations and deflections of the slabs were restrained by L4x3x1/2 angles on the perimeter and C4x7.25 channel sections on top of the slab bolted through the slab and the supporting beam flanges. A detail of the restraint system is illustrated in Fig. 4-5.

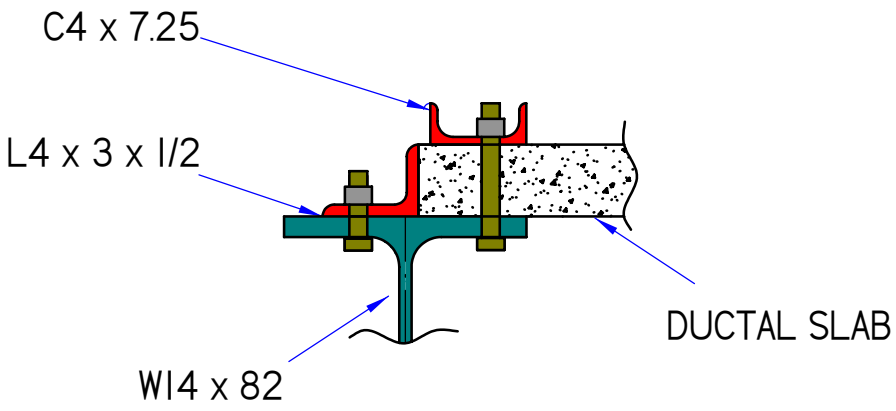

Figure 4-5 – Detail of Frame Restraint System

4.3.2 Instrumentation

The slabs tested were loaded from the bottom using a 300 ton ram and a 150 kip load cell. The slabs were loaded with the formed surface facing up; this allowed for observation of tensile crack propagation on the smooth face of the slab.

Each of the slabs was outfitted with a series of strain gauges on the top and bottom face to aid in monitoring of the strain response. The placement of the strain gauges was based on the likely location of crack formation, and adjusted during the testing to account for inaccuracies in the prediction. The strain gauge nomenclature was based on a relative reference with respect to the Virginia Tech Structures Laboratory, with East in the

direction of the main bay door and North in the direction of the machine shop. The expected flexural failure mechanism for a slab fully restrained with a point load at the center is illustrated in Fig. 4-6. The strain gauges were positioned in directions that were perpendicular to the predicted crack pattern; the goal was to observe the strain response and compare the results to the limiting strain values proposed by Park *et al.* (2003). The general placement locations for strain gauges for the top and bottom faces are illustrated in Fig. 4-7. It should be noted that the final strain gauge placement was dependent on the predicted failure mechanism determined prior to testing as well as the failure mechanism predicted based on previous tests.

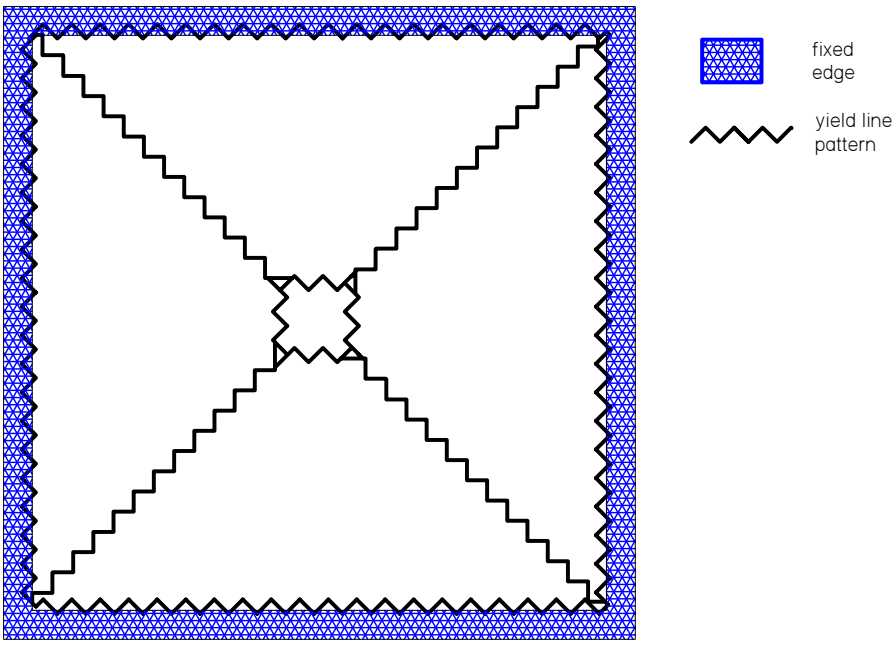

Figure 4-6 – Fully Restrained Yield Line Pattern

A maximum of nine strain gauges were used on each slab due to the limitations on the data acquisition system used. Vishay Micro-Measurements strain gauges were used on all slabs with CEA-06-500UW-350 (1/2 in. – 350 Ω - G.F. = 2.100) gauges used on the first 11 slabs and CEA-06-500UW-120 (1/2 in. – 120 Ω - G.F. = 2.085) gauges used on the final slab. Prior to mounting the gauges on the slab, the surface was ground with a masonry grinding pad to ensure a smooth surface for adhesion. The gauges were

mounted directly to the Ductal® surface using Vishay Measurements Group M-Bond 200 adhesive.

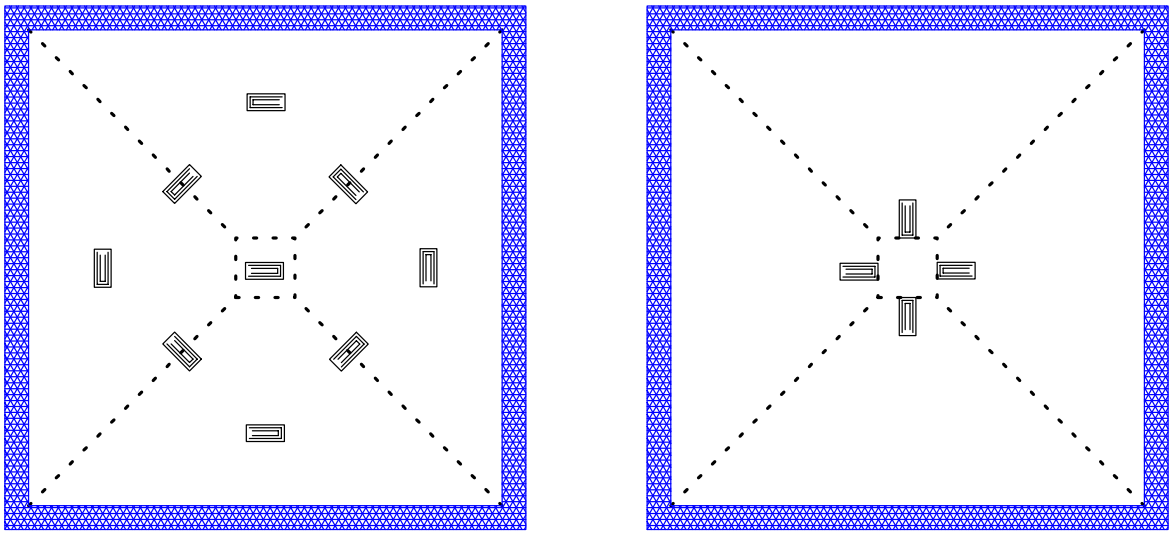

(a) Top Face *(b) Bottom Face*

Figure 4-7 – Strain Placement Configurations

To apply and measure the loads during testing, a ram/load cell combination as illustrated in Fig. 4-8 was used. Steel plates of various sizes were used as the punch area and were

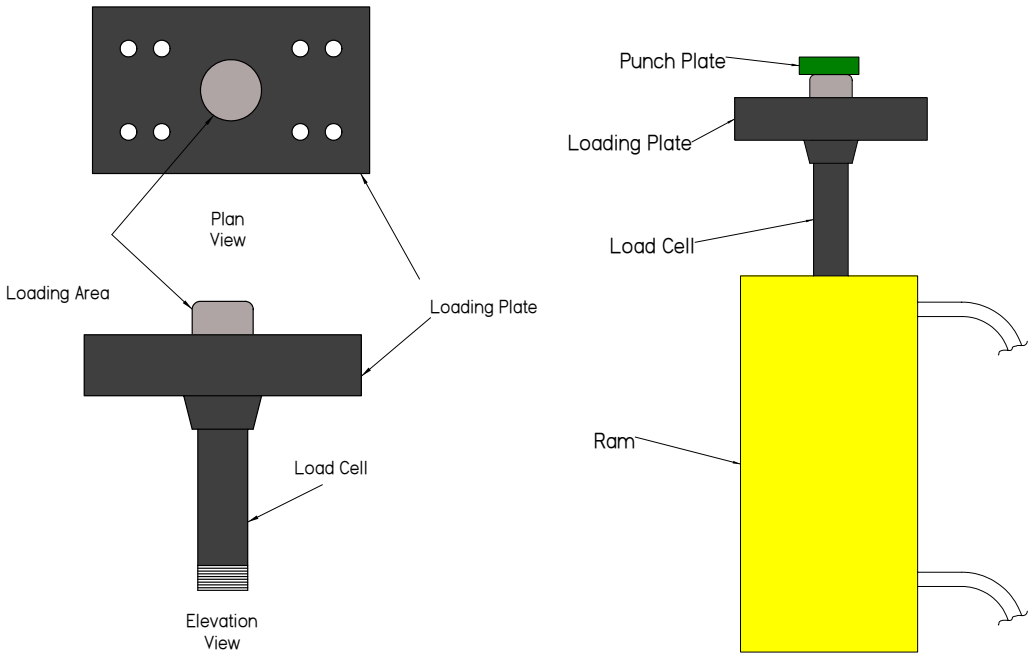

Figure 4-8 – Ram/Load Cell Combination

placed on top of the loading area to transfer the load from the ram to the plate specimen. A list of the punch sizes used are summarized later in this chapter. To measure the displacement of the slab at the point of load application, one wire pot displacement transducer was attached to each side of the ram to provide a redundant system for measuring displacements (Fig. 4-9). The wire pots were not attached directly to the slabs due to the inability to bore into the slab with a conventional drill and masonry bit.

(Latin Tech website)

Figure 4-9 – Wire Pot Displacement Transducer

During the initial series of tests, two linear variable displacement transducers (LVDTs) were mounted on the frame and positioned to record the displacement at the top of the angles on perpendicular faces. The LVDTs were used to verify the stiffness of the angles, but were not used after the initial series of tests due to the negligible deflections observed. A generic diagram of a typical LVDT is shown in Fig. 4-10. Due to the number of unknowns in the design of the frame, assumptions were made about the acceptable deflections of the angles.

Figure 4-10 – Linear Variable Displacement Transducer

The output was recorded using a Vishay Measurements Group System 5000 Scanner. The acquisition system used contained two strain gauge cards and two high-level cards capable of supporting 10 strain gauges and 10 high-level instruments (wire pots, plunger displacement transducers, and potentiometers). The software used for recording and

processing the test data was Smart Strain. For all of the tests, the data was recorded on a continuous basis with sampling rates varying from 1-2 recordings per second; the software allowed for real-time monitoring of results during testing.

4.4 Test Matrix

4.4.1 Trial Specimens

Prior to testing the Ductal® slabs in the frame, two conventional concrete slabs reinforced with welded wire fabric were tested to ensure that the proper failure mechanism was achieved and that the frame behaved as predicted. This additional testing was important due to the high cost of Ductal® and the difficulty in producing additional slabs for testing.

4.4.2 Test Parameters and Series Details

The testing was conducted on three series of slabs (2.0 in., 2.5 in., and 3.0 in.) with varying punch sizes. One of the goals of the testing was to determine the boundary between a punching shear failure and a flexural failure with the majority of tests failing in punching so strength could be characterized. The philosophy in determining the punching area was to produce a punching shear failure in the first test of each series where the punching shear capacity was determined from the preliminary analysis results. The subsequent tests varied the plate area to produce failures on both sides of the spectrum, punching shear and flexure, that would help define the boundary between the two failure mechanisms.

4.4.2.1 Series 1

The first series tested were the 2.0 in. thick slab specimens. These slabs were tested first due to the limited knowledge of the behavior of Ductal® in punching shear and the unlikelihood that a 2.0 in. slab would be used in a bridge application based on the study by Park *et al.* (2003). Initially the plan was to test four plates in each series, but due to

excessive thickness of one of the 2.0 in. slabs it was evaluated as a 3.0 in. slab in Series 3. The test matrix for Series 1 is shown in Table 4-1.

Table 4-1 – Series 1 Matrix (2.0 in. slabs)

Test #	Punch Area	Punch Dimensions	Predicted Failure Load	Predicted Failure Mechanism
1	2.25 in^2	1.5 in. x 1.5 in.	30.8 k	Punching
2	4.0 in^2	2.0 in. x 2.0 in.	33.2 k	Flexural
3	1.0 in^2	1.0 in. x 1.0 in.	26.4 k	Punching

4.4.2.2 Series 2

The specimens evaluated in Series 2 were 2.5 in. thick slab specimens. These were tested second in order to provide more results prior to testing the 3.0 in. slabs. Initially only three slabs were tested because the bolt holes were misaligned on the fourth due to improper placement of the block-outs during casting, but a total of four slabs were tested after modifications were made to the frame. The test matrix for Series 2 is shown in Table 4-2.

Table 4-2 – Series 2 Matrix (2.5 in. slabs)

Test #	Punch Area	Punch Dimensions	Predicted Failure Load	Predicted Failure Mechanism
1	4.0 in^2	2.0 in. x 2.0 in.	49.5 k	Punching
2	9.0 in^2	3.0 in. x 3.0 in.	52.7 k	Flexural
3	2.25 in^2	1.5 in. x 1.5 in.	44.0 k	Punching
4	6.25 in^2	2.5 in. x 2.5 in.	51.9 k	Flexural

4.4.2.3 Series 3

The last specimens evaluated in Series 3 were 3.0 in. thick slab specimens. These slabs were the most critical in the testing series because 3.0 in. was the minimum allowable thickness predicted in the study by Park *et al.* (2003). In Series 3 a total of five slabs

were tested due to the additional slab gained from the excessive pouring of a 2.0 in. slab. The test matrix for Series 3 is shown in Table 4-3.

Table 4-3 – Series 3 Matrix (3.0 in. slabs)

Test #	Punch Area	Punch Dimensions	Predicted Failure Load	Predicted Failure Mechanism
1	6.25 in^2	2.5 in. x 2.5 in.	72.6 k	Punching
2	2.25 in^2	1.5 in. x 1.5 in.	59.4 k	Punching
3	1.0 in^2	1.0 in. x 1.0 in.	52.8 k	Punching
4	4.0 in^2	2.0 in. x 2.0 in.	66.0 k	Punching
5	4.0 in^2	1.75" x 1.75"	62.7 k	Punching

4.5 Test Procedures

4.5.1 Loading

The slabs were brought into the lab using a forklift and placed near the frame. Eyebolts were then installed in two of the opposite corner block-outs with lifting eyes installed. The slabs were then lifted into place using the overhead crane with slings threaded through the eyebolts and lowered into the correct position on the frame.

4.5.2 Testing

The slabs were tested through a 300 ton ram with pressure applied through a hydraulic hand pump that allowed loading to be applied in 0.5 – 1.0 kip increments. The slabs were loaded in 3 – 5 kip increments and after each increment cracks were marked on the specimen. The marking for cracks continued until the load was within 6 kips of the predicted failure load, which was based on the preliminary analysis and previous test results. For the punching shear failures, the slabs were loaded until a decrease in load was observed in the load-deflection curve following the peak load. The criterion for termination of loading on the flexural failures was more subjective and was determined from the load-deflection curve as the point at which the curve reached a plateau after the peak load.

Chapter 5 - Presentation of Results and Analysis

5.1 Overview

The slabs tested in this research effort failed in one of two mechanisms: punching shear or flexure. This section summarizes the results from each test and discusses the failure mechanisms. The results of each test are then compared to the predicted response from the preliminary analysis and a few other proposed equations for predicting punching shear capacity. Modifications are then suggested to improve the response prediction for future experiments.

5.2 Failure Mechanisms

As previously stated, there were two possible failure mechanisms for the slabs tested: punching shear or flexure. The primary goal of this research effort was to force the majority of the slabs to fail in punching shear and then determine the boundary for a flexural failure.

A punching shear failure is typically a brittle failure that occurs with limited warning, and for the Ductal® slabs this occurred when the slab failed to support additional load followed by a conical punching failure. An example of a typical punching shear failure for Ductal® is shown in Fig. 5-1. Cracking on the tensile face began near the center and radiated out to one of the edges, and as the load was increased the cracking migrated to the opposite face. For all of the slabs that failed in punching shear, the direction of cracking tended to be in one direction; this led to the conclusion that the fibers were not as randomly oriented as expected. This phenomenon was attributed to the casting technique used where the slabs were poured in a uniaxial direction with a trough system, resulting in alignment of the fibers parallel to the direction of pour. This enabled the cracks to form between the fibers (Fig 5-2). This theory is in agreement with the trend described by the AFGC recommendations (2002) in that the fibers tend to align with the direction of the pour and along the formwork. Failure of the slab occurred when the cone of failure radiating outward from the point of load application pushed up through the slab

body. At failure the slab was no longer capable of taking additional load and the majority of the cracking had occurred in one direction, as illustrated in Fig. 5-3.

(a) Tensile face of typical slab failing in punching shear

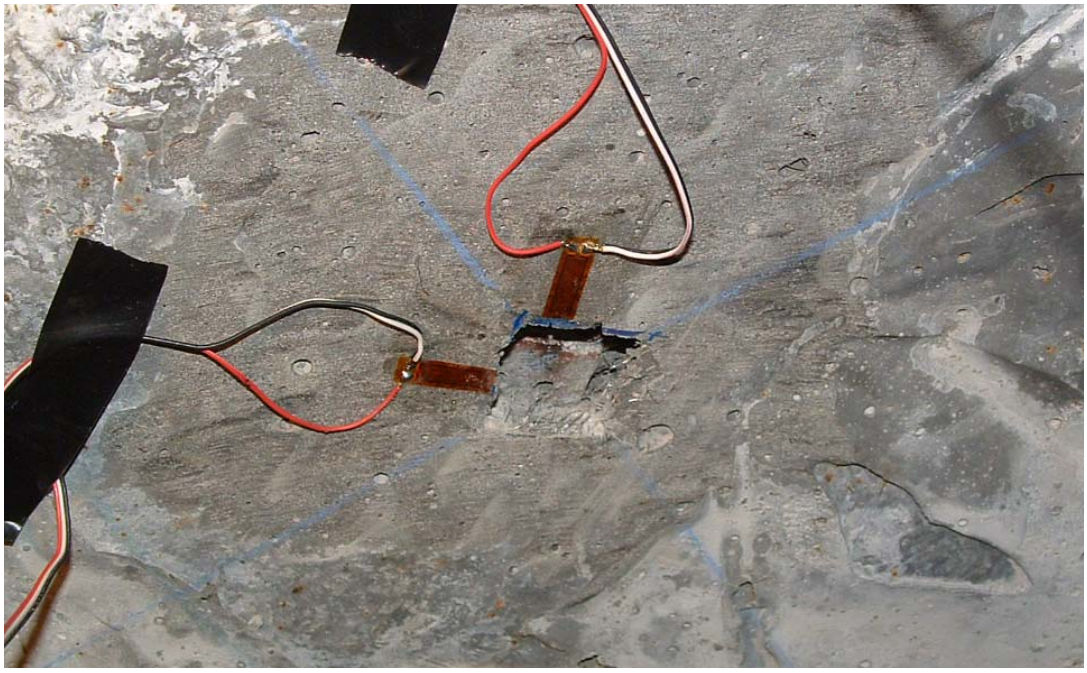

(b) Loading face of typical slab failing in punching shear

Figure 5-1– Typical Punching Shear Failure for Ductal®

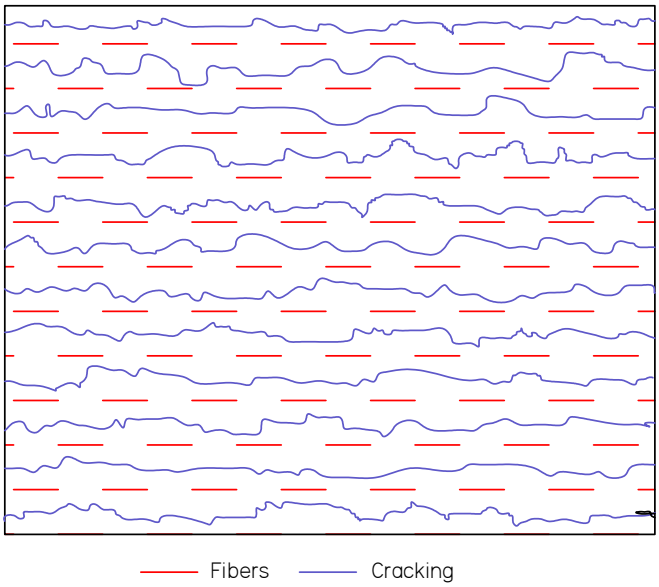

Figure 5-2 - Fiber Orientation vs. Crack Pattern

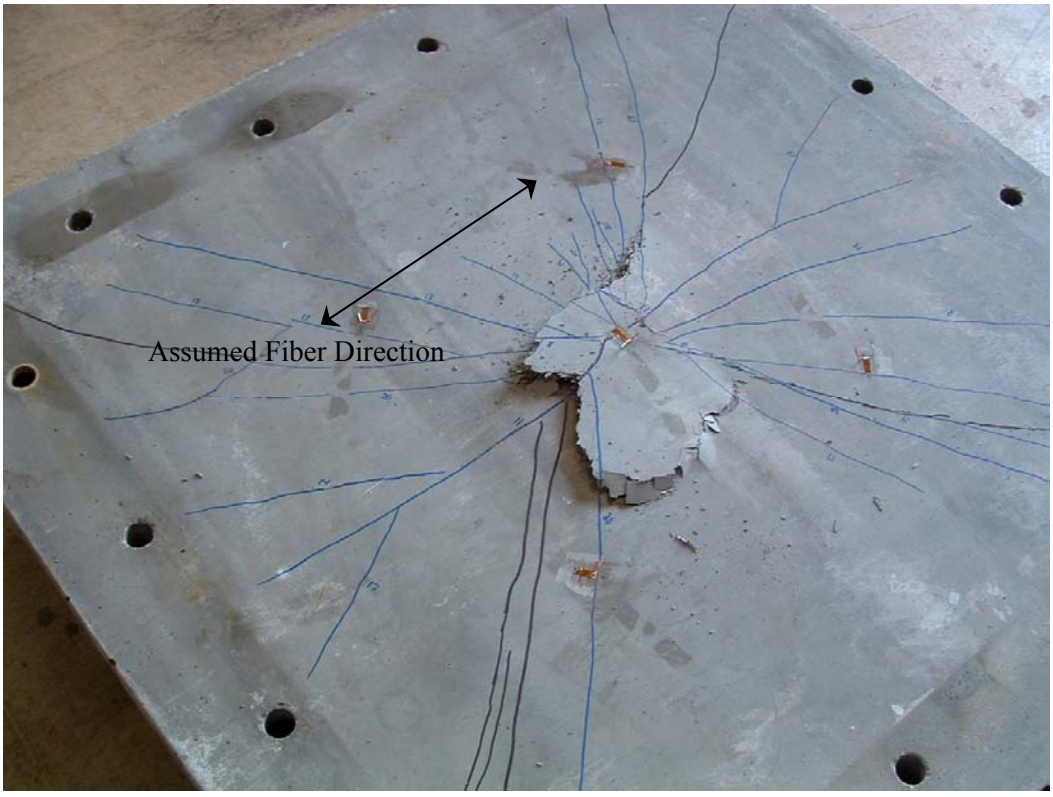

Figure 5-3 - Typical Crack Pattern for Punching Shear Failure

Contrary to punching shear failures, a flexural failure is a gradual failure that allows for the support of a reduced load after the formation of plastic hinges in the slab. A slab is capable of additional deformation, even after the peak load is achieved, which produces a more ductile failure, the preferred failure mechanism in design. An example of a typical flexural failure for Ductal® is shown in Fig. 5-4 with representations for both the tensile face and the loading face.

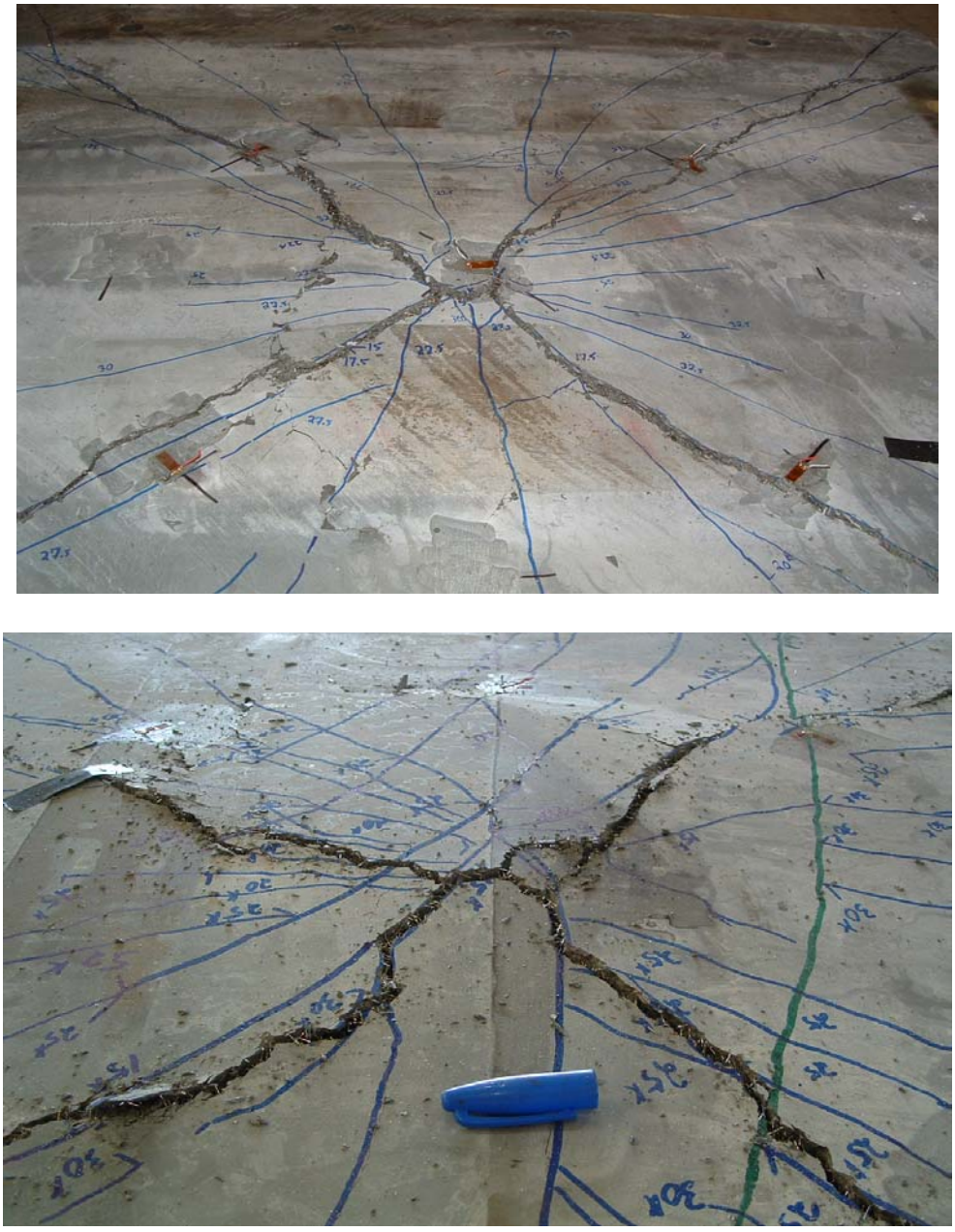

(a) Tensile face of typical slab failing in flexure

(b) Loading face of typical slab failing in flexure

Figure 5-4 – Typical Flexural Failure for Ductal®

Similar to the punching shear failure mechanism, cracks initially formed near the center of the slab on the tensile face and radiated to the edge. As loading continued, the cracks along the diagonals on the tensile face widened and extended through the slab thickness to the loading face with additional cracks forming at the fixed support on the loading face. The failure load was not as obvious in the flexural failures because there was no distinct failure cone as in the punching failures. The slabs that failed in flexure reached a peak load followed by a gradual decrease in load while continuing to deform.

All of the slabs tested failed at loads lower than predicted in both flexure and punching shear. The overestimation of the flexural failure loads can be attributed to a number of factors including the use of yield line analysis, inaccurate assumption of moment capacity, and the degree of fixity at the supports. Yield line analysis serves as an upper bound on the load carrying capacity of the slabs considered. The use of yield line analysis requires knowledge of the moment capacity in orthogonal directions, but based on the crack patterns observed during testing, the two were not the same as assumed in the yield line analysis. Full restraint of the slab edges was essential for forcing punching shear failures according to the preliminary analysis because it requires the largest load to cause a flexural failure. Investigation of the slabs after testing showed that the flexural hinges at the support face were not as distinct as the diagonal hinges, indicating that the slabs may not have been fully restrained along the edges. This could have also resulted in a lower load than predicted from the yield line analysis of a fully restrained slab. It was also observed that corner effects were not a factor in the flexural failures. The overestimation of the punching failure loads can simply be attributed to the lack of knowledge about the punching behavior of Ductal® slabs. As indicated in the preliminary analysis section, the starting point for the prediction equation was the ACI equation for punching shear, with a modification to account for the tensile strength of Ductal®. The term that historically represents the tensile strength of concrete ($4\sqrt{f'_c}$) was replaced with the tensile strength of Ductal® reported by Park *et al.* (2003). During this experiment the only variables that were considered were the slab thickness and punch plate area; changes in other variables

such as punch plate aspect ratio or percent fiber content may have provided more insight into the factors that affect the punching shear behavior of Ductal®.

5.3 Testing Results

5.3.1 Series 1 Results

The slabs tested in Series 1 were all approximately 2.0 in. thick specimens. These slabs were tested first, due to the unlikelihood that slabs this thin would be used in a real bridge application. The 2.0 in. slabs also served as a good starting point because the data obtained from testing would provide a good lower bound for the punching shear capacity of UHPC. The results from the 2.0 in. slabs are shown in Table 5-1. Series 1 consisted of three tests because one of the slab specimens was poured in excess of 2.0 in. and was deemed unacceptable for testing as a 2.0 in. slab, but was tested in Series 3 as a 3.0 in. slab.

Table 5-1 – Series 1 Test Results

			Predicted			***Actual***		
Test #	Plate Thickness (in.)	Punch Plate Size (in.)	Punching Failure Load (kips)	Flexural Failure Load (kips)	Failure Mechanism	Failure Mechanism	Failure Load (kips)	Average Maximum Deflection$_{(midspan)}$ (in.)
1	2.17	1.5	35.0	38.2	Punching	***Punching***	***23.3***	***.724***
2	2.32	2	44.1	44.3	Flexure	***Punching***	***27.2***	***.796***
3	2.12	1	29.1	36.1	Punching	***Punching***	***22.6***	***No data***

The results from Series 1 indicated that a very small loading area would be required to force a punching shear failure in Ductal® slabs, but further testing was required for a more accurate interpretation. As shown in Table 5-1, all of the Series 1 specimens tested failed in punching shear, the slabs were loaded to the maximum load, and the failure mechanism was abrupt, ending with the slab not capable of supporting additional load.

The response is best illustrated with a load-deflection curve as shown in Fig. 5-5. As expected, the slabs were capable of undergoing a significant amount of deformation prior to failure, around 3/4 in. for a 2.0 in. slab which equates to approximately L/48. The failure mode for each of the specimens was similar to the description for punching shear provided earlier in the chapter.

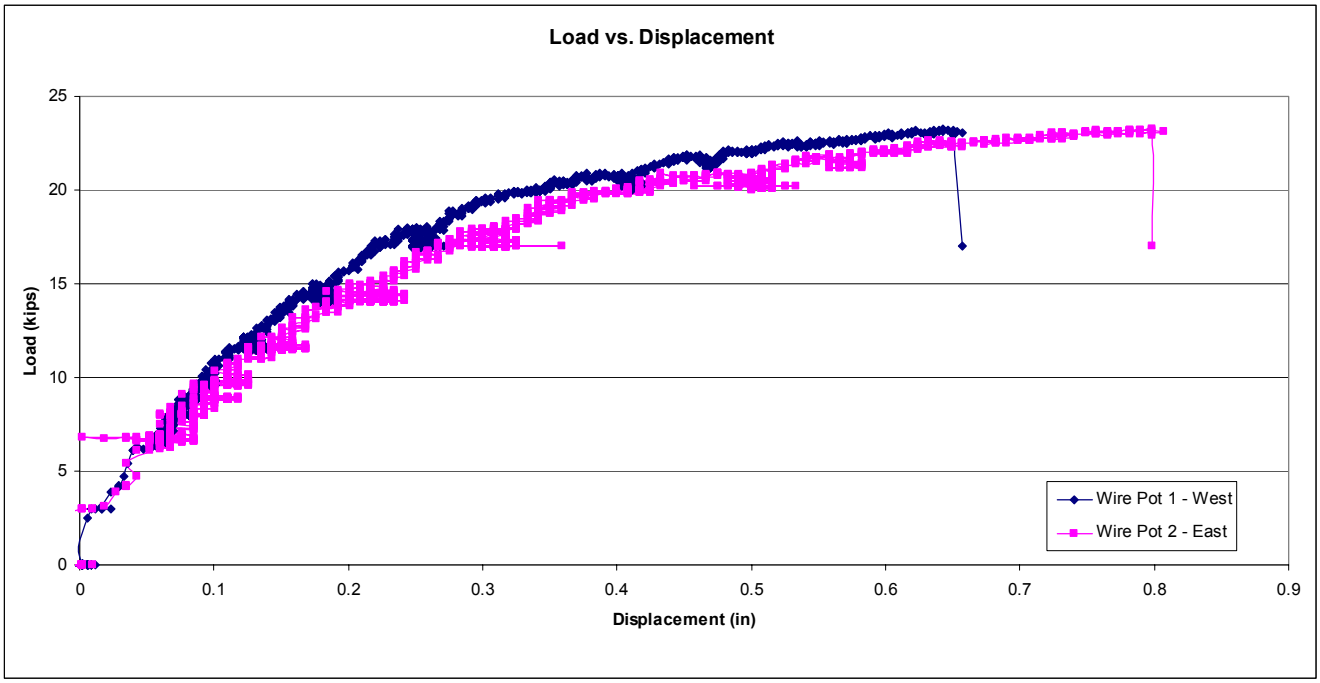

Figure 5-5 – Typical Load vs. Displacement Curve for Series 1 - Slab #1

The strains recorded from the mounted strain gauges were highly dependent on the crack pattern observed during the test. The strain values on the gauges located on the diagonals of the slab varied depending on the path of the diagonal cracking, with high tensile strains observed when the cracking passed near or through the gauge location. An example of this trend is illustrated in Fig. 5-6 with the NE strain gauge experiencing significantly higher tensile strain than the other gauges; a major crack likely formed underneath or within very close proximity to this gauge. It can also be observed that the SE strain gauge experienced an increase in tensile strain, but at a much higher load than the NE strain gauge. This likely resulted from the strain induced at the gauge from the growth of a crack that previously did not have a major influence on the gauge. As previously stated in Chapter 3, the limiting strain is defined as follows:

Limiting strain criterion

$\varepsilon_{lim} \leq \omega_{lim} / l_c = 1.5\ \omega_{lim} / h$ for unreinforced sections

$\varepsilon_{lim} \leq \omega_{lim} / l_c = \min (3\ L_f / 8h;\ 3/200)$ for reinforced UHPC sections

where:

ω_{lim} = maximum admissible crack opening

L_f = fiber length

ε_{lim} = maximum admissible strain

l_c = characteristic length = 2/3h

h = height of structure

A consistent measure of the orthogonal strains was not achieved in Series 1 due to inconsistent placement of the gauges for this series. The orthogonal gauges were placed at varying locations for Series 1 with no placement duplicated in the series. The inconsistency in Series 1 resulted from a number of factors, including testing learning curve factors and strain gauge availability. While a consistent measure of the orthogonal strains was not achieved within Series 1, the placement on two of the slabs was consistent

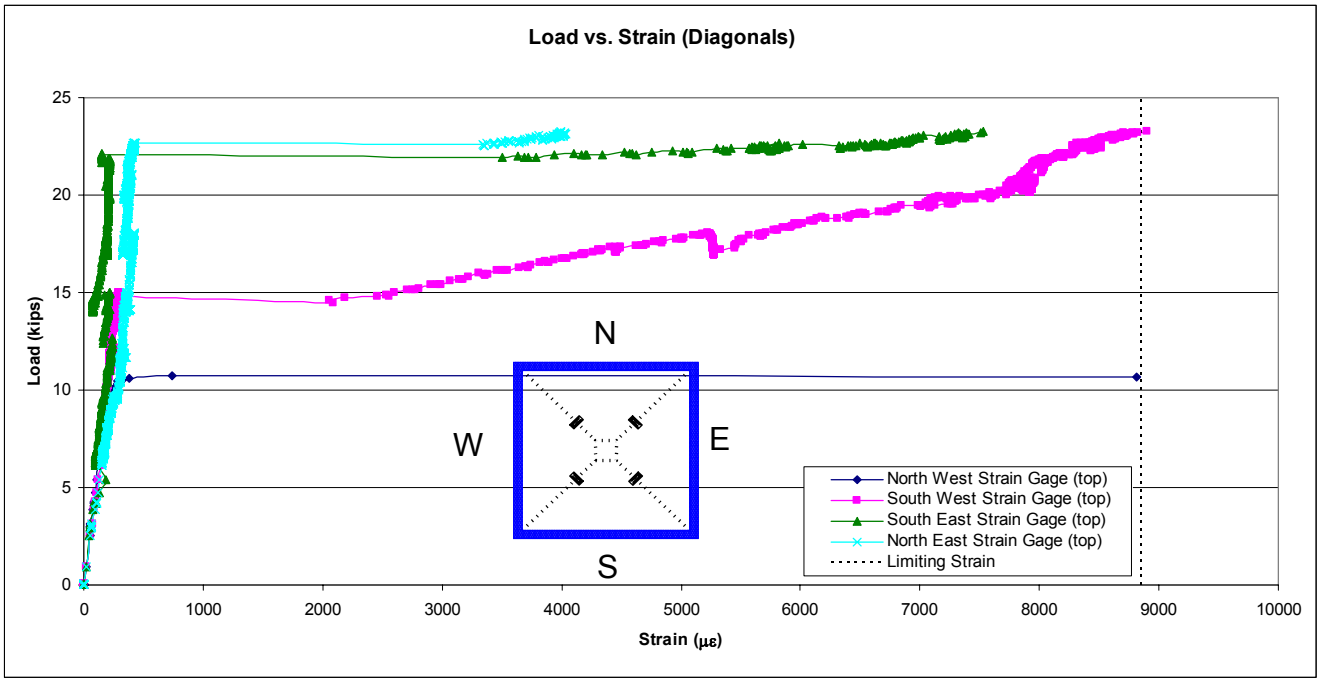

Figure 5-6 – *Typical Load vs. Strain (Diagonal) for Series 1 – Slab #2 (Tensile Face)*

with slabs tested in the other two series. The general trend was similar to that observed along the diagonal, with strain response dependent on crack location, and is illustrated in Fig. 5-7. The strain response of the gauges on the loading face was different as a result of the gauges being in compression throughout the testing, compression shown as a negative strain value. The general trend observed in Series 1 is illustrated in Fig. 5-8; the compressive strain increases proportional to load increases until failure, after which the compressive strain is relieved as the loading area punches through the plate.

The results from Series 1 were consistent over the limited number of tests, with an increase in failure load observed with increasing punch plate dimensions. The initial predictions did not provide very accurate results when compared to the actual results as shown in Table 5-2. When the compared to the prediction from the preliminary analysis, the failure load is overestimated in all cases (~62% maximum), but when compared to the ACI 318-02 design equations (Building Code Requirements 2002) the failure load is underestimated in all cases (~18% maximum). This trend illustrates that neither equation provides an accurate measure of the punching shear capacity of Ductal, but the ACI 318-02 equation (Building Code Requirements 2002) would be conservative for the 2.0 in. slabs tested in Series 1.

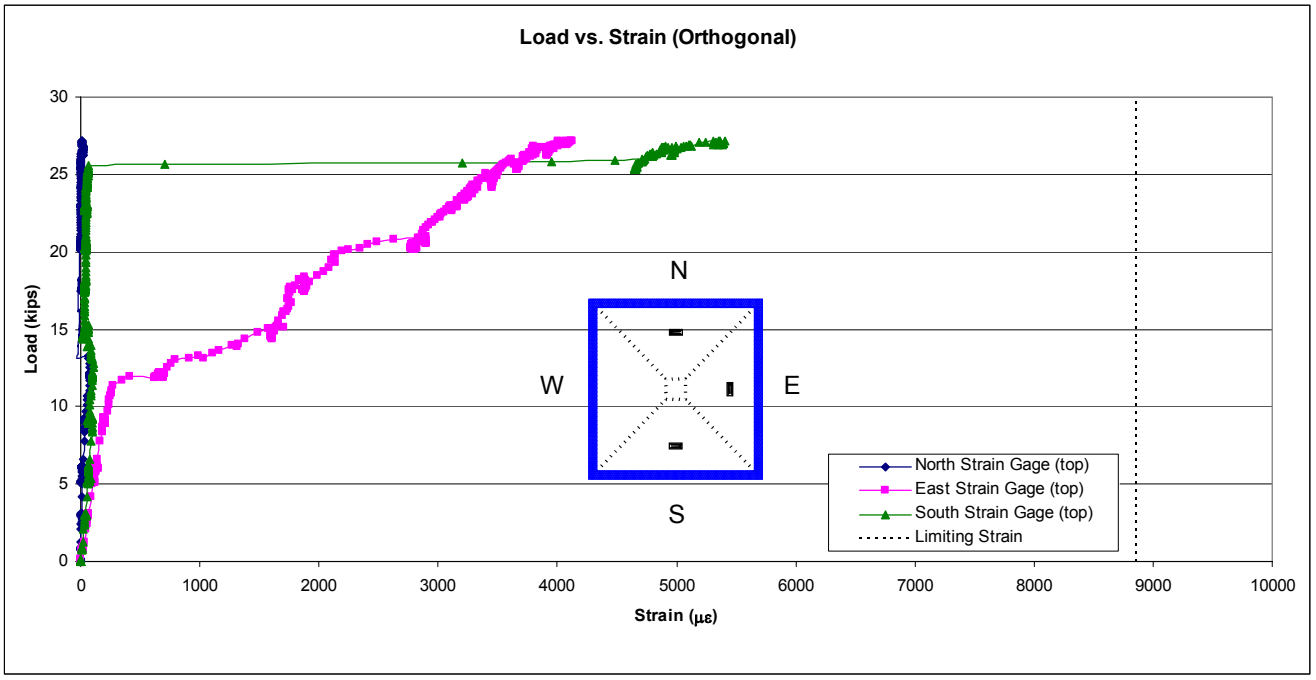

Figure 5-7– Load vs. Strain (Orthogonal) for Series 1 – Slab #2 (Tensile Face)

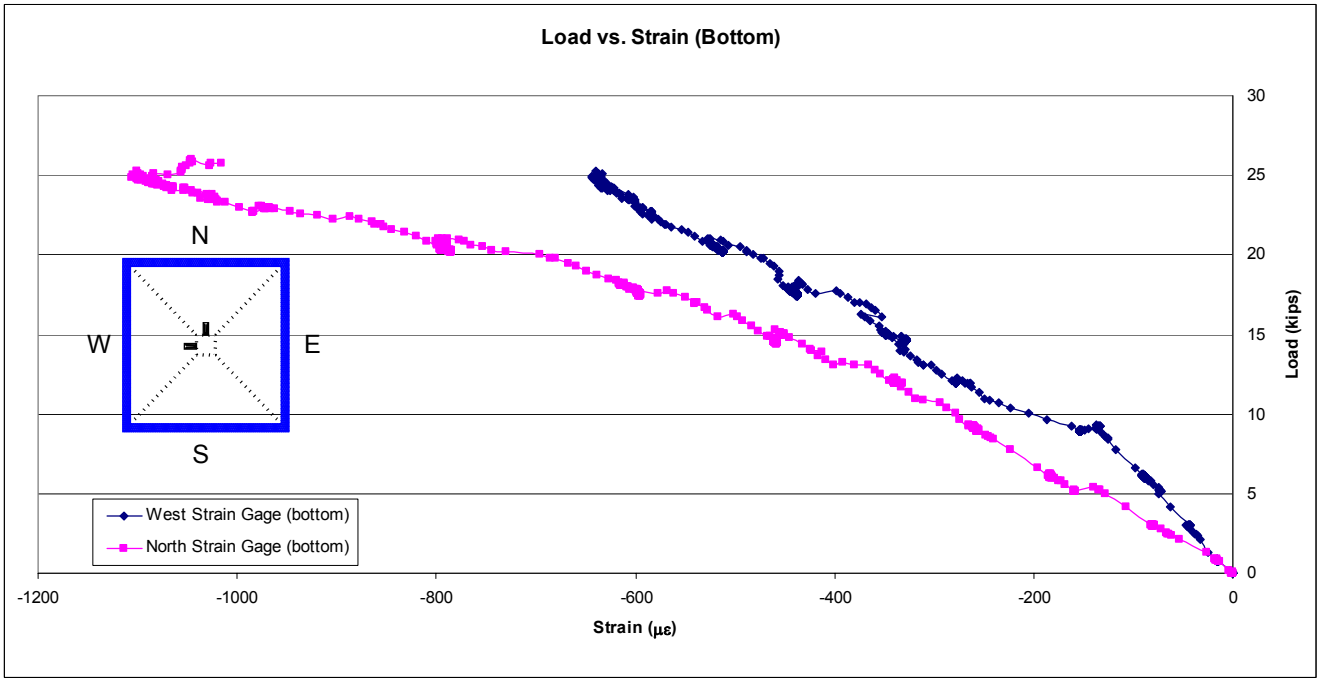

Figure 5-8 – Typical Load vs. Strain for Series 1 – Slab #2 (Loading Face)

Table 5-2 – Series 1 Comparison of Predicted vs. Actual

Test #	Punch Dimension (in.)	Actual Failure Load (kips)	Predicted Failure Load (kips)	% Difference	ACI Equation Failure Load (kips)	% Difference
1	1.5	***23.3***	35.0	50.4%	22.4	-3.7%
2	2	***27.2***	44.1	62.1%	28.2	3.8%
3	1	***22.6***	29.1	28.9%	18.6	-17.5%

5.3.2 Series 2 Results

The slabs tested in Series 2 were all approximately 2.5 in. thick specimens. This series was tested second in order to provide additional data prior to testing the more critical 3.0 in. slab specimens. The results from Series 2 are shown in Table 5-3. A total of four slabs were tested in Series 2, but the final slab was not tested immediately after the third slab due to a fabrication error with the restraint block-out locations, which required modifications to the testing frame.

Table 5-3 – Series 2 Test Results

			Predicted			***Actual***		
Test #	Plate Thickness (in.)	Punch Plate Size (in.)	Punching Failure Load (kips)	Flexural Failure Load (kips)	Failure Mechanism	Failure Mechanism	Failure Load (kips)	Average Maximum Deflection$_{(midspan)}$ (in.)
1	2.61	2	53.1	55.8	Punching	**Punching**	**33.0**	**0.57**
2	2.58	3	63.2	55.9	Flexure	**Flexure**	**35.9**	***2.11***
3	2.54	1.5	45.2	52.0	Punching	**Punching**	**30.5**	***1.26***
4	2.76	2.5	64.0	63.1	Flexure	**Flexure**	**34.2**	***1.87***

As a whole, the results observed from Series 2 were comparable to those from Series 1. While all of the specimens tested in Series 1 failed in punching shear, the specimens tested in Series 2 experienced both flexural and punching shear failures. The punching shear and flexural failures were similar in nature to the descriptions earlier in the chapter.

Similar to the specimens from Series 1, the punching shear failure is best illustrated through the load-deflection curve in Fig. 5-9. The load-deflection curve (Fig. 5-10) for a flexural failure illustrates the ability of the Ductal® slabs to continue to support a reduced load while continuing to deform beyond the peak load. The strain response amongst the two failure mechanisms was observed to be similar in nature and dependent on the location of the strain gauge placement relative to the crack formation pattern. Representative load-strain responses for Series 2 are illustrated in Figs. 5-11, 5-12, and 5-13 for the diagonal, orthogonal, and loading face locations, respectively.

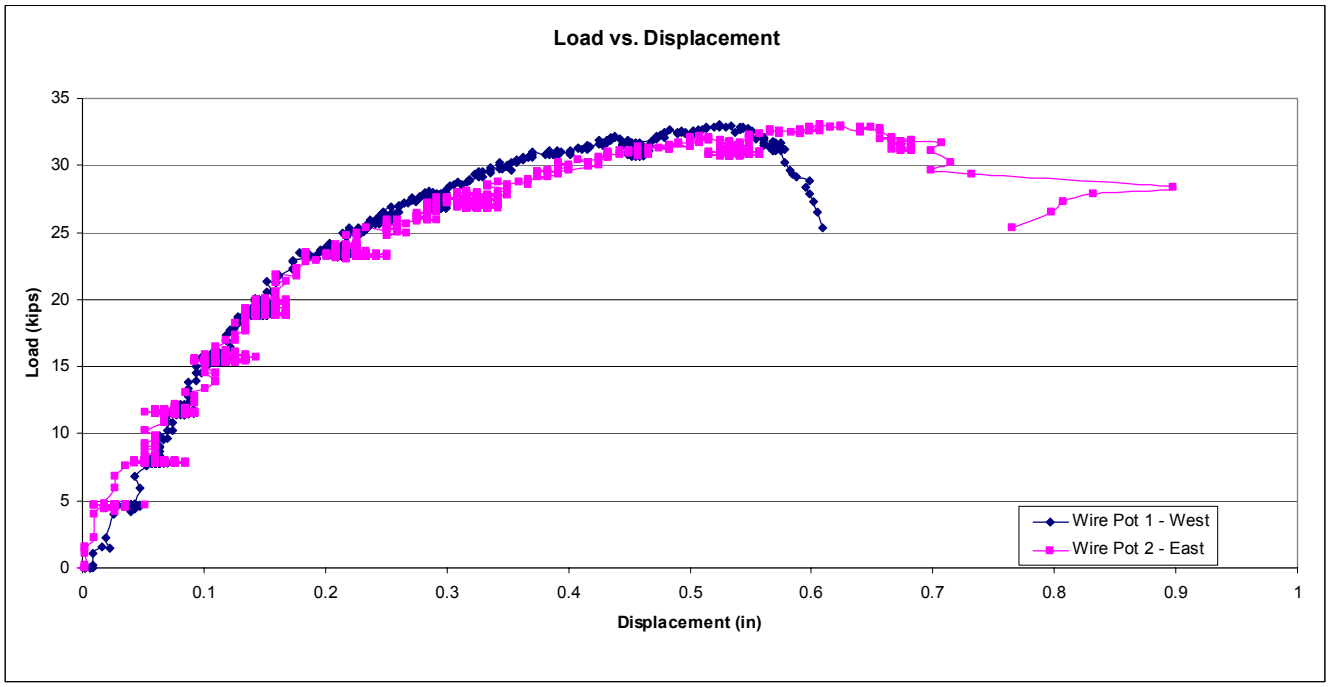

Figure 5-9 – Typical Load vs. Displacement Curve for Series 2 – Slab #1 (Punching Shear Failure)

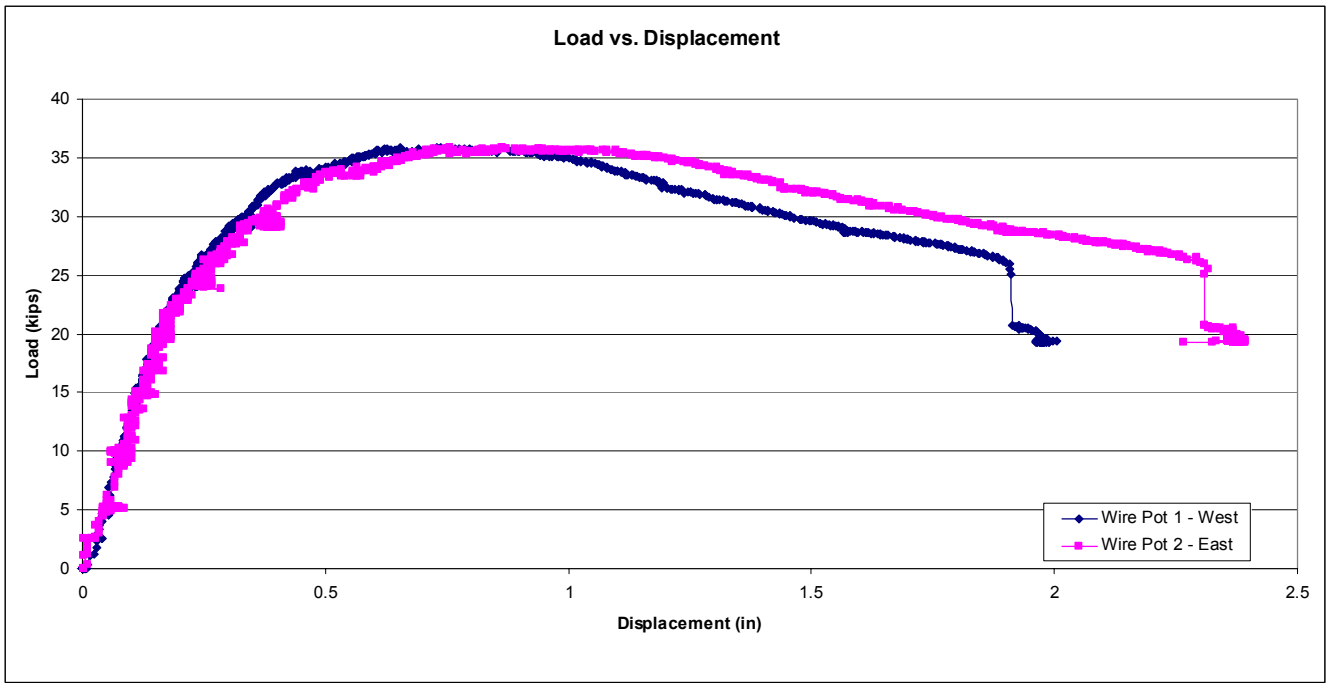

Figure 5-10– Typical Load vs. Displacement Curve for Series 2 – Slab #2 (Flexural Failure)

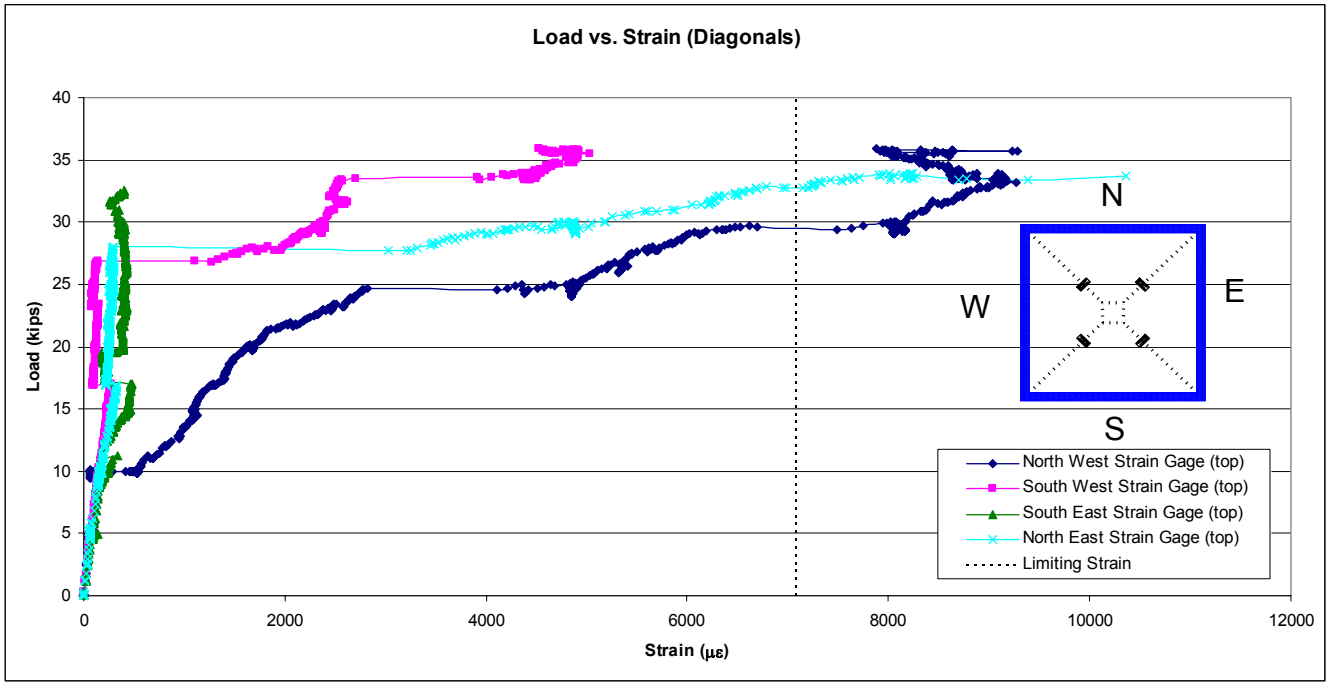

Figure 5-11 – Typical Load vs. Strain (Diagonal) for Series 2 – Slab #2 (Tensile Face)

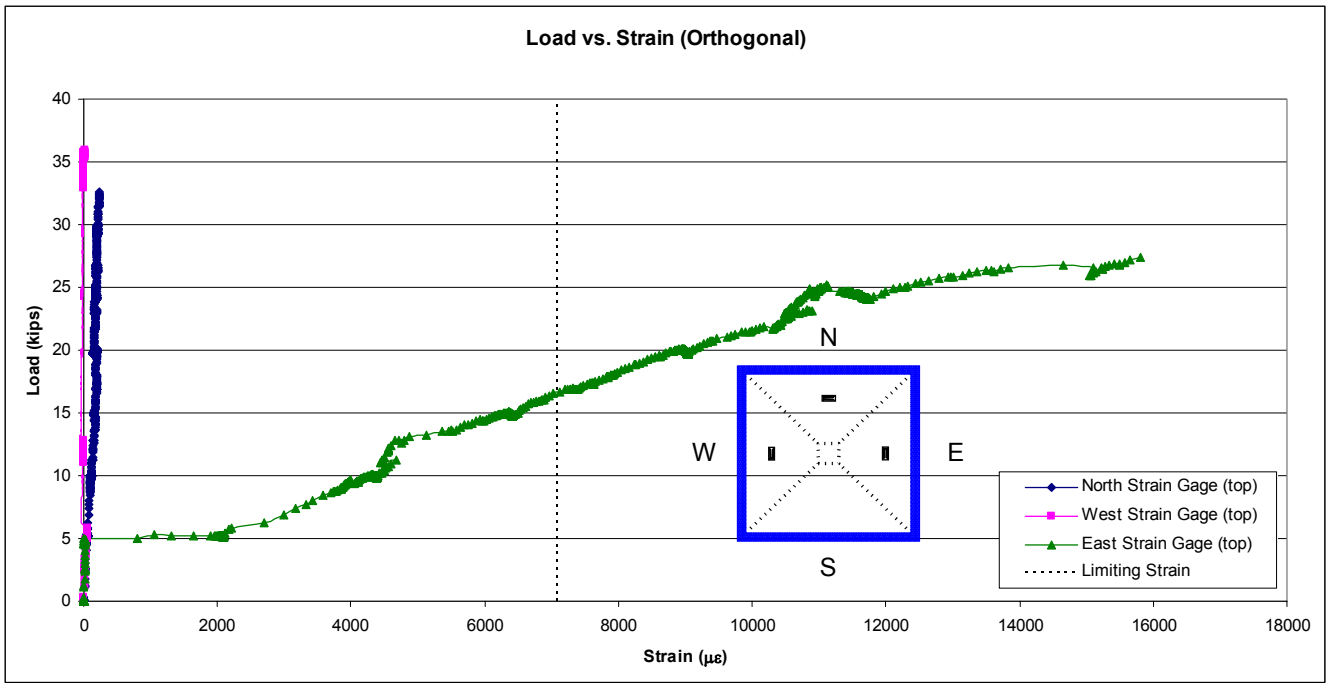

Figure 5-12 – Typical Load vs. Strain (Orthogonal) for Series 2 – Slab #2 (Tensile Face)

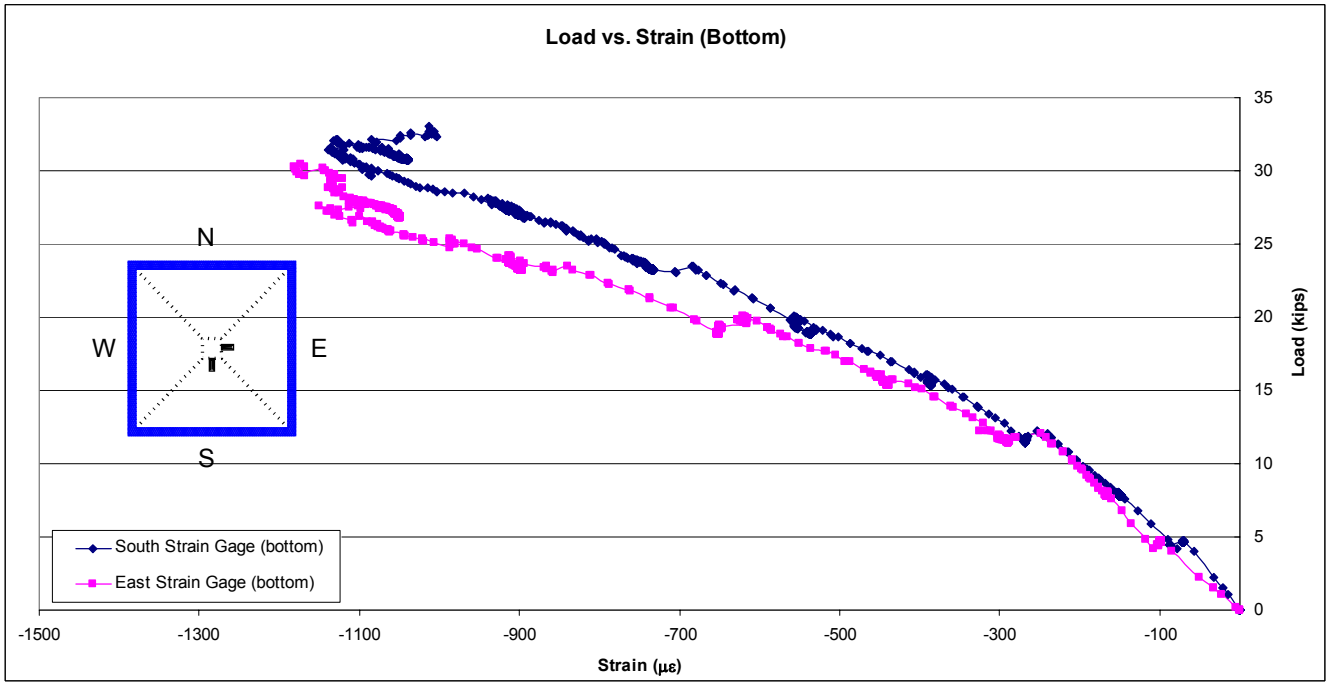

Figure 5-13 – Typical Load vs. Strain (Loading Face) for Series 2 – Slab #1

As was the case with the slabs from Series 1, the slabs tested in Series 2 experienced an increase in failure load as the punch plate dimensions increased, but failed to accurately match the predicted response (Table 5-4). In both the flexural and punching shear failure,

the predicted failure loads were higher than the actual failure loads. This trend is understandable for the flexural failures because the prediction is based on yield line analysis which provides an upper bound estimate on the failure load; the interpretation of this difference can likely be attributed to a failure mode different from the predicted mode (~87% maximum). The comparison to the prediction for the punching shear capacity further illustrates that the prediction model overestimates the capacity of Ductal® in punching shear (~61% maximum). Similar to the results from Series 1, the ACI 318-02 equation (Building Code Requirements 2002) underestimates the punching shear capacity, but to a lesser degree in Series 2 (~5% maximum). The trend from Series 2 illustrates that the ACI 318-02 equation (Building Code Requirements 2002) is more accurate in predicting the punching shear capacity of 2.5 in. slabs than the prediction equation from the preliminary analysis. Unfortunately, this hypothesis carries little validity because there were only a limited number of tests for comparison in Series 2 and it is not valid for Series 1.

Table 5-4 – Series 2 Comparison of Predicted vs. Actual

Test #	Punch Dimension (in.)	Actual Failure Load (kips)	Predicted Failure Load (kips)	% Difference	ACI Equation Failure Load (kips)	% Difference
1	2	***33.0***	53.1	60.8%	34.0	2.9%
2	3	***35.9***	55.9	55.6%	*	-
3	1.5	***30.5***	45.2	47.8%	28.9	-5.3%
4	2.5	***34.2***	63.1	84.5%	*	-

** No ACI Equation for predicting flexural failure load*

5.3.3 Series 3 Results

The slabs tested in Series 3 were all approximately 3.0 in. thick specimens. This series was tested last in order to gain a good understanding of the expected response from the Series 1 and 2 specimens. During the testing of the slabs from Series 1 and 2, all of the slabs failed in the predicted mechanism except one slab from Series 1, but all failed at a load significantly lower than predicted. The results from the previous tests allowed for a

better estimate of the failure load to be predicted. This prediction had no theoretical basis, but aided gauging the anticipated failure load during testing. In Series 3 a total of five slabs were tested; the fifth slab tested was originally cast as a 2.0 in. slab, but was poured in excess and was measured to be approximately 3.0 in. over the unsupported region. This slab specimen provided an additional data point between the punching shear and flexural failure boundary. The results from Series 3 are shown in Table 5-5.

Table 5-5 – Series 3 Test Results

			Predicted			***Actual***		
Test #	Plate Thickness (in.)	Punch Plate Size (in.)	Punching Failure Load (kips)	Flexural Failure Load (kips)	Failure Mechanism	Failure Mechanism	Failure Load (kips)	Average Maximum Deflection$_{(midspan)}$ (in.)
1	3.10	2.5	76.5	78.8	Punching	**Flexural**	**39.0**	**1.51**
2	2.83	1.5	54.0	64.2	Punching	**Punching**	**35.2**	***0.60***
3	3.03	1	53.9	72.3	Punching	**Punching**	**40.1**	***1.08***
4	2.85	2	60.9	66.0	Punching	**Flexural**	**38.4**	***1.66***
5	3.27	1.75	72.3	85.4	Punching	**Flexural**	**39.4**	***1.80***

Similar to the results from the other series, a small plate was required to produce a punching shear failure. Additionally, the prediction equations were not as accurate in predicting the failure mechanism as in previous tests. While this is still conservative, the prediction equation cannot be assumed valid for predicting the failure load or mode.

Similar to the specimens from Series 1 and 2, the punching shear and flexural failures are best illustrated through load-deflection curves (Figs. 5-14 and 5-15). The punching shear failures in Series 3 differed from those in Series 1 and 2 in that the specimens were able to sustain a reduced load while continuing to deform, similar to a flexural failure. For the specimens of Series 3, the failure mechanisms were titled punching shear failures based on the abrupt conical failure during testing, even though the load deflection curve does not illustrate this with a rapid drop in load. The load-strain responses for both the

flexural and punching shear failures were similar for both failure types and of similar form to the responses observed in Series 1 and 2. Representative load-strain responses for Series 3 are illustrated in Figs. 5-16, 5-17, and 5-18 for the diagonals, orthogonal, and loading face locations, respectively.

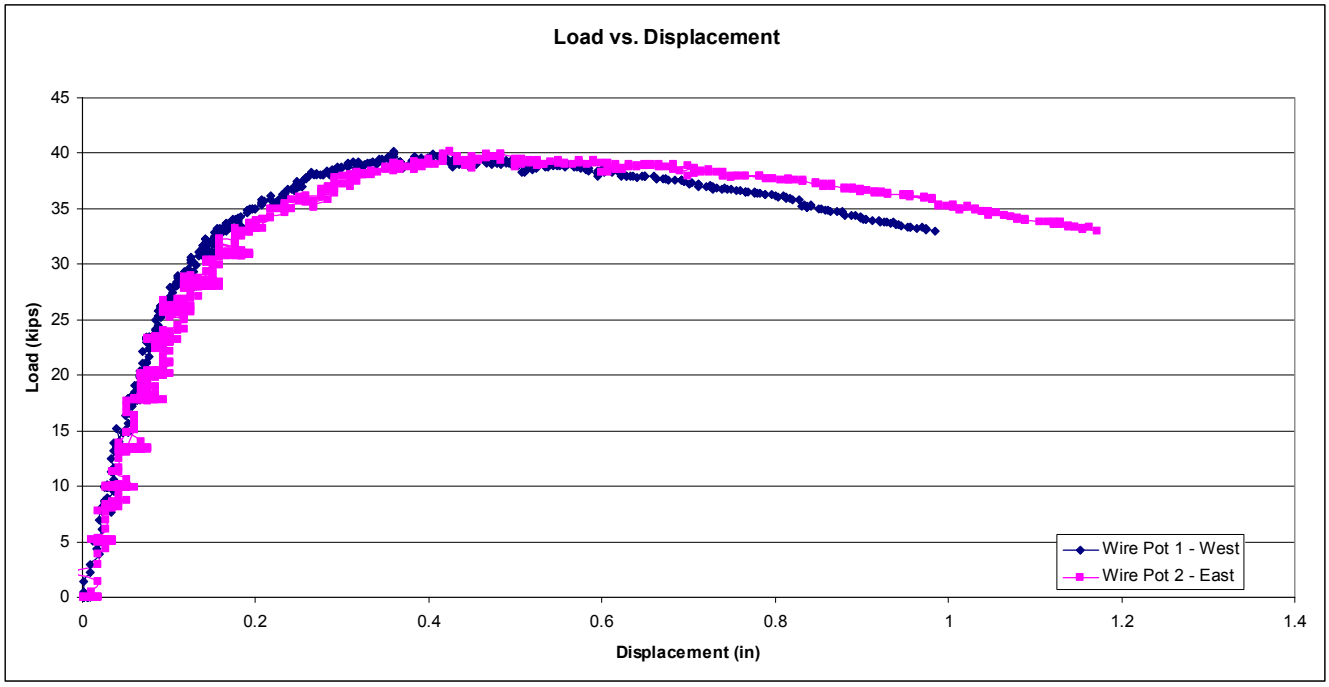

Figure 5-14 – Typical Load vs. Displacement Curve for Series 3 – Slab #3 (Punching Shear Failure)

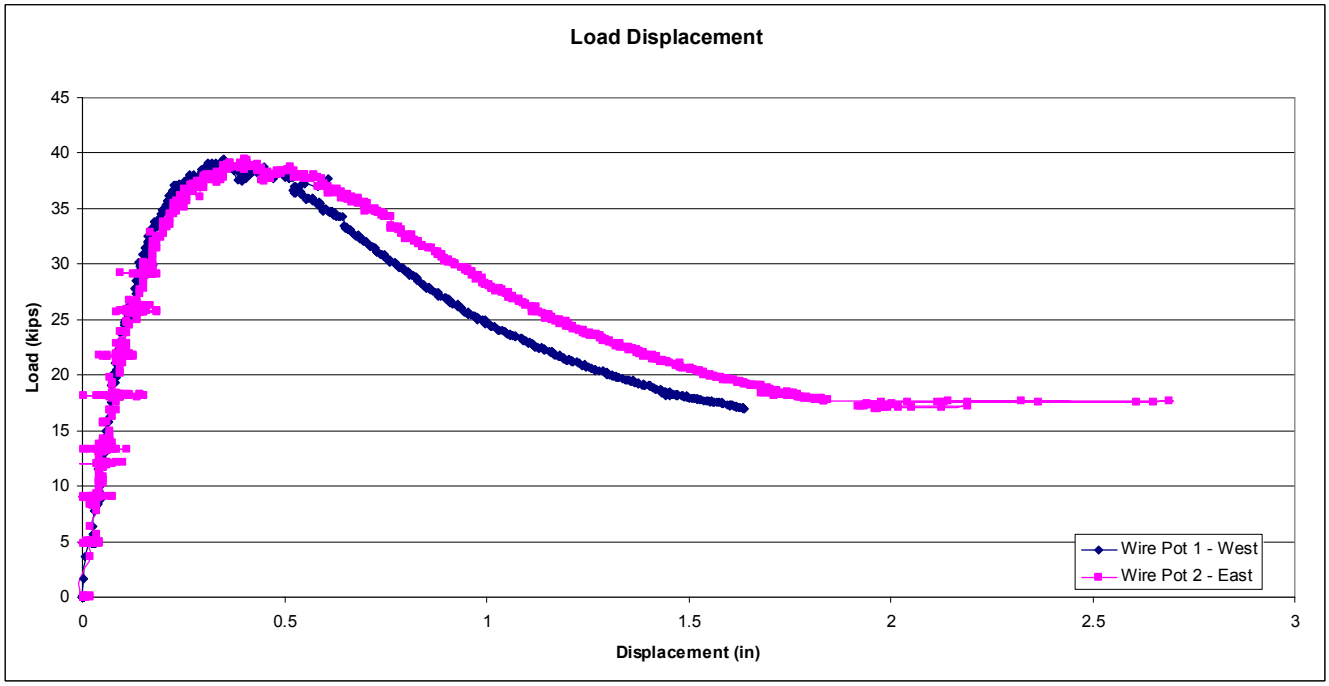

Figure 5-15– Typical Load vs. Displacement Curve for Series 3 – Slab #5 (Flexural Failure)

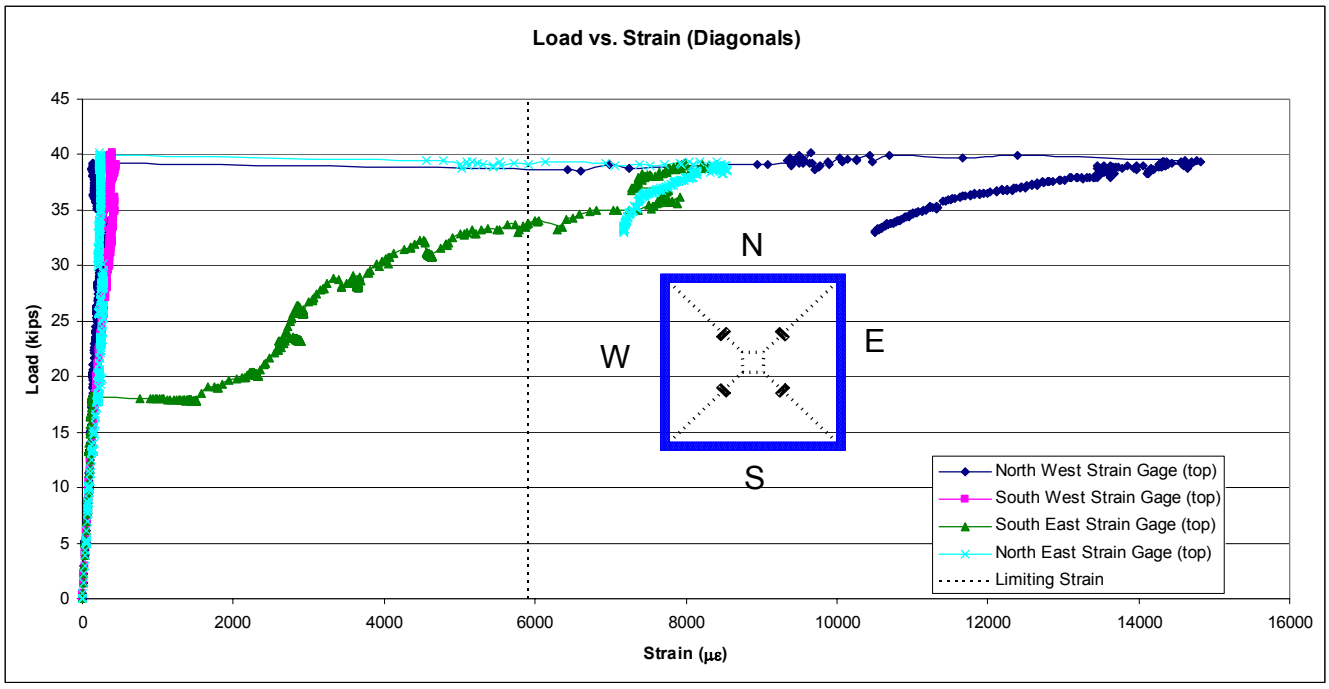

Figure 5-16 – Typical Load vs. Strain (Diagonal) for Series 3 – Slab #3

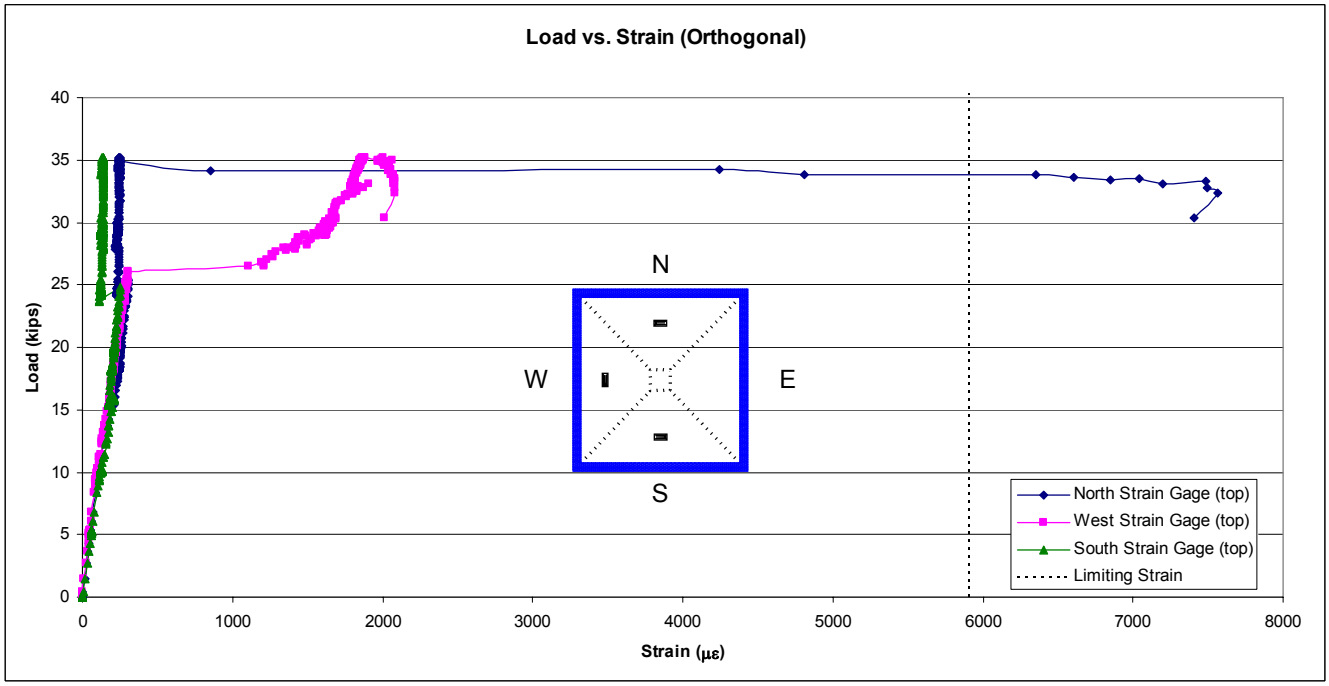

Figure 5-17 – Typical Load vs. Strain (Orthogonal) for Series 3 - Slab #2

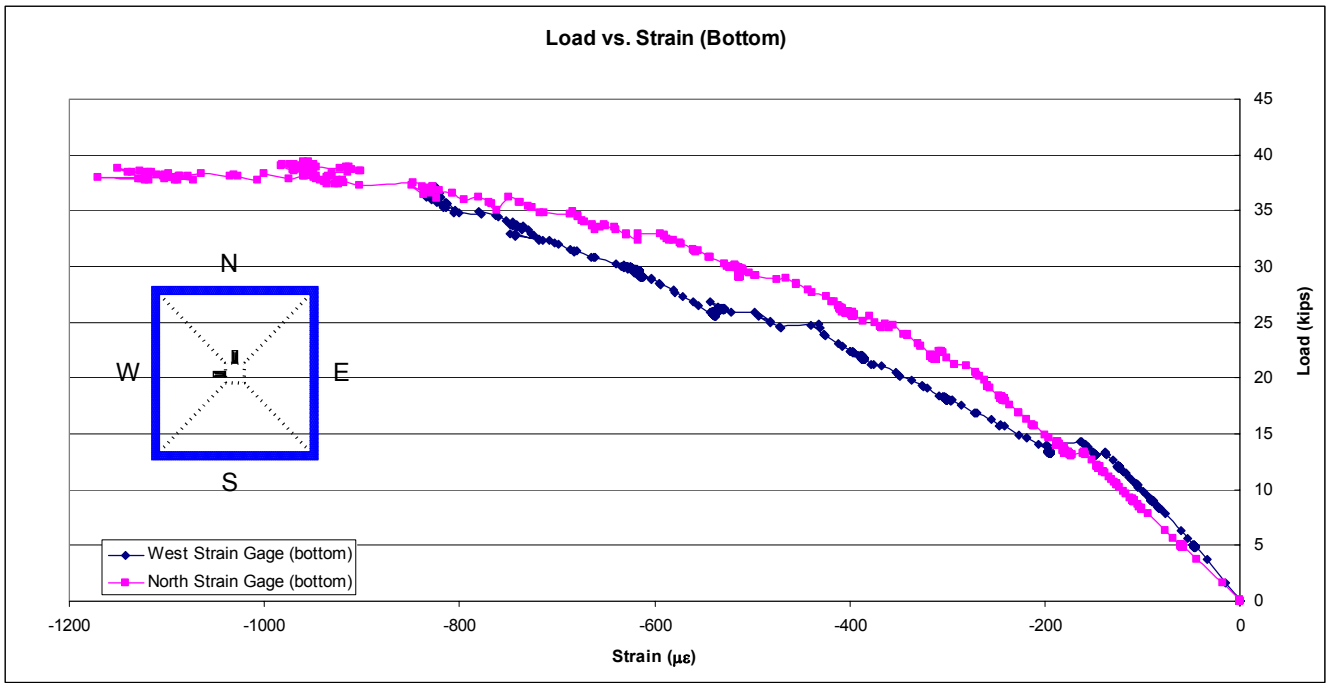

Figure 5-18 – Typical Load vs. Strain (Loading Face) for Series 3 - Slab #5

Similar to results from Series 1 and 2, the slabs tested in Series 3 experienced an increase in failure load as the punch plate dimensions increased, but failed to accurately match the predicted response (Table 5-6). For both failure modes, the predicted failure loads were higher than the actual failure loads. Additionally, the predicted failure mechanism was not always in agreement with the actual failure mechanism. The overestimation of the flexural failure loads can again be attributed to the upper bound estimate from the yield line analysis, but this does not aid in the interpretation of the inaccuracies in the punching shear prediction. Similar to the results from Series 1 and 2 the prediction equation consistently overestimates the punching shear capacity (~ 53% maximum). A comparison of the results to the ACI 318-02 equation (Building Code Requirements 2002) produces results that are more accurate (~ 14% maximum), but overestimates for one case and underestimates for the other. Based on the results of Series 3, neither the equation developed in the preliminary analysis nor the current ACI 318-02 equation (Building Code Requirements 2002) provide a good prediction for the punching shear capacity of UHPC, and additional analysis is required.

Table 5-6 – Series 3 Comparison of Predicted vs. Actual

Test #	Punch Dimension (in.)	Actual Failure Load (kips)	Predicted Failure Load (kips)	% Difference	ACI Equation Failure Load (kips)	% Difference
1	2.5	**39.0**	78.8	*	**	**
2	1.5	**35.2**	54.0	53.4%	34.6	-1.8%
3	1	**40.1**	53.9	34.2%	34.5	-14.1%
4	2	**38.4**	66.0	*	**	**
5	1.75	**39.4**	85.4	*	**	**

** Original prediction assumed to be punching shear, but failure was flexure (incorrect comparison)*

*** No ACI Equation for predicting flexural failure load*

The results from all tests are included in Appendix B.

5.4 Comparison of Results to Other Models

In this section a series of models and equations will be presented and compared to the results obtained during testing. Some of the equations presented will be from the work of other researchers' studies of punching shear, others will be models from derived from the ACI 318-02 code (Building Code Requirements 2002), and the last will be equations modeled to fit the results using curve fitting software. The models are first presented in this section, then compared to results in section 5.4.5.

5.4.1 Narayanan and Darwish Equation

Narayanan and Darwish (1987) studied the effect of steel fiber reinforcement on the punching shear capacity of micro-concrete slabs by testing 12 simply supported slabs to failure. The parameters considered in the study were volume fraction of fibers, amount of tensile reinforcement, and concrete strength. The results indicated that an increase in fiber content improved the shear strength and modified the position of the critical perimeter. The authors proposed that the design of concrete slabs for shear can be similar to that for beams and suggested the following equation for the prediction of punching shear

$$\nu_u = \xi_s \cdot (A' f_{spf} + B'' \rho + \nu_b) \ \textit{(MPa)} \qquad \textit{Equation 5-1}$$

where:

ζ_s = empirical depth factor

A' = non dimensional constant = 0.24

f_{spf} = split cylinder strength of fiber reinforced concrete (MPa)

B" = dimensional constant = 16

ρ = area percent of tensile steel reinforcement (%)

ν_b = vertical fiber pull-out stress along inclined crack (MPa)

The equation proposed by Narayanan and Darwish (1987) was further expanded by Tan and Paramasivam (1994) as

$$\nu_u = \frac{P_u}{\zeta_s \cdot u_b \cdot d} = 0.24 fsp + 16\rho + 0.41\tau_u \rho_f d_f \frac{L}{D} \ \textit{(MPa)} \qquad \textit{Equation 5-2}$$

where:

u_b = critical perimeter = $(1 - 0.55 \cdot \rho_f \cdot d_f \cdot \frac{L}{D}) \cdot (4 \cdot r + 3 \cdot \pi \cdot h)$

h = slab thickness (mm)

r = width of loading platen (mm)

d = average effective depth to tension reinforcement (mm)

ζ_s = empirical depth factor = $(1.6 - 0.002 \cdot h)$

f_{spf} = split cylinder strength of fiber reinforced concrete (MPa)

ρ = area percent of tensile steel reinforcement (%)

τ_u = average fiber matrix interfacial bond stress = 4.15 MPa

ρ_f = volume fraction of steel fibers (%)

d_f = factor for fiber type = 0.5 (round), 0.75 (crimped), 1.0 (duoform-steel fibers)

L = length of fibers (mm)

D = diameter of fibers (mm)

In the form proposed by Tan and Paramasivam (1994), the contribution by the concrete (term 1), the tensile reinforcement (term 2), and the steel fibers (term 3) can be distinguished. In order to use this equation, the term that represents the tensile steel

contribution was excluded because no tensile reinforcement was used in the Ductal® slabs tested. The final equation form is

$$v_u = \frac{P_u}{\zeta_s \cdot u_b \cdot d} = 0.24 fsp + 0.41 \tau_u \rho_f d_f \frac{L}{D} \ (MPa) \qquad \text{Equation 5-3}$$

: .

5.4.2 Shaaban and Gesund Equation

Shaaban and Gesund (1994) studied the effects of steel fibers on the punching shear strength of reinforced concrete slabs (flat plates), specifically whether the addition of steel fibers significantly enhanced the punching shear capacity. Thirteen slabs with varying fiber contents were tested to failure and produced results that demonstrated the enhancement in punching shear capacity achieved with the addition of fibers. The authors proposed an equation of the same form as the ACI 318-02 code (Building Code Requirements 2002) equation for punching shear, but modified it to account for the fiber contribution. The equation proposed is

$$V_c = \left[\left(0.3 \cdot W_f + 6.8\right) \cdot \frac{\sqrt{f'_c}}{1000} \right] \cdot b_o \cdot d \ \ (kips) \qquad \text{Equation 5-4}$$

where:

W_f = percent of fibers by weight of concrete (%)

f'_c = concrete compressive strength (psi)

b_o = critical perimeter as defined by ACI (in.)

d = average effective depth to tension reinforcement (in.)

The advantage of this equation is that it maintains the general form of the ACI 318-02 code equations for punching shear (Building Code Requirements 2002), but for the testing performed in this research effort there was no variation in the percent of fibers by weight of concrete (W_f) because a standard 2% by volume was used in all slabs.

5.4.3 Modified ACI Equation for Concrete Breakout Strength

Observations were made of the failure surface of the test specimens and it was concluded that the conical failure was similar in appearance to the breakout cone for concrete as shown in ACI 318-02 (Building Code Requirements 2002) for a surface with an embedded bolt in tension (Fig. 5-19). The only significant difference observed was that in the ACI 318-02 code the size of the bolt head has no impact on the failure cone. The equation proposed by the ACI 318-02 code (Building Code Requirements 2002) is

$$N_b = k \cdot \frac{\sqrt{f'_c}}{1000} \cdot h_{ef}^{1.5} \text{ (kips)} \qquad \textit{Equation 5-5}$$

where: N_b = basic concrete breakout strength in tension for single anchor in cracked concrete (lb)

k = coefficient for basic concrete breakout strength in tension = 24 (cast-in anchors), 17 (post-installed anchors)

f'_c = concrete compressive strength (psi)

h_{ef} = effective anchor embedment depth

Modifications were made to this equation to predict the strength of Ductal® subjected to a tensile load; this tensile load was assumed to be equivalent to the applied punching load. Similar to the bolt head applying load to the slab through the head (Fig. 5-19), the load applied to the Ductal® slabs results from the loading plate (Fig. 5-20).

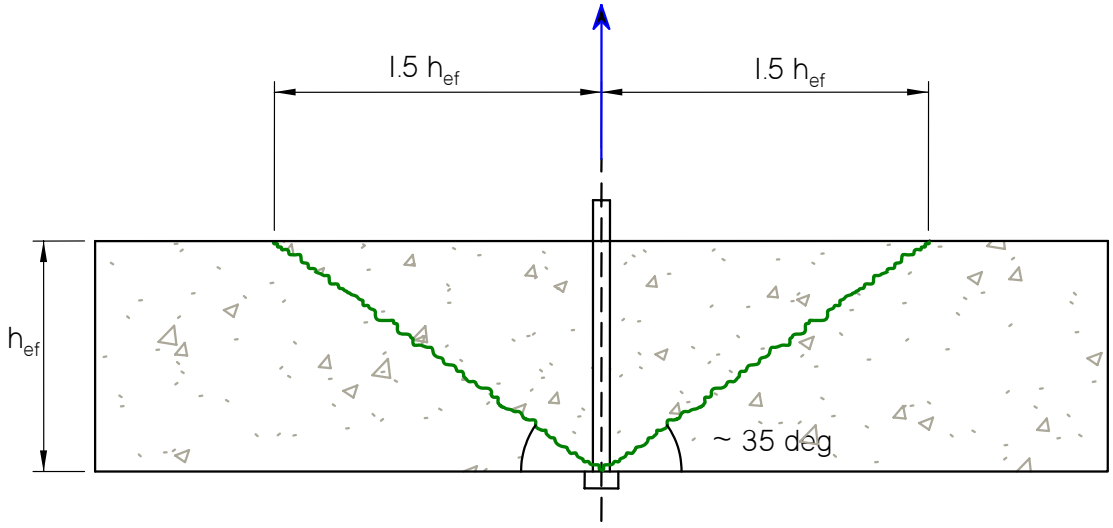

Figure 5-19 – Concrete Breakout Failure Surface

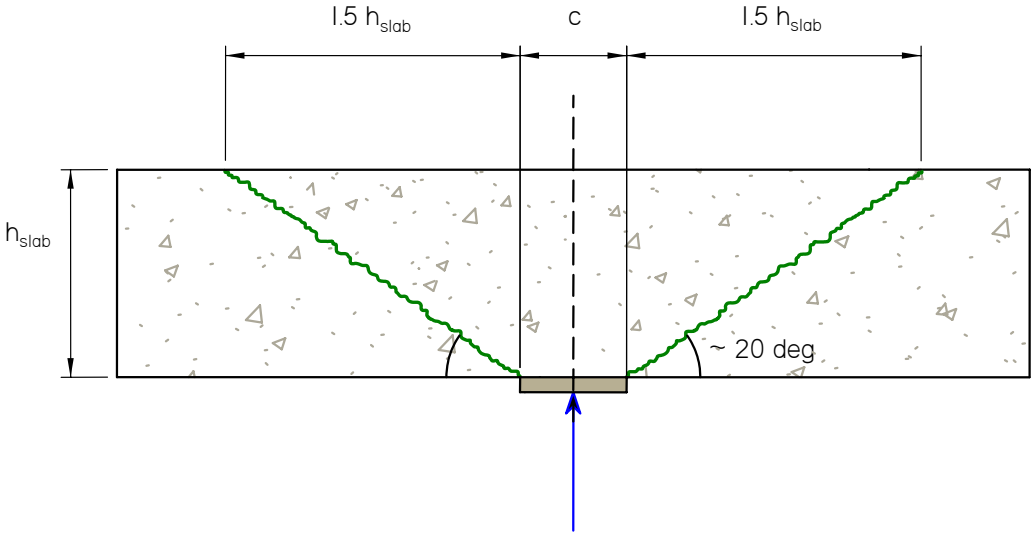

Figure 5-20 – Ductal® Breakout (Punching Shear) Failure Surface

For concrete breakout strength, the ACI 318-02 code refers to the work of Fuchs *et al.* (1995) which states that the concrete conical failure depends on the tensile capacity of the concrete, considered to be proportional $\sqrt{f'_c}$. With the increased tensile capacity achieved with Ductal®, it would be expected that an increase in the concrete breakout

strength could be achieved. The proposed equation based on the work by Fuchs *et al.* (1995) is

$$V_c = N_b = k_1 \cdot f_t \cdot \frac{(3 \cdot h + c)^2 - c^2}{\sqrt{h}} \text{ (kips)} \qquad \textit{Equation 5-6}$$

where: f_t = split cylinder tensile strength (ksi)

k_1 = empirical constant derived using NLREG software = 0.38

h = slab thickness (in.)

c = loading plate dimension (in.)

The proposed equation reduces to the original ACI equation as ***c*** approaches zero, and the modified equation is in terms of h^2 as opposed to $h^{1.5}$ proposed in the ACI equation. The significant difference between the original ACI equation for concrete breakout strength and the modified equation is the consideration of the bolt head and loading plate area. The ACI equation does not consider the area of the bolt head in the conical failure surface, while the plate area is included and then removed in the modified equation; the difference is best illustrated in Figs. 5-19 and 5-20.

5.4.4 ACI Curve – Fit Equations

The use of empirical equations, historically, has served as the foundation for the ACI prediction of punching shear capacity; the equations were developed based on the test data with little emphasis placed on a model to characterize the true failure mechanism (ASCE-ACI Task Committee 1974). The use of these empirically developed equations has continued over the years with only minor changes, but the general form is still maintained. This illustrates that the use of empirical equations is not uncommon, but the trend in recent years has been to develop empirical equations that maintain the same general form of the ACI 318-02 design equations (Building Code Requirements 2002); this was the method used in the preliminary analysis.

Using a nonlinear regression and curve fitting software package (NLREG), numerous iterations were performed to fit an equation similar in form to the ACI design equations for punching shear to the test data for the UHPC slabs. The general form of the equation developed is

$$V_c = K \cdot (c + a \cdot h + M) \cdot 4 \cdot a \cdot h \quad \textit{(kips)} \qquad \textit{Equation 5-7}$$

where:

K = empirical constant representative of material tensile capacity = *0.25*

c = loading plate dimension (in.)

a = empirical factor relating slab thickness to equivalent effective depth = 5.29

h = slab thickness (in.)

M = empirical constant (assumed to represent the fiber contribution to the critical perimeter) = *7.81* (in.)

The appearance of the equation can be modified to a more familiar format by replacing the empirical constant representing the tensile capacity with $k\sqrt{f'_c}$, where k is an empirical constant relating tensile strength to compressive strength:

$$V_c = k_2 \cdot \frac{\sqrt{f'_c}}{1000} \cdot b_o \cdot d_{equiv} \quad \textit{(kips)} \qquad \textit{Equation 5-8}$$

where:

k_2= empirical constant relating tensile strength to compressive strength = *0.14*

f'_c = concrete compressive strength (psi)

b_o = critical perimeter = $4 \cdot (c + a \cdot h + M)$

c = loading plate dimension (in.)

h = slab thickness (in.)

d_{equiv} = equivalent effective depth = $a \cdot h$ (in.)

a = empirical factor relating slab thickness to equivalent effective depth = 5.29

M = empirical constant (assumed to represent the fiber contribution to the critical perimeter) = *7.81* (in.)

Replacing the representative tensile capacity with the actual tensile capacity determined from split cylinder testing, the equation can be expressed in the following form:

$$V_c = k_3 \cdot f_t \cdot b_o \cdot d_{equiv} \text{ (kips)} \qquad \textit{Equation 5-9}$$

where:

k_3 = empirical constant relating tensile strength to compressive strength = *0.02*

f_t = split cylinder tensile strength (ksi)

b_o = critical perimeter = $4 \cdot (c + a \cdot h + M)$ (in.)

h = slab thickness (in.)

d_{equiv} = equivalent effective depth = $a \cdot h$ (in.)

a = empirical factor relative slab thickness to equivalent effective depth = *5.29*

M = empirical constant (assumed to represent the fiber contribution to the critical perimeter) = *7.81 (in.)*

These empirical equations were derived with the ACI design equations for punching shear capacity as the foundation, but were modified to provide a reasonable fit to the test results. These modifications left some uncertainty in the interpretation of the model; the empirical factor M cannot be physically defined in the term for the critical perimeter. It has been assumed that this empirical factor, M, represents the contribution of the fibers to an increase in the critical perimeter, but based on the limited test data this cannot be verified.

5.4.5 Comparison of Results to Model Equations

In general the various models previously discussed performed well when compared to the results of the tests. None of the established models was capable of fitting the data with good precision, but most provided a reasonable representation of the response.

5.4.5.1 Preliminary Analysis

The equation derived during the preliminary analysis overestimated the punching shear capacity of the test slabs. As illustrated in Fig. 5-21, the predictions are consistently unconservative with all of the predicted failure loads exceeding the measured capacities. The results from this equation could be factored down to better match the measured data, but this would be interpreted as the tensile capacity not being fully utilized. Additionally, the predicted capacity was calculated based on the tensile capacity ($f_t + k_m = 0.1 + 1.0$ ksi) proposed by Park *et al.* (2003) which was lower than the tensile capacity measured from the split cylinder tests conducted by Graybeal (2004) which ranged from 1.5 – 1.7 ksi. Using the actual tensile capacity would make the prediction more unconservative. The lack of full tensile capacity could be attributed to the fiber orientation that did not appear to be random as predicted. Random orientation was not likely achieved due to the thinness of the slab which did not allow for orientation of the fibers perpendicular to the formed surface. This differs significantly for the tensile test specimens where the fibers are randomly oriented.

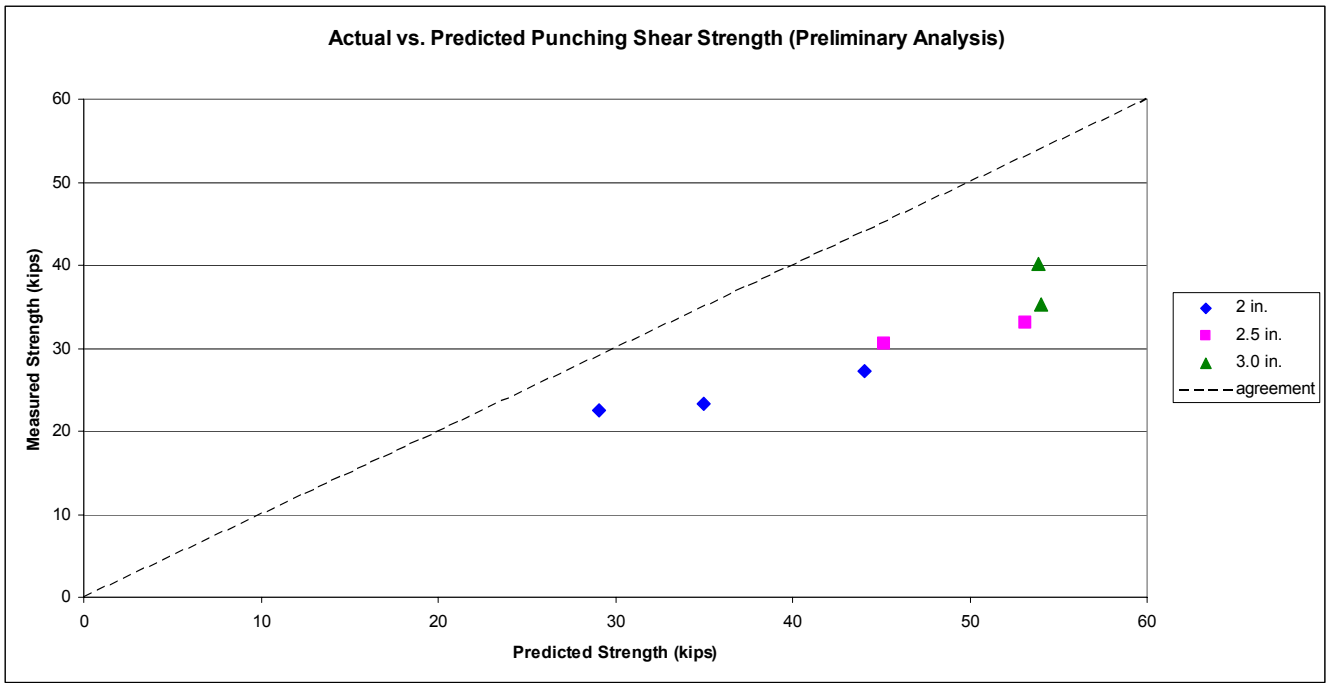

Figure 5-21 – Preliminary Analysis Prediction for Punching Shear Capacity vs. Actual

5.4.5.2 ACI Punching Shear Design Equation

The ACI 318-02 punching shear equation (Building Code Requirements 2002) provided a more reasonable prediction of the punching shear capacity than the preliminary analysis equation as illustrated in Fig. 5-22. The only observed flaw with this method is that it considers the effective depth of the tensile reinforcement which was replaced with the slab thickness because no tensile reinforcement was used in the test slabs. The ACI equation assumes a constant relationship between the tensile strength (f_t) and compressive strength (f'_c), which appears to be reasonable so long as the fiber volume does not change. The term $4 \cdot \sqrt{f'_c}$ is roughly half of the tensile capacity ($f_t = 7.5 \cdot \sqrt{f'_c}$) suggested for design by ACI, which is about what was observed in the punching shear failures.

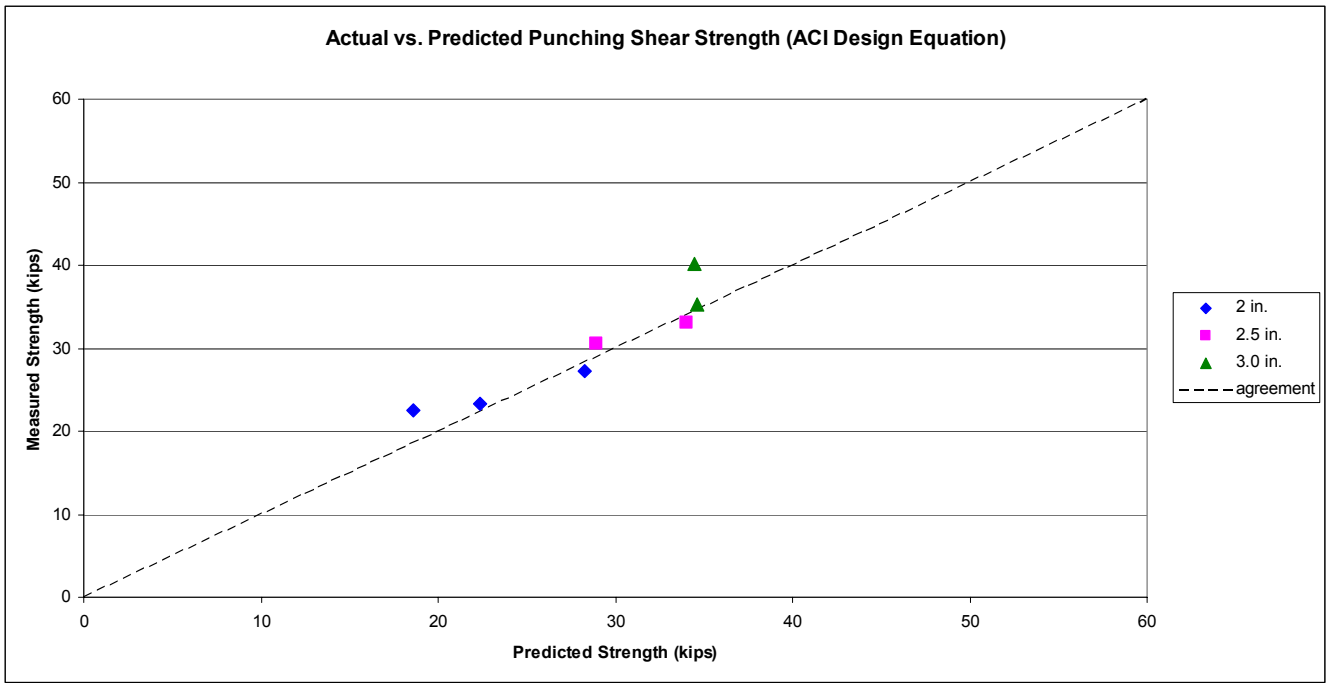

Figure 5-22 – ACI 318-02 Prediction for Punching Shear Capacity vs. Actual

5.4.5.3 Narayanan and Darwish Equation

The equation proposed by Narayanan and Darwish (1987) provided an excellent prediction for some of the test slabs, specifically the 2.0 in. slabs, but was unconservative for the other thicknesses. The comparison is illustrated in Fig. 5-23.

5.4.5.4 Shaaban and Gesund Equation

The equation proposed by Shaaban and Gesund (1994) provided similar results to the ACI equation, as expected, because this is the equation from which the form was derived (Fig. 5-24). The difficulty that arises from using this equation is that the basis for its derivation is that the fiber content is a factor in the punching shear capacity prediction and for this experiment the fiber content was not varied.

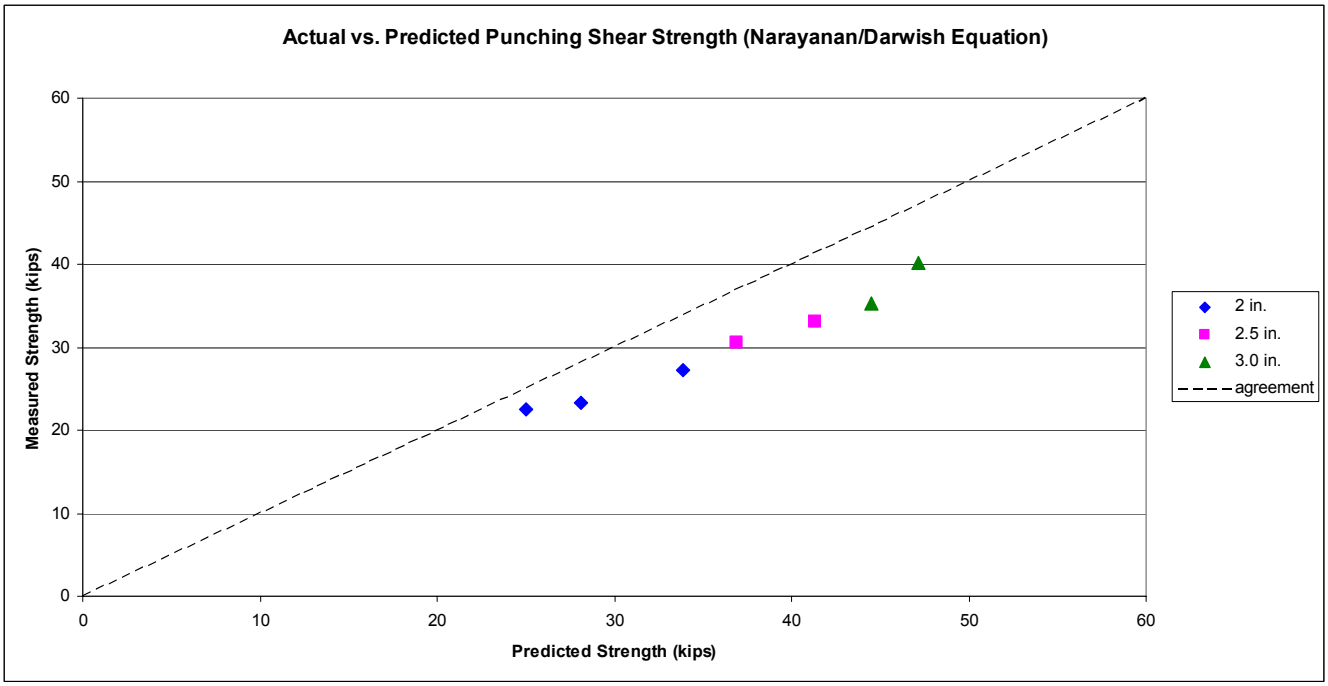

Figure 5-23– Narayanan & Darwish Prediction for Punching Shear Capacity vs. Actual

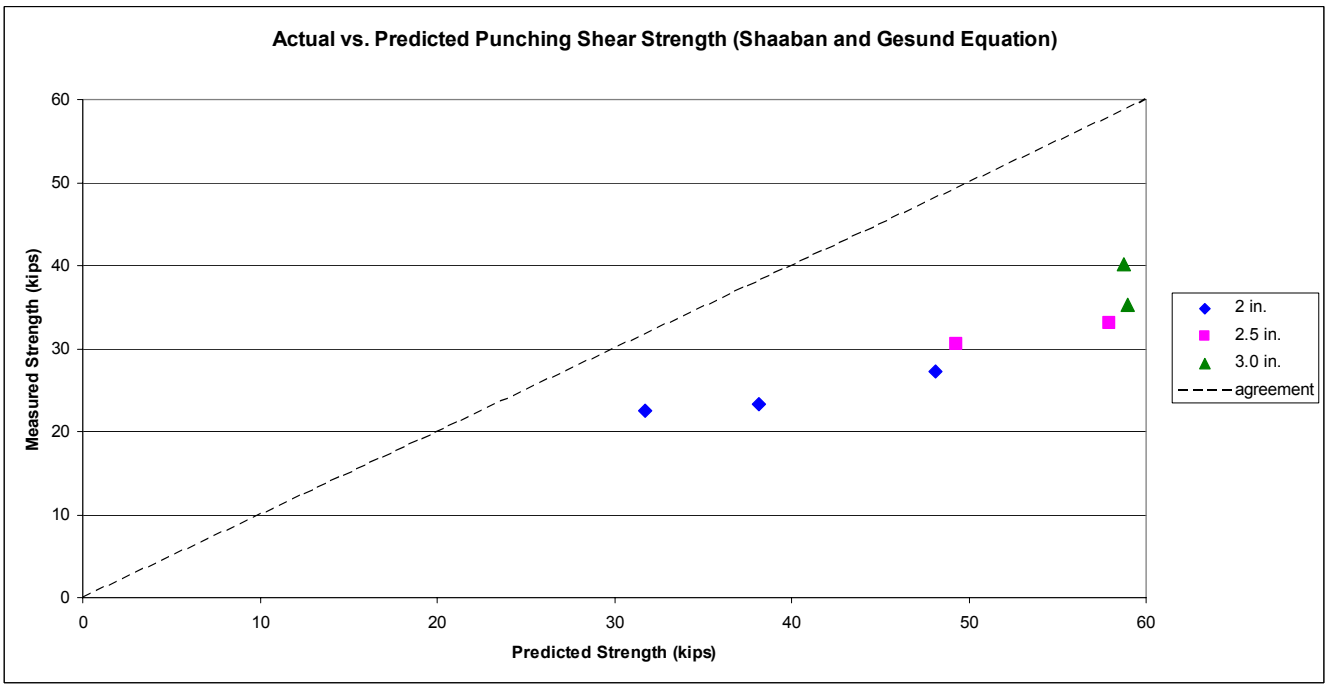

Figure 5-24– Shaaban & Gesund Prediction for Punching Shear Capacity vs. Actual

5.4.5.5 ACI Concrete Breakout Equation

The equation for concrete breakout strength from the current ACI 318-02 Code (Building Code Requirements 2002) is not considered to be an equation for the punching shear capacity of concrete, but results in a similar failure mechanism. As illustrated in Fig. 5-25, this equation provides a good prediction of the punching shear capacity, but this is as a result of the empirical constant being derived from curve-fitting using NLREG. A similar trend could be observed in the original ACI prediction equation if a curve fit were used to improve the fit of the curve to the data (i.e., modifications made to the constant relating compressive strength to tensile strength).

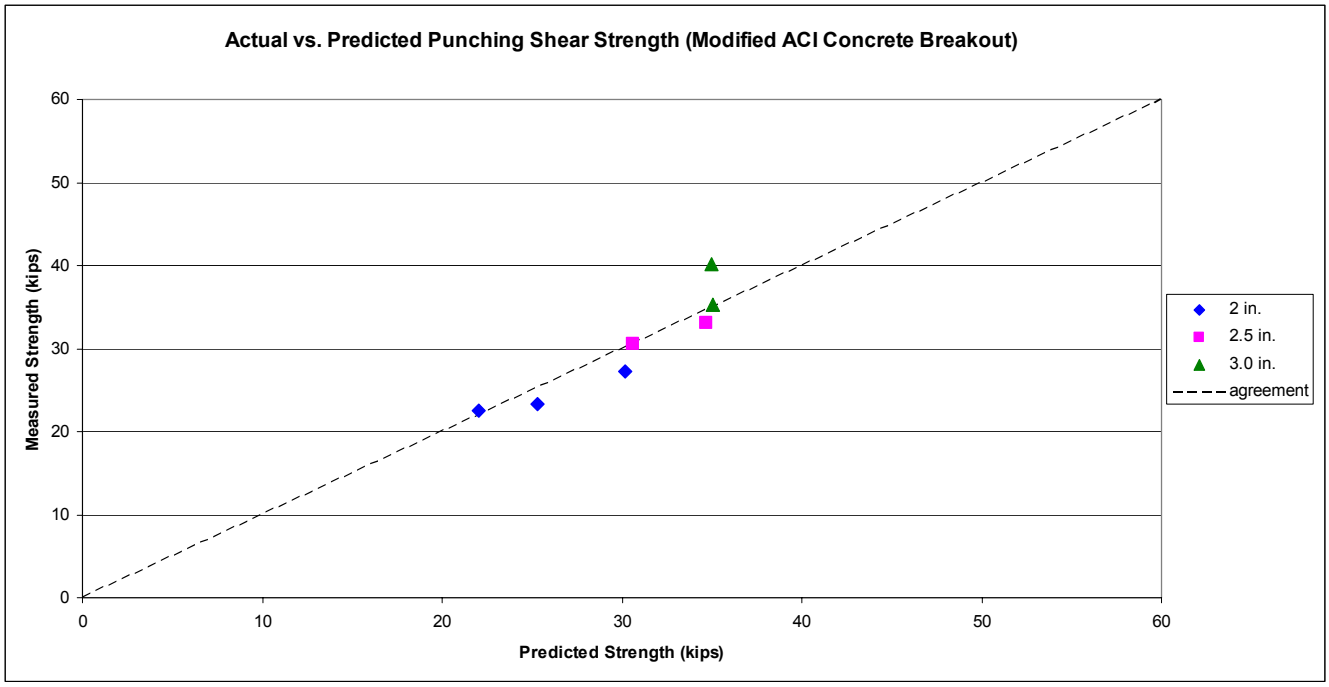

Figure 5-25 – Modified ACI Prediction for Concrete Breakout (Punching) Capacity vs. Actual

5.4.5.6 ACI Curve-Fit Equation

As would be expected with any curve fit equation, the predictions match the actual results very well. The curve fit was based on the general form of the ACI 318-02 punching shear equation (Building Code Requirements 2002) with terms for the tensile capacity, critical perimeter, and effective depth adjusted to provide the best fit to the data set. The difficulty that arises from using this equation is the limited number of data points to

develop the curve and the unknown interpretation of the empirical constant ***M*** (Eqs. 5-7, 5-8 and 5-9). The performance of the equation is illustrated in Fig. 5-26.

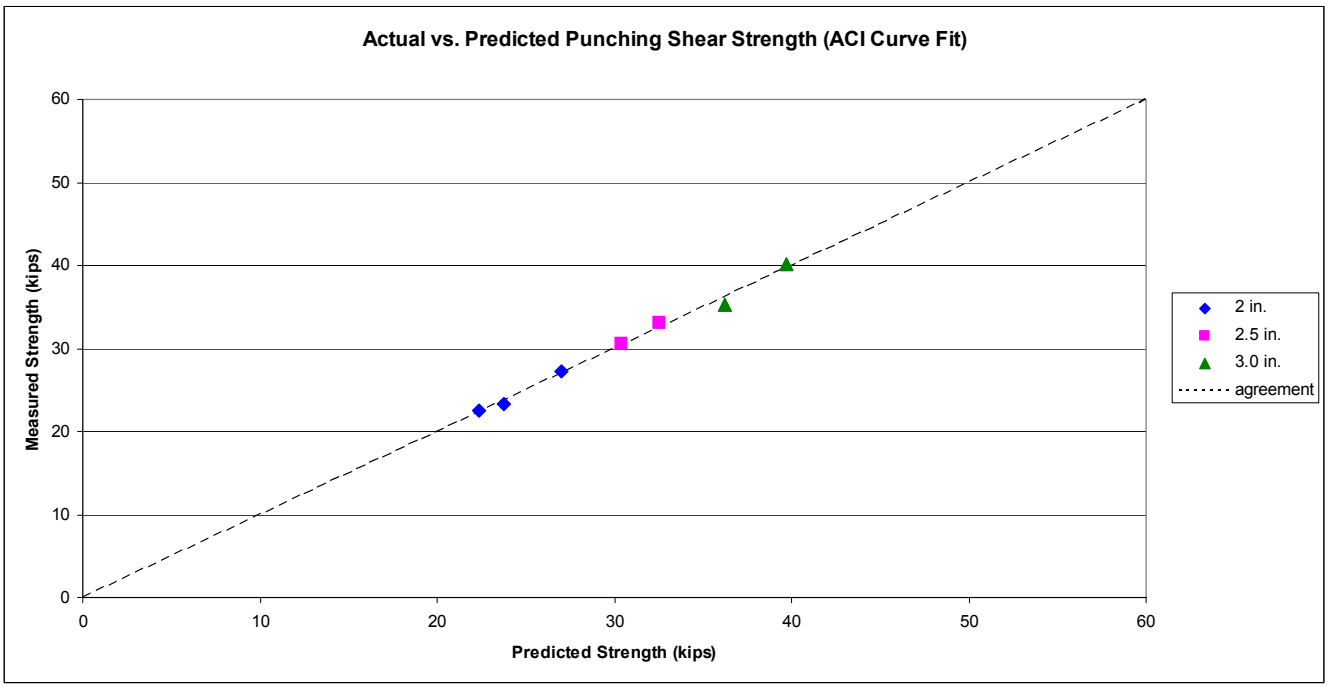

Figure 5-26 – Curve-Fit Prediction for Punching Shear Capacity vs. Actual

5.4.5.7 Comparison of Prediction Equations

Each of the presented equations provides some advantages and disadvantages, but all tend to provide a reasonably consistent measure of the response. Each of the equations could be modified for design purposes to provide a conservative prediction of the punching shear capacity, but a more useful method would be to compare the predictions statistically to determine the best predictor. Although the data set is limited, there is not a significant amount of scatter in the data and the use of statistical comparisons should provide a good measure of the relative effectiveness of each equation. A statistical analysis of the measured response to the predicted response is provided in Table 5-7.

Table 5-7 – Statistical Results

			Prediction Equation					
			Preliminary Analysis	ACI	Narayanan/ Darwish	Shaaban/ Gesund	Modified Concrete Breakout	Curve Fit
Slab Thickness	Punch Size	Actual	V_{act}/V_{cal}	V_{act}/V_{cal}	V_{act}/V_{cal}	V_{act}/V_{cal}	V_{act}/V_{cal}	V_{act}/V_{cal}
in.	in.	kips						
2.12	1	22.6	0.78	1.21	1.11	0.71	1.03	1.01
2.17	1.5	23.3	0.66	1.04	1.21	0.61	0.92	0.98
2.32	2	27.2	0.62	0.96	1.24	0.57	0.90	1.01
2.54	1.5	30.5	0.68	1.06	1.21	0.62	1.00	1.00
2.61	2	33.0	0.62	0.97	1.25	0.57	0.95	1.01
3.03	1	40.1	0.75	1.16	1.18	0.68	1.15	1.01
2.83	1.5	35.2	0.65	1.02	1.26	0.60	1.01	0.97
Mean			***0.68***	***1.06***	***1.21***	***0.62***	***0.99***	***1.00***
Standard Deviation			***0.06***	***0.09***	***0.05***	***0.06***	***0.08***	***0.02***
Standard Error			***0.02***	***0.04***	***0.02***	***0.02***	***0.03***	***0.01***
Confidence Level (95.0%)			***0.06***	***0.09***	***0.05***	***0.05***	***0.08***	***0.02***
Coefficient of Variation			***8.9%***	***8.9%***	***4.5%***	***8.9%***	***8.3%***	***1.7%***

Definitions of statistical terms

Term	**Symbol**	**Definition**	**Equation**
Mean (x)	$\bar{x}$	Average of the results	$\frac{\sum x}{n}$
Standard Deviation (s)	σ	The root mean square of the set of deviations between each point of the set and the mean of the set	$\sqrt{\frac{\sum d^2}{(n-1)}}$
Standard error (of the mean)	σ_n	Measure of how far a variable is likely to be from the expected value	$\frac{\sigma}{\sqrt{n}}$
Confidence Level	-	An interval constructed from data in such a way that the probability that the interval contains the true value is 95%	From student t-table
Coefficient of Variation	CV	A statistical representation of the precision of the tests	$\frac{\sigma}{\bar{x}}$

All of the models considered provided reasonable estimates for the prediction of punching shear capacity of UHPC. The results illustrate that the range of the mean of the measured load to the predicted load ranges from 0.62 – 1.21 while the coefficient of variation only ranges from 1.7 – 8.9%, excellent agreement for a cementitious material. This agreement is likely achieved due to the uniformity of UHPC resulting from the controlled batching environment and the lack of coarse aggregate which could reduce the uniformity. The results of the analysis indicate that the best model for predicting the punching shear capacity is the *Curve Fit Equation* as should be expected, but as previously stated there is some uncertainty in the defined critical perimeter and this equation will not be recommended for design. The next model considered was the *Modified Concrete Breakout Equation* due to its low mean and coefficient of variation. The mean of the ratio of measured to the predicted strength (V_{act}/V_{cal}) is not the lowest (a low ratio close to 1.0 would indicate good agreement), but it is in line with the other models, and the coefficient of variation is significantly lower than that in the remaining models. A low mean indicates that the model overall reasonably predicts the punching shear strength of UHPC slabs, and the coefficient of variation indicates that there is little fluctuation in the ratio of the measured to the actual strength when compared to the mean. For these reasons, the *Modified Concrete Breakout Equation* will be considered the best model for the prediction of the punching shear capacity of UHPC slabs. The current *ACI 318-02 Code equation* (Building Code Requirements 2002) could also have been used, but the mean was similar and the coefficient of variation was higher, indicating more scatter around the mean.

5.5 Proposed Slab Thickness

The results of the optimized section modeling performed by Park *et al.* (2003) suggested that the minimum slab thickness to be used in bridge applications is 4.0 in. This prediction was based on the no cracking SLS criterion proposed by the French Association of Civil Engineering (AFGC) which did not allow for any cracking to occur. Based on the results of the testing conducted, this criterion is unrealistic because the load that caused cracking was significantly lower than the final failure load. The load to cause first cracking ranged from ~ 5 – 15 kips (presented in Appendix B) depending on the

specimen thickness and the loading plate area, but these cracking loads were significantly lower than the peak loads that ranged from 22.6 – 40.1 kips. This illustrates that the SLS criterion may be excessively conservative for UHPC slab systems. Based on the results obtained from the testing, a very small loading plate is required in order to produce a punching shear failure, even on the 2.0 in. slab specimens, but in the absence of flexural failures in Series 1 it is recommended that the slab thickness be limited to 2.5 in. For a 2.5 in. slab system, a plate size of 2.0 in. x 2.0 in. was required to cause a punching shear failure, which occurred at a peak load of 30.1 kips. This failure load is greater than the load that would be experienced with the AASHTO HL-93 truck (16 kips per tire) or the Tandem truck (12.5 kips per tire) over a much smaller loading area, 2 in. x 2 in. vs. 8 in. x 20 in. (Cousins 2003). Modification of the proposed concrete breakout equation to account for variations in the loading plate aspect ratio results in the following equation

$$V_c = k_1 \cdot f_t \cdot \frac{(3 \cdot h + a) \cdot (3 \cdot h + b) - a \cdot b}{\sqrt{h}}$$

where a and b are the dimensions of the loading plate

Using this modified equation with the standard 8 in. x 20 in. loading area results in punching shear capacities of 88, 102, and 117 kips for 2.0, 2.5 and 3.0 in. thick slabs, respectively. These capacities far exceed the anticipated loads from the standard AASHTO trucks even with the addition of impact factors and factors of safety.

5.6 Flexural Failures

While the purpose of this research was to develop a prediction measure of the punching shear capacity of UHPC, a number of flexural failures occurred during the testing that cannot be ignored. The sole method used to predict the flexural capacity of UHPC was yield line analysis, which serves as an upper bound analysis technique. The results of the Ductal® flexural failures did not exhibit good agreement with the predictions from yield line analysis as illustrated in Fig. 5-27. Yield line analysis overestimated the flexural

capacity of Ductal® slabs in all tests and all cases by a significant amount (~ 117% maximum) as shown in Table 5-8. The disagreement with the prediction model can likely be attributed to two main factors; the difference in flexural capacity between orthogonal directions from fibers not being randomly oriented, and the material not being ideal for use of yield line analysis based on moment-curvature relationships observed. Further analysis of the flexural capacity is required to gain a better understanding of the behavior, but that is beyond the scope of this research effort.

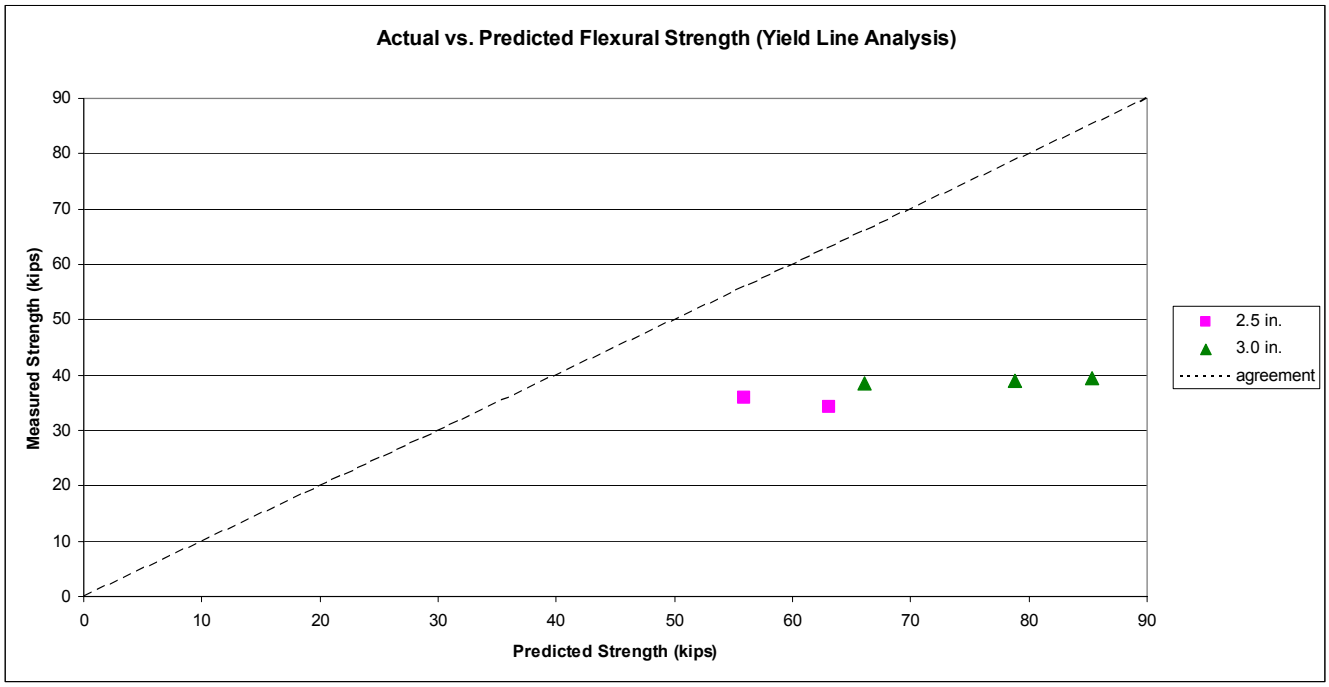

Figure 5-27 – Yield Line Analysis Prediction for Flexural Capacity vs. Actual

Table 5-8 – Summary of Flexural Failure Results

Slab Thickness (in)	Punch Dimension (in.)	Actual Failure Load (kips)	Predicted Failure Load (kips)	% Difference
2.58	3	**35.9**	55.9	55.6%
2.76	2.5	**34.2**	63.1	84.5%
3.10	2.5	**39.0**	78.8	102.1%
2.85	2	**38.4**	66.0	71.8%
3.27	1.75	**39.4**	85.4	116.7%

5.7 Summary of Results

The results obtained from the experimental testing illustrate some of the advantages of using UHPC as a replacement for other construction materials, such as increased strength, the ability to undergo significant deflections, the small punch size required to cause a flexural failure, and the ability to support a reduced load beyond the peak load in flexural failures and in some punching shear failures. These results were not in good agreement with the prediction models proposed in the preliminary analysis, but appear to achieve good agreement with other models, particularly the Modified Concrete Breakout Equation derived from the ACI 318-02 Code (Building Code Requirements 2002) equation for concrete breakout resulting from a bolt anchored in concrete. The limited number of data points makes the statistical analysis questionable, but the minimal variance leads to the assumption that the model is sufficiently accurate for design purposes. It should also be noted that the results do not take into consideration the effects of axial loads on the slab systems, which would be the case for a prestressed system as proposed by Park *et al.* (2003). The addition of prestressing in the slab system could result in an increase in the applied tensile load and produce a tensile failure prior to service loads being applied, but could significantly improve the punching shear capacity when service loads are applied. Further analysis would be required to verify the effects of prestressing, but it is beyond the scope of this research project.

Chapter 6 - Summary, Conclusions, Recommendations

6.1 Summary

UHPC is considered to be a new material for use in structural applications, and as a result very little research has been performed. The properties of UHPC make the material ideal for uses in applications that require high strength, ductility, and corrosion resistance, but the current cost limits the potential for use in many structural applications. With the significantly improved properties of UHPC, compared to reinforced concrete and in some cases steel, the ability to make smaller and thinner sections at lower cost is the most viable option for making the material more competitive.

From the work of Park *et al.* (2003) an optimized section was developed that minimized the material usage and resulted in a thin section for use as a bridge girder. The optimized section utilized a thin top flange which would serve as the riding surface for vehicular traffic, but utilized no shear reinforcement. Additionally, the optimized section, specifically the top flange section developed by Park *et al.* (2003), was not verified with experimental data and relied primarily on Finite Element Analysis to characterize the local effects. Due to the poor historical performance of cementitious materials in tension, the lack of tensile reinforcement in the slab/riding surface and unverified slab response served as the foundation for this research effort.

The objectives of the research effort were primarily to characterize the punching shear capacity of UHPC slabs and to determine the minimum slab thickness that could be used to prevent a punching shear failure. The lack of tensile reinforcement in the top flange of the optimized section allowed for the potential of a punching shear failure occurring from a tire patch load. Additionally, due to the high cost of the material, an attempt was made to minimize material usage in the testing. From these objectives, a preliminary analysis was performed to attempt to predict the failure response and mechanisms for UHPC slabs

utilizing yield line analysis for the flexural response and the ACI 318-02 design equations for punching shear modified to account for the tensile capacity of UHPC. With the objective of the research effort being the characterization of UHPC, the philosophy was to determine the boundary between flexural and punching shear failures. From this preliminary analysis, specimens were sized sufficiently small to minimize material usage, but large enough that a punching shear failure could be forced provided a sufficiently small loading plate was used. Based on the yield line analysis, this required the use of fully restrained supports in order to maximize the load to cause a flexural failure to allow for an increased likelihood that a punching shear failure would occur.

From the preliminary analysis, a total of twelve specimens were cast with thicknesses of 2.0 in., 2.5 in., and 3.0 in. with four slabs per thickness. The only other variable considered in the testing was the area of the square loading plate. One of the 2.0 in. specimens cast was poured in excess of the desired thickness and was tested as a 3.0 in. thick slab. All of the specimens were loaded to failure and measurements of the load, displacement, and strain were recorded for interpretation. The loaded specimens failed in either a flexural or punching shear failure, depending on the loading plate area and slab thickness. The failure loads were then compared to the predicted capacity of the preliminary analysis and it was determined that the prediction significantly overestimated the capacity. As a result, this prediction equation was deemed inadequate for predicting the failure load, and other models were evaluated for agreement. Due to the limited research conducted on UHPC, models that produced a similar failure mechanism were also considered. Based on the agreement with test data, a model was chosen to represent the best method for prediction of punching shear capacity of UHPC slabs.

6.2 Conclusions

The following conclusions are made based on the test results and analysis:

- The tensile capacity inherent to UHPC can significantly improve the punching shear capacity for a slab.
- A sufficiently small loading area is required to force a punching shear failure in a UHPC slab system. Based on this assessment, a 2.5 in. slab thickness should provide sufficient punching shear capacity for bridge applications. The actual slab thickness selected for design should also consider factors such as web spacing, flexural capacity, and deflection criteria.
- The modified ACI equation for concrete breakout strength provides the best measure of the punching shear capacity of UHPC slabs:

$$V_c = N_b = k_1 \cdot f_t \cdot \frac{(3 \cdot h + c)^2 - c^2}{\sqrt{h}}$$

with variables defined in section 5.4.3.

- The limiting strain criterion proposed in the MIT Report (Park *et al.* 2003) should be followed due to the lack of consistent data from the testing. The measured strains were highly dependent on the location of crack formation.
- Fibers tend to align in the direction of the flow of the material and also with the formwork; this may result in different flexural capacities in different directions.
- UHPC is more suited for precast operations due to the controlled environment and special formwork required.
- The brittle punching shear failure mechanism exhibits limited warning prior to failure, but is still significantly less abrupt than for a reinforced concrete punching shear failure.

6.3 Recommendations for Future Research

- Further verification of the proposed equation for the prediction of punching shear capacity of UHPC slabs should be performed. The specimen sample was limited and only a few parameters were varied; more data would aid in validating the model.
- Additional testing on UHPC slab specimens should be performed with variations in the following parameters:
    - Slab thickness
    - Slab aspect ratio
    - Compressive strength
    - Tensile strength
    - Fiber volume
    - Loading plate area
    - Loading plate aspect ratio
    - Restraint conditions
    - Loading rate effects
    - Dynamic effects
    - Contribution of tensile reinforcement
- Testing of full-scale slab specimens of the dimensions proposed for the top flange in the optimized section should be conducted. Three full scale specimens will be tested in the Virginia Tech Structures Laboratory in December 2004.

References

AFGC Scientific and Technical Documents (2002) – Ultra High Performance Fibre-Reinforced Concretes – Interim Recommendations (Documents scientifiques et techniques – Bétons fibrés à ultra-hautes performances – Recommandations provisoires), French Association of Civil Engineering (Association Française de Génie Civil).

ASCE-ACI Task Committee 426 (1973). "The Shear Strength of Reinforced Concrete Members", ASCE – Journal of the Structural Division, 99 (6), 1091-1187.

ASCE-ACI Task Committee 426 (1974). "The Shear Strength of Reinforced Concrete Members-Slabs", ASCE – Journal of the Structural Division, 100 (8), 1543-1591.

Building Code Requirements for Structural Concrete, ACI 318-02, and Commentary, ACI 318R-02 (2002), American Concrete Institute, Farmington Hills, MI.

Cousins, T.E. (2003), "Load", CEE 5484 – Advanced Bridge Design Course Presentation, Virginia Polytechnic Institute and State University.

Fuchs, W., Eligenhausen, R., Breen, J.E. (1995). "Concrete Capacity Design (CCD) Approach for Fastening to Concrete", ACI Structural Journal, 92 (1), 73-94.

Graybeal, B.A., Hartmann, J.L. (2003). "Strength and Durability of Ultra-High Performance Concrete", 2003 PCI National Bridge Conference.

Graybeal, B.A. (2004), e-mail communication, August, 2004.

Keenan, W.A. (1969). "Strength and Behavior of Restrained Reinforced Concrete Slabs Under Static and Dynamic Loadings", Technical Report R 621 – Naval Civil Engineering Laboratory, Port Huenueme, CA.

Latin Tech Inc., accessed October 10 (2004). "Position Transducers", Latin Tech Inc., Miami, FL. Internet Address: http://www.lt-automation.com/PositionTransducers.htm

Lafarge North America Inc., accessed September 7 (2004). "Ductal's Durability Properties", Lafarge North America Inc., Herndon, VA. Internet Address: http://www.imagineductal.com/imagineductal/home.asp

Narayanan, R., Darwish, I.Y.S. (1987). "Punching Shear Tests on Steel Fibre Reinforced Micro-concrete Slabs", Magazine of Concrete Research, 39 (138), 42-50.

Park, H., Ulm, F-J., Chuang, E. (2003). "Model-Based Optimization of Ultra High Performance Concrete Highway Bridge Girders", CEE Report R03-01 – Massachusetts Institute of Technology.

Park, R., Gamble, W.L. (2000). Reinforced Concrete Slabs – Second Edition, John Wiley & Sons, Inc., NY, 551-620.

Perry, V.H. (2003). "A Revolutionary New Material for New Solutions", Technical Forum Presentation, Lafarge North America.

Perry, V.H., Zakariasen, D. (2003). "Overview of UHPC Technology, Materials, Properties, Markets and Manufacturing", 2003 Concrete Bridge Conference, Orlando, FL.

Semioli, W.J. (2001). "The New Concrete Technology", Concrete International, 23 (11), 75-79.

Shaaban, A.M., Gesund, H. (1994). "Punching Shear Strength of Steel Fiber Reinforced Concrete Flat Plates", ACI Structural Journal, 91 (3), 406-414.

Tan, K.-W., Paramasivam, P. (1994). "Punching Shear Strength of Steel Fiber Reinforced Concrete Slabs", Journal of Civil Engineering Materials, 6 (2), 240-253.

TFRC – Turner Fairbanks Highway Research Center, accessed November 11 (2004). "High Performance Concrete Bridge Project Fact Sheets – Virginia Avenue Over the Clinch River, Richlands", McLean, VA. Internet Address: http://www.tfhrc.gov/structur/hpc/flyers.htm

Ulm, F-J., Chuang, E. (2003). "UHPC Design Issues", Technical Forum Presentation, Massachusetts Institute of Technology, Cambridge, MA.

Yankelevsky, D.Z., Leibowitz, O. (1999). “Punching Shear in Concrete Slabs”, International Journal of Mechanical Sciences, 41 (1), 1-15.

APPENDIX A

Edge Condition: Four Edges Pinned

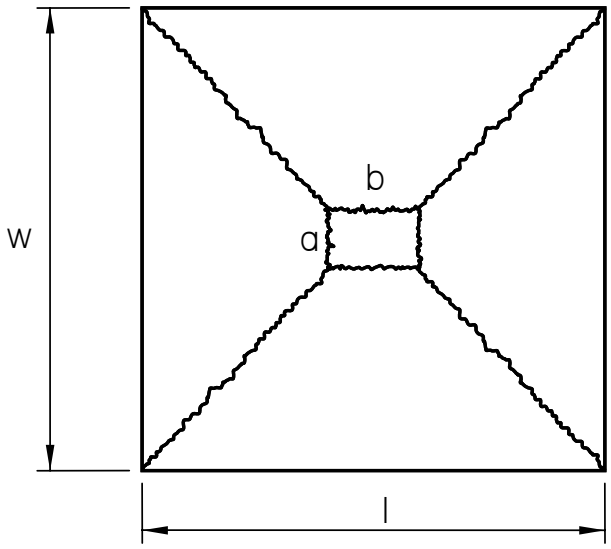

Figure A-1 - Case A

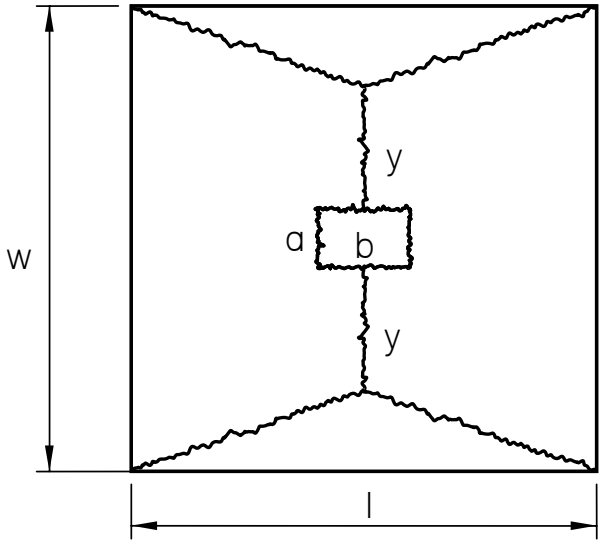

Figure A-2 - Case B

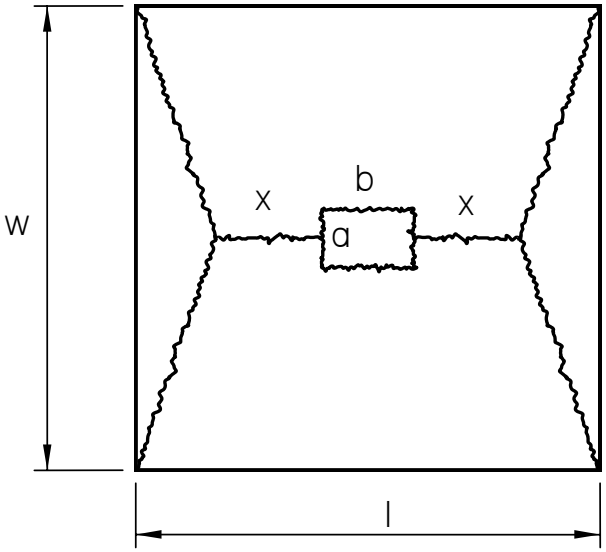

Figure A-3 - Case C

Edge Condition: Three Edges Pinned / One Edge Fixed

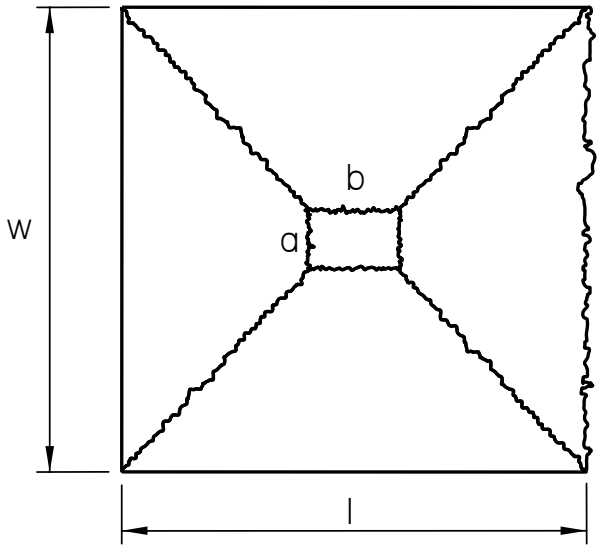

Figure A-4 - Case D

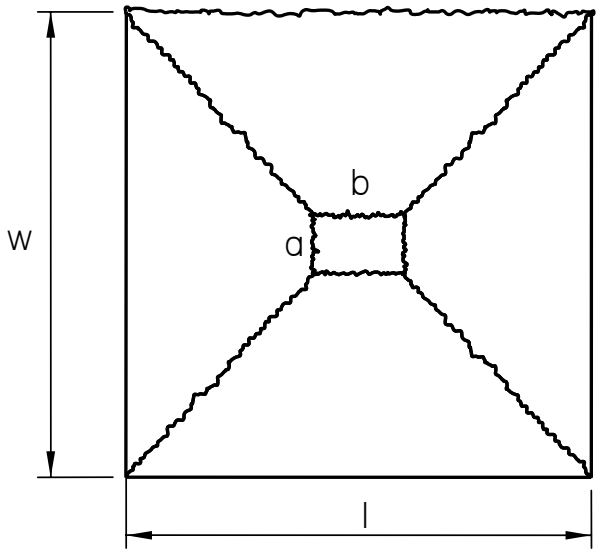

Figure A-5 - Case E

Edge Condition: Two Edges Pinned / Two Edges Fixed

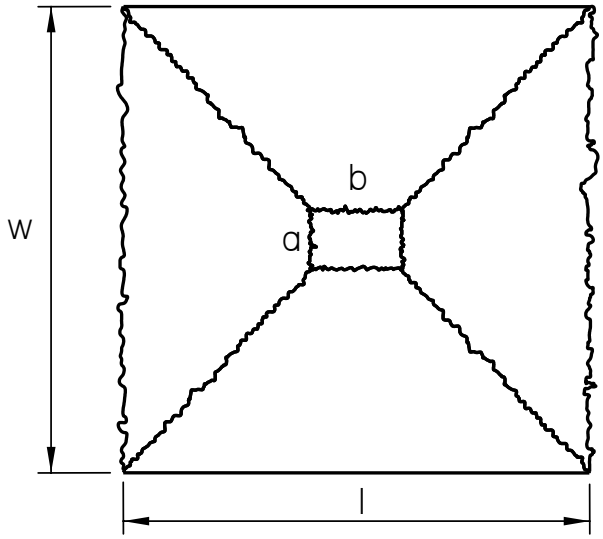

Figure A-6 - Case F

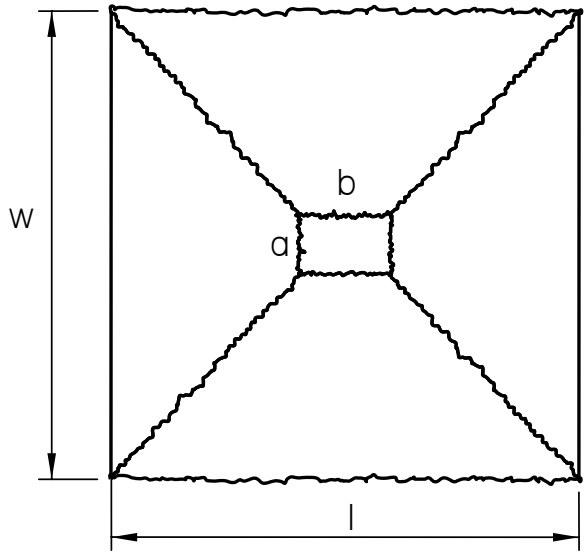

Figure A-7 - Case G

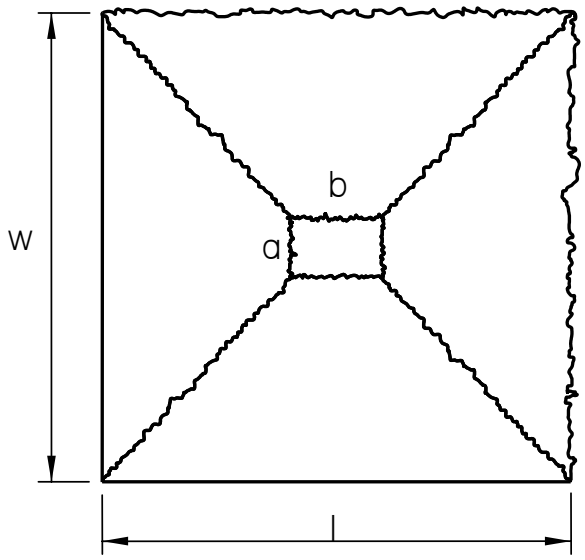

Figure A-8 - Case H

Edge Condition: One Edge Pinned / Three Edges Fixed

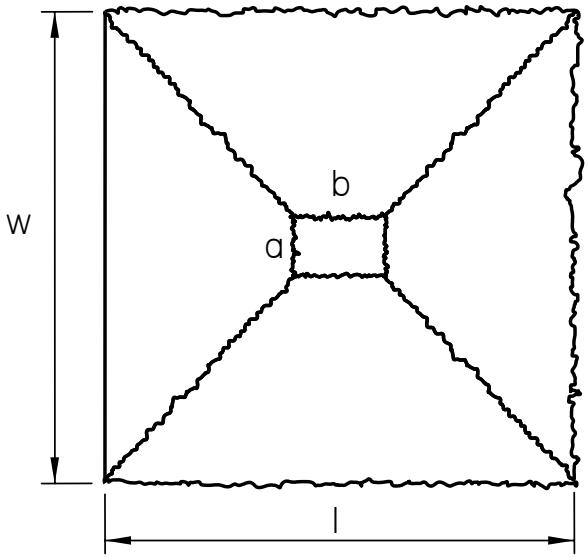

Figure A-9 - Case I

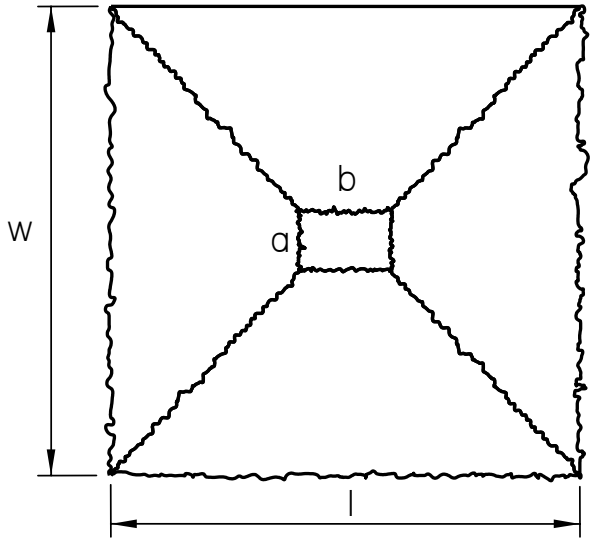

Figure A-10 - Case J

Edge Condition: Four Edges Fixed

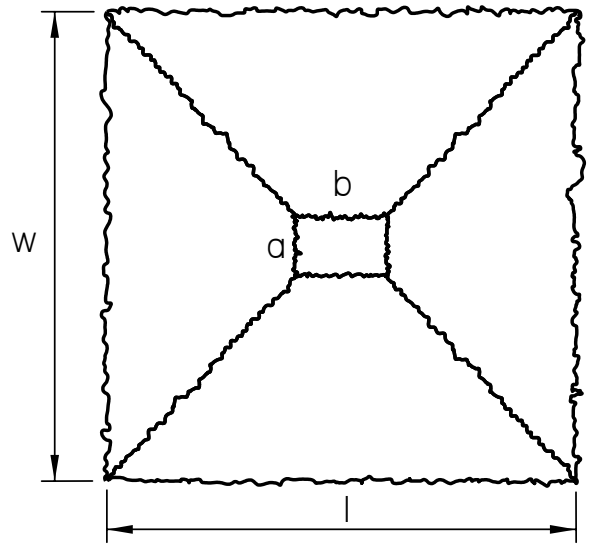

Figure A-11 - Case K

Edge Condition: Radial Pattern

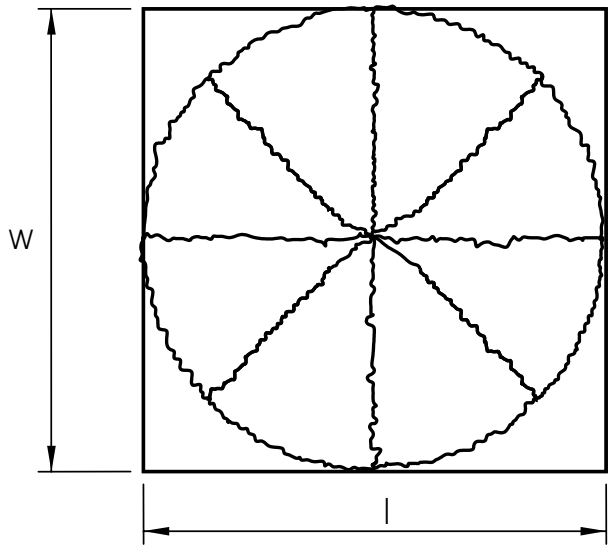

Figure A-12 - Case L

APPENDIX B

Summary of Results

Table B-1 -Summary of Results

Slab Thickness	Square Punch Size	Observed 1st Cracking Deflection	Observed 1st Cracking Load	Actual Failure Load	Mechanism of Failure
in.	in.	in.	kips	kips	
2.17	1.5	**.06**	**6.7**	**23.3**	Punching Failure
2.32	2	**.05**	**6.1**	**27.2**	Punching Failure
2.12	1	**no data**	**8.0**	**22.6**	Punching Failure
2.61	2	**.06**	**7.9**	**33.0**	Punching Failure
2.58	3	**.08**	**9.9***	**35.9**	Flexural Failure
2.54	1.5	**.05**	**8.0**	**30.5**	Punching Failure
2.76	2.5	**.06**	**9.1**	**34.2**	Flexural Failure
3.10	2.5	**.05**	**14.9**	**39.0**	Flexural Failure
2.83	1.5	**.11**	**19.8**	**35.2**	Punching Failure
3.03	1	**.05**	**14.9**	**40.1**	Punching Failure
2.85	2	**.12**	**15.1**	**38.4**	Flexural Failure
3.27	1.75	**.06**	**13.4**	**39.4**	Flexural Failure

* Slab was accidentally loaded prior to starting test, resulting in an initial crack (no measurements). Load indicated is when the first crack was observed after testing began.

Table B-2 – Summary of Material Properties
(Graybeal communication)

Compressive Strength – No Modulus Test (ksi)	32.1
Compressive Strength – Modulus Test (ksi)*	31.6
Tensile Strength (ksi)	1.6
Elastic Modulus (ksi)	7857

*Compressive strength – modulus test was loaded in the elastic region to record the modulus and then loaded to failure. Compressive strength – no modulus test was directly loaded to failure.

Series 1

Figure B-13 – Failure Surface (2.0 in. slab - 1.5 in. plate)

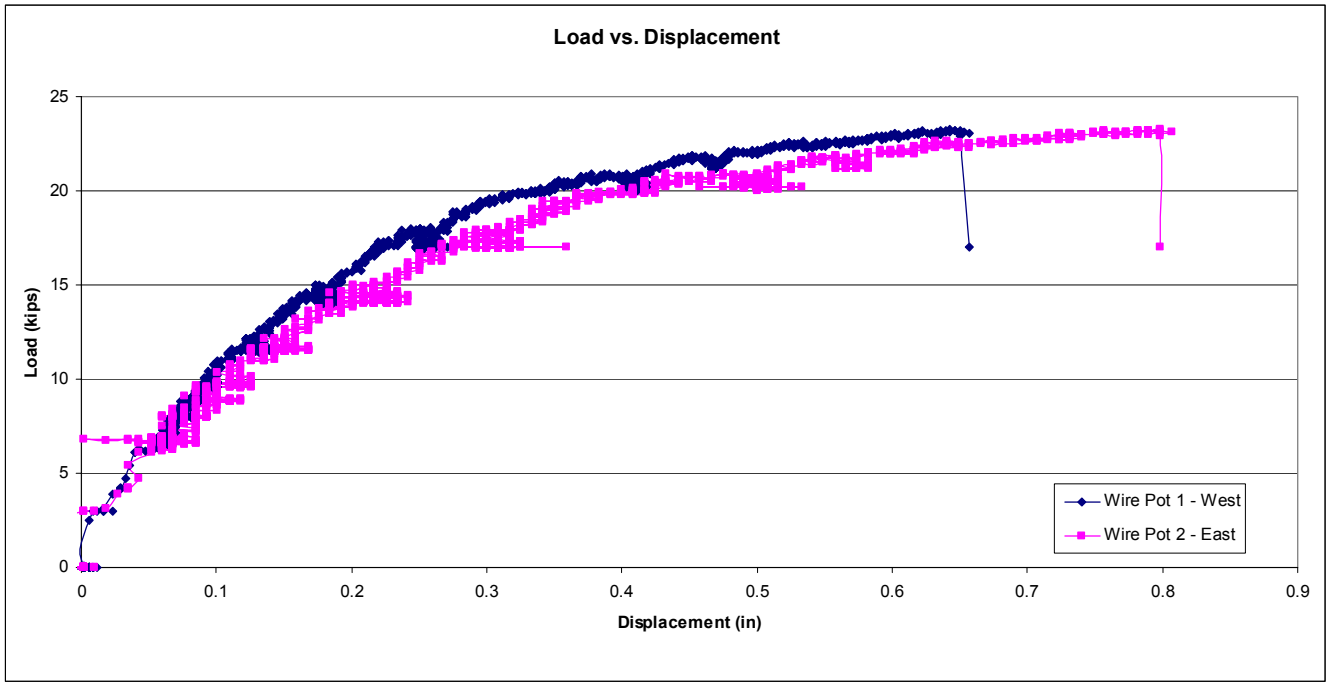

Figure B-14 - Load vs. Displacement (2.0 in. slab - 1.5 in. plate)

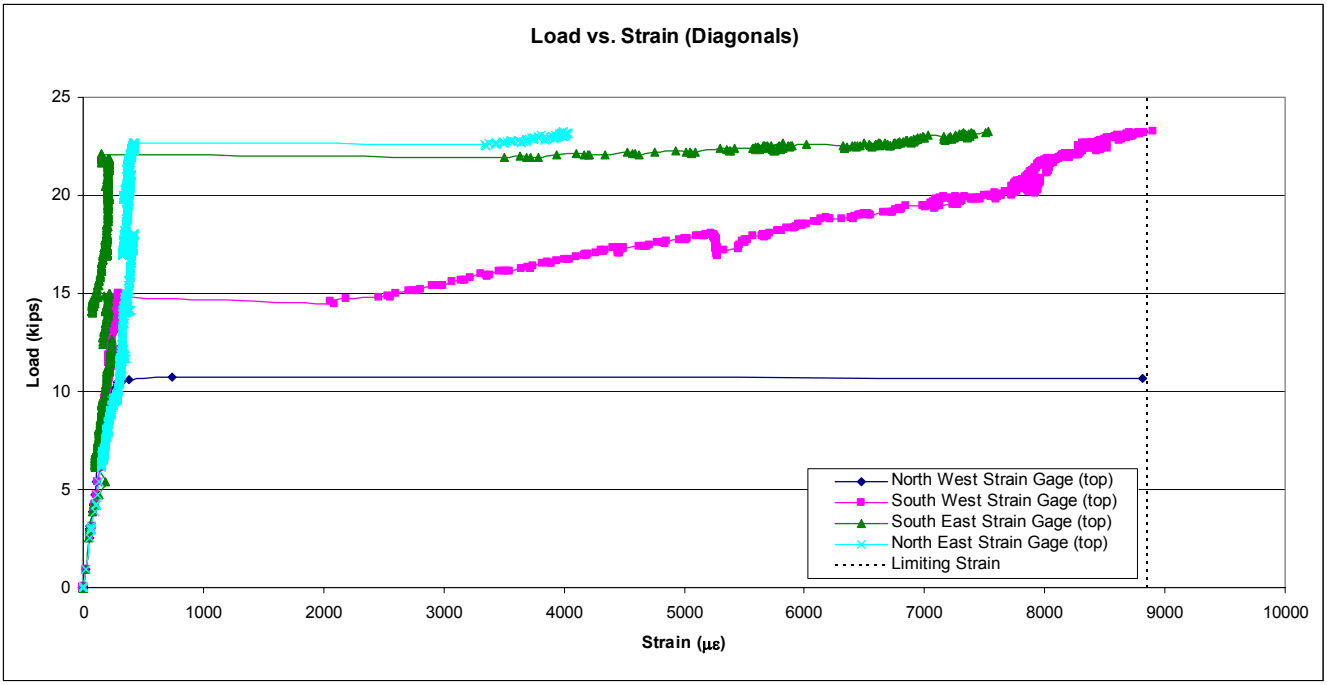

Figure B-15 – Load vs. Diagonal Strain (2.0 in. slab - 1.5 in. plate)

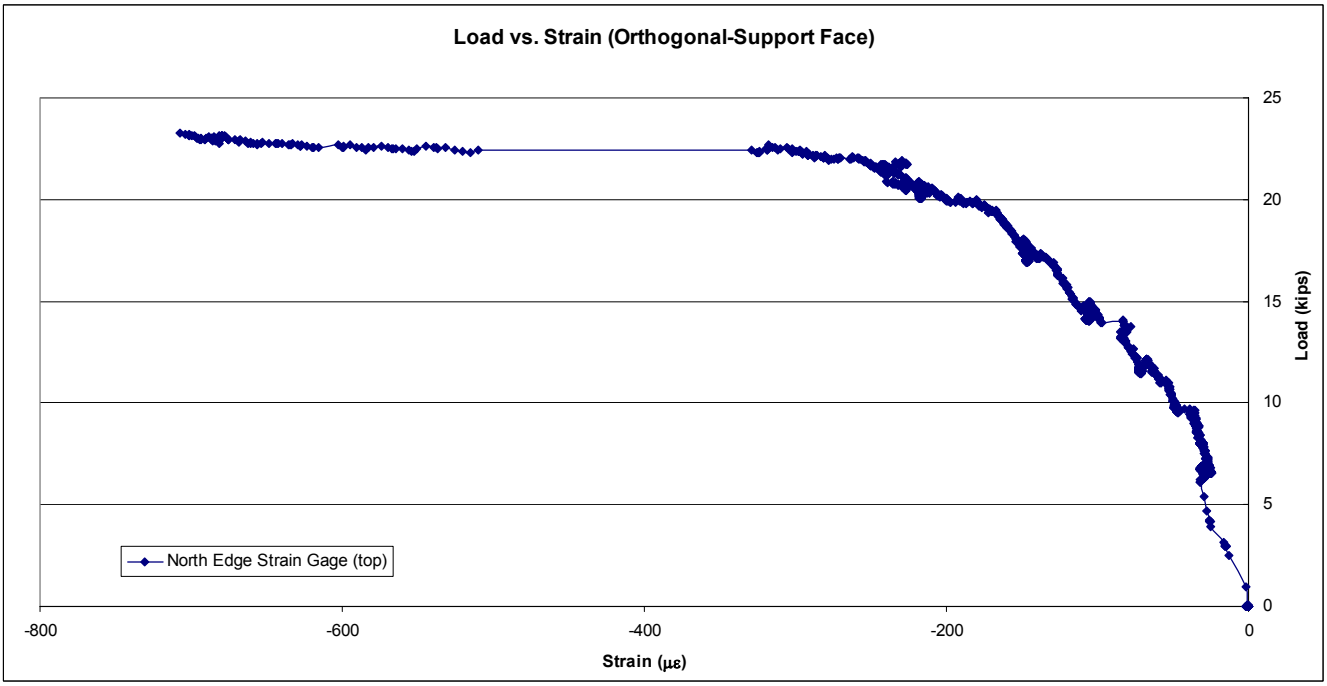

Figure B-16 - Load vs. Orthogonal Strain (2.0 in. slab - 1.5 in. plate)

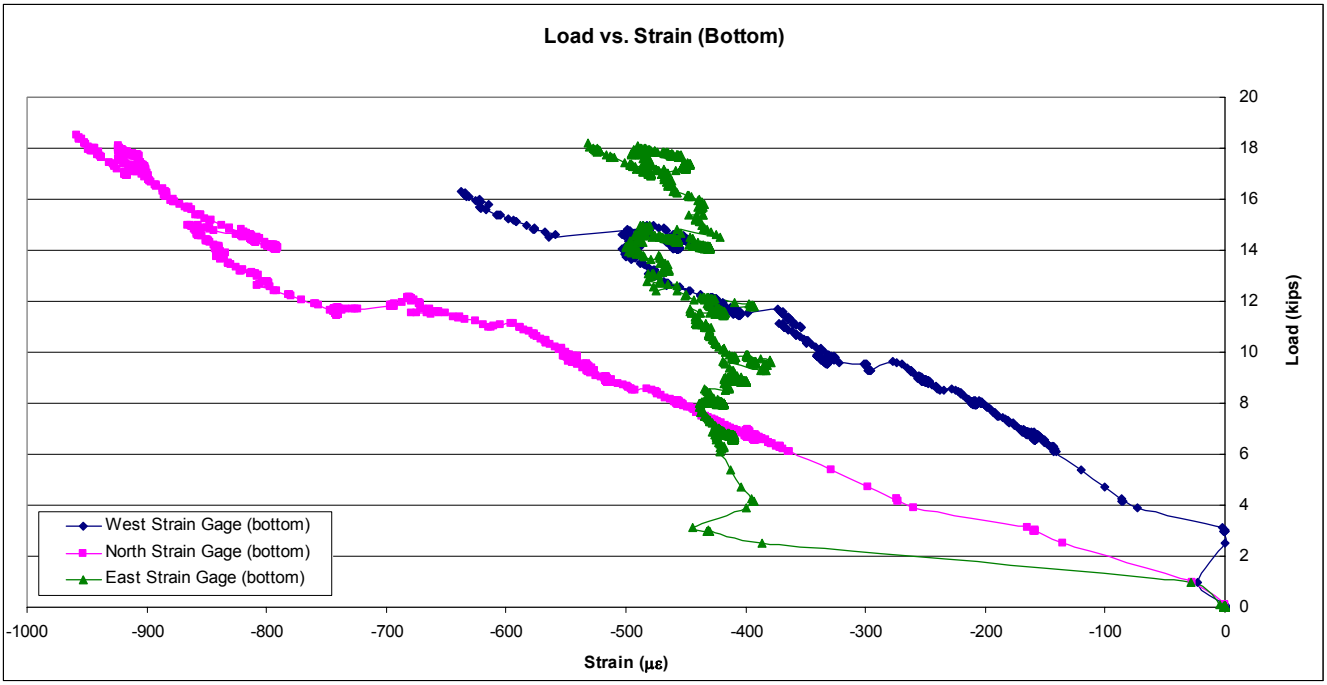

Figure B-17 - Load vs. Bottom Strain (2.0 in. slab - 1.5 in. plate)

Figure B-18 – Failure Surface (2.0 in. slab – 2.0 in. plate)

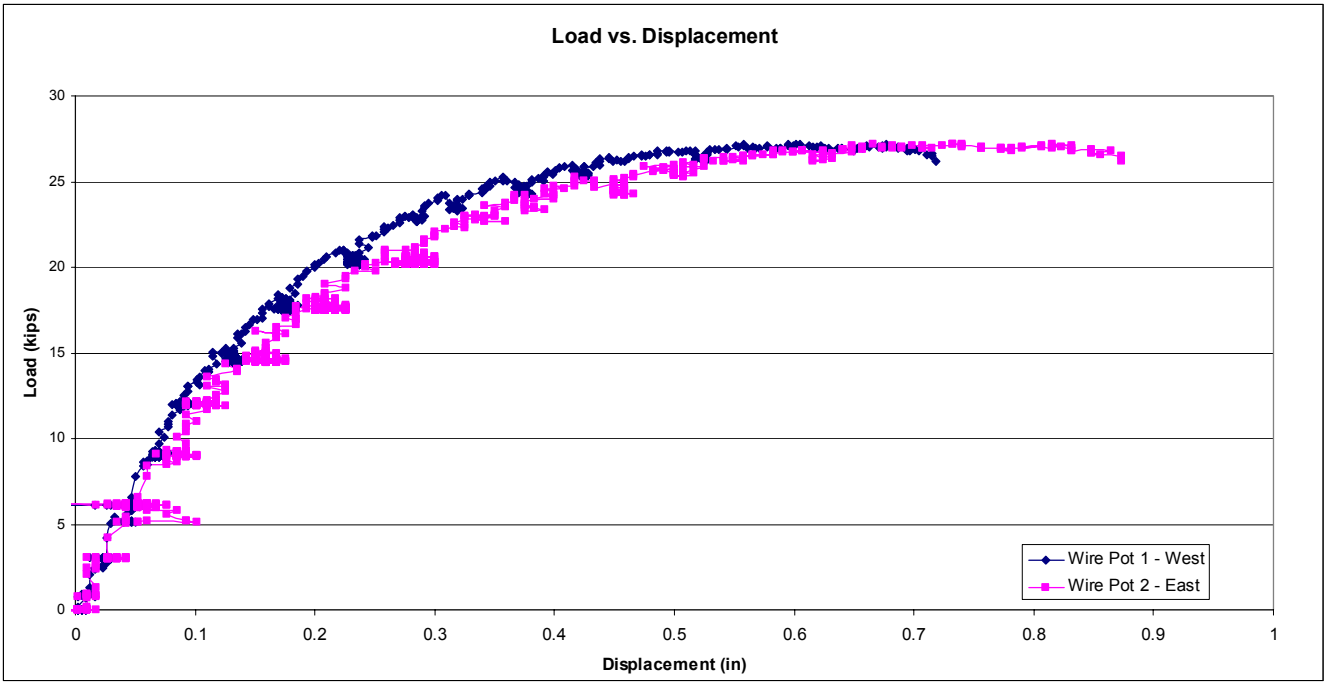

Figure B-19 - Load vs. Displacement (2.0 in. slab – 2.0 in. plate)

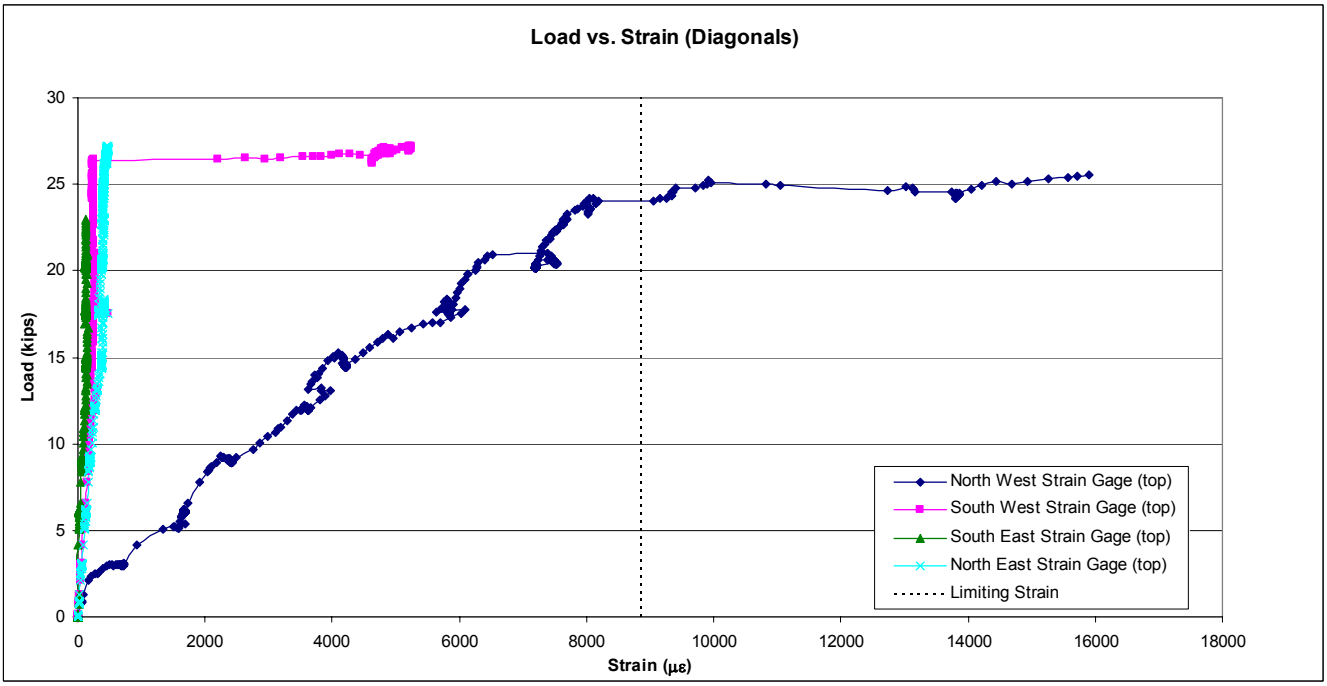

Figure B-20 - Load vs. Diagonal Strain (2.0 in. slab – 2.0 in. plate)

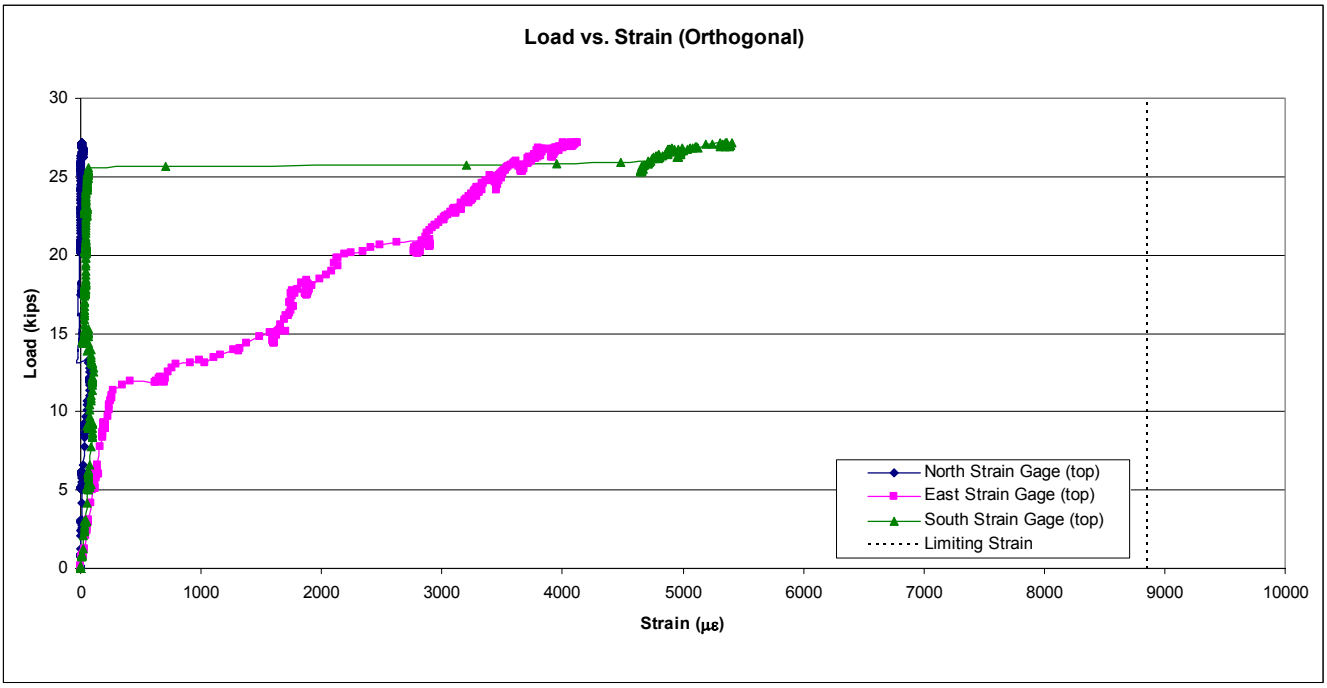

Figure B-21 - Load vs. Orthogonal Strain (2.0 in. slab – 2.0 in. plate)

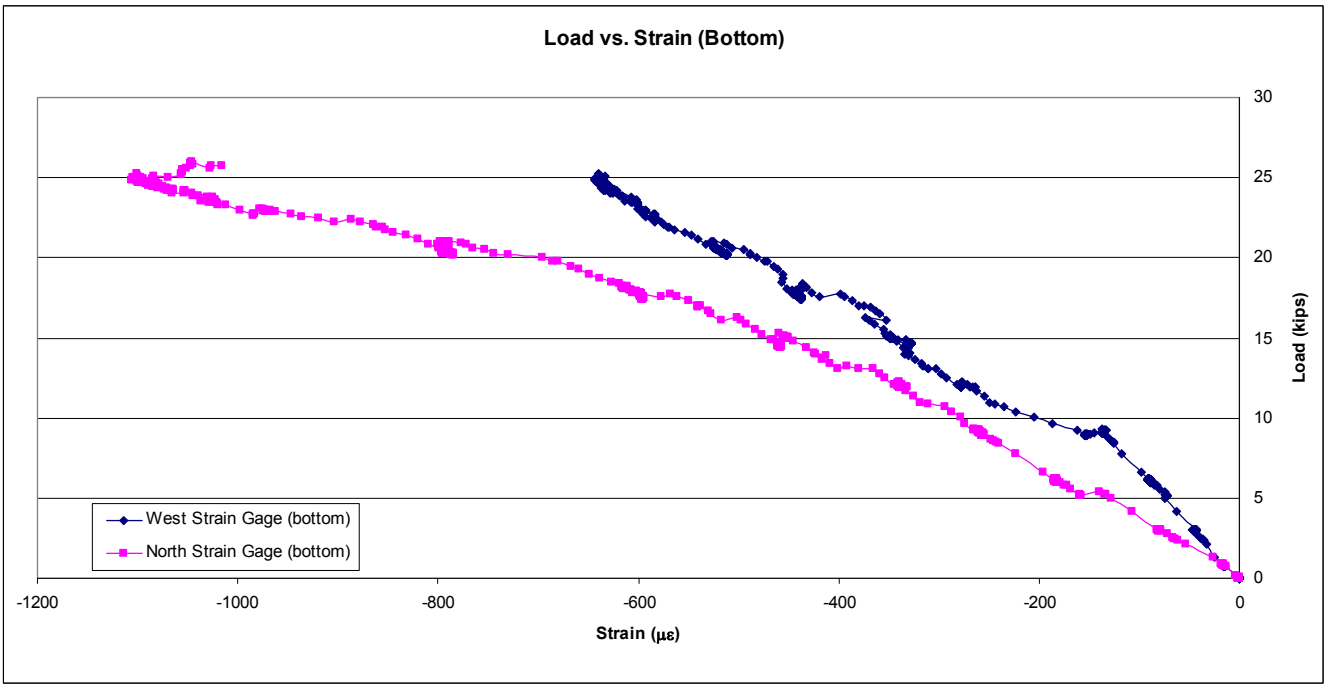

Figure B-22 - Load vs. Bottom Strain (2.0 in. slab – 2.0 in. plate)

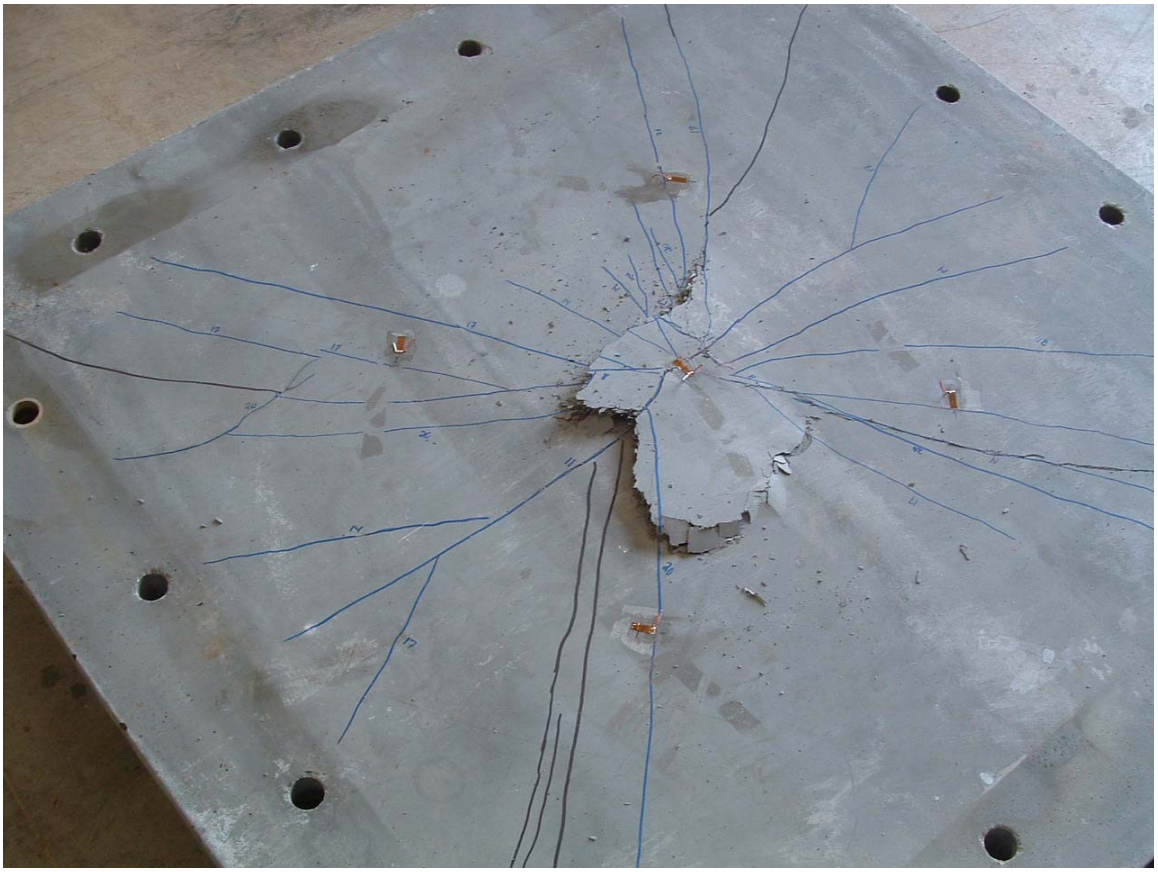

Figure B-23 – Failure Surface (2.0 in. slab – 1.0 in. plate)

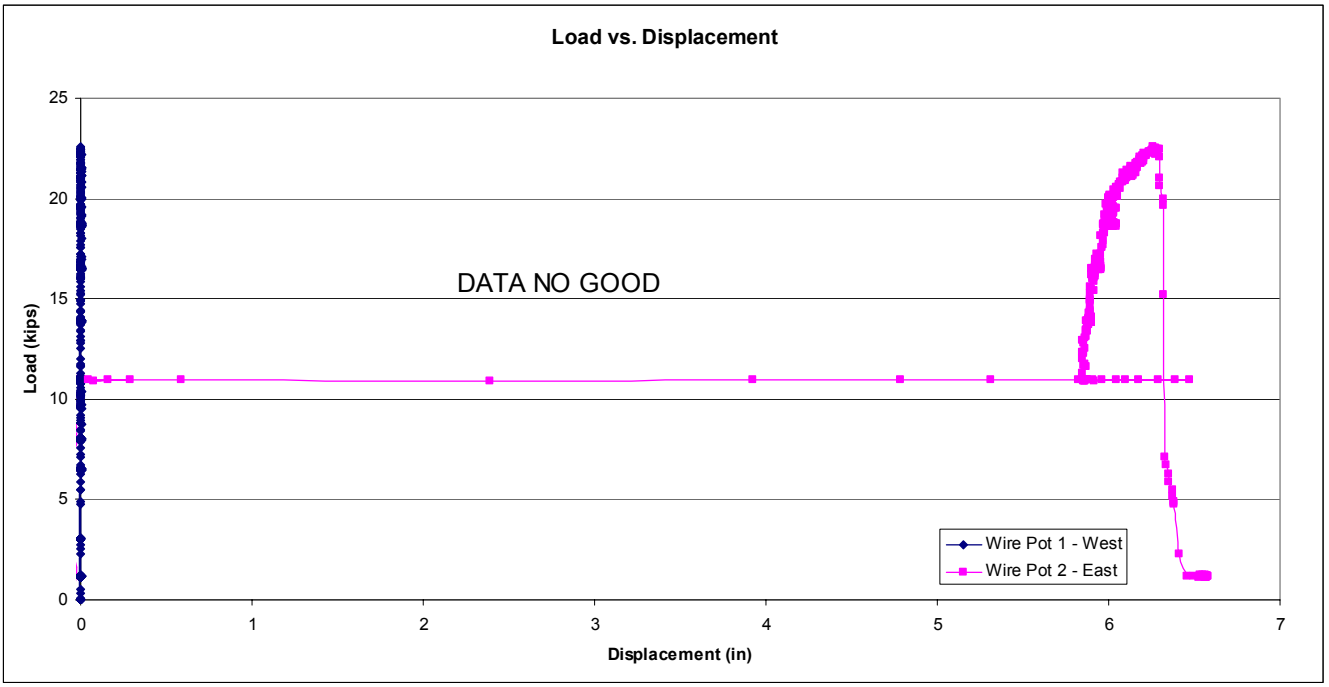

Figure B-24 - Load vs. Displacement (2.0 in. slab – 1.0 in. plate)

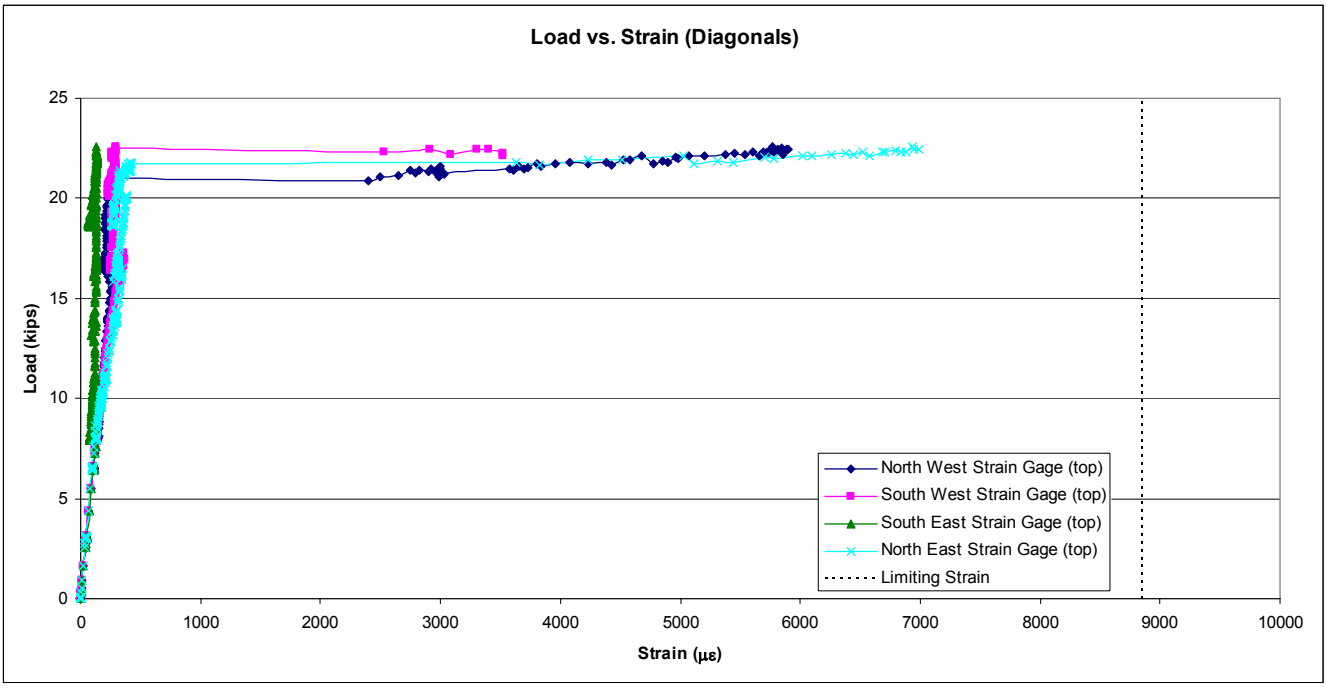

Figure B-25 - Load vs. Diagonal Strain (2.0 in. slab – 1.0 in. plate)

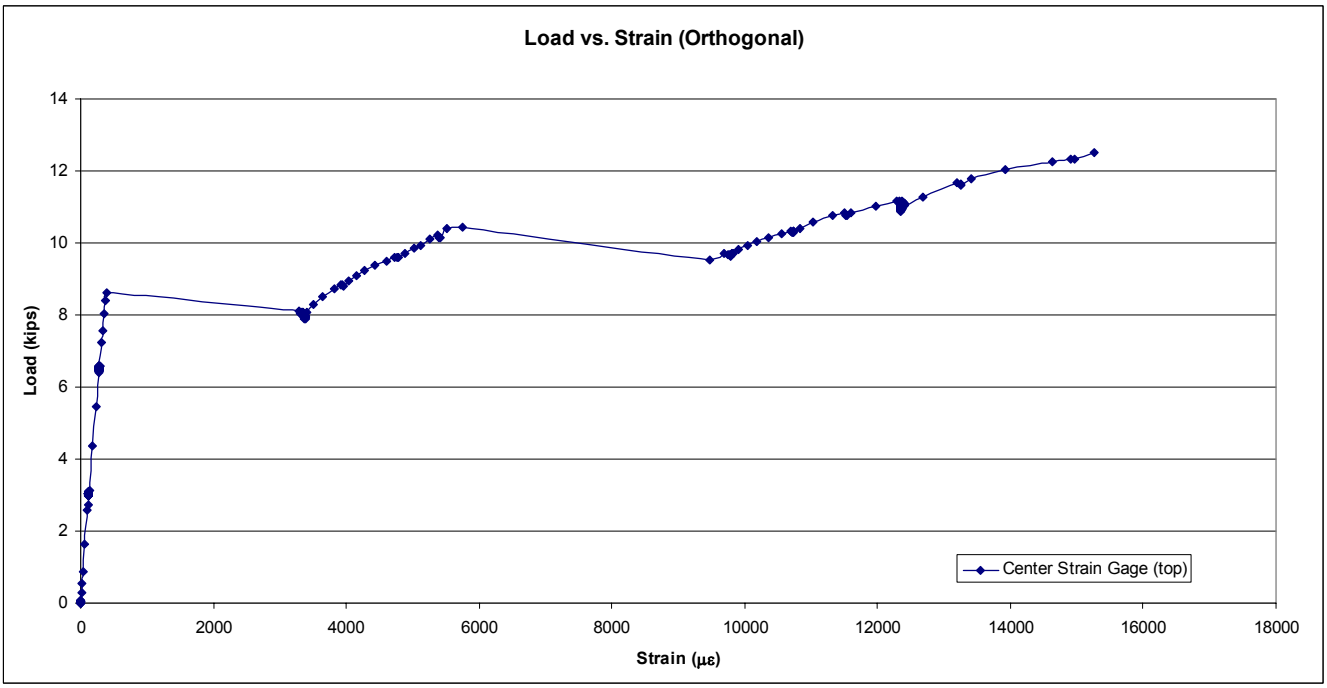

Figure B-26 - Load vs. Orthogonal Strain (2.0 in. slab – 1.0 in. plate)

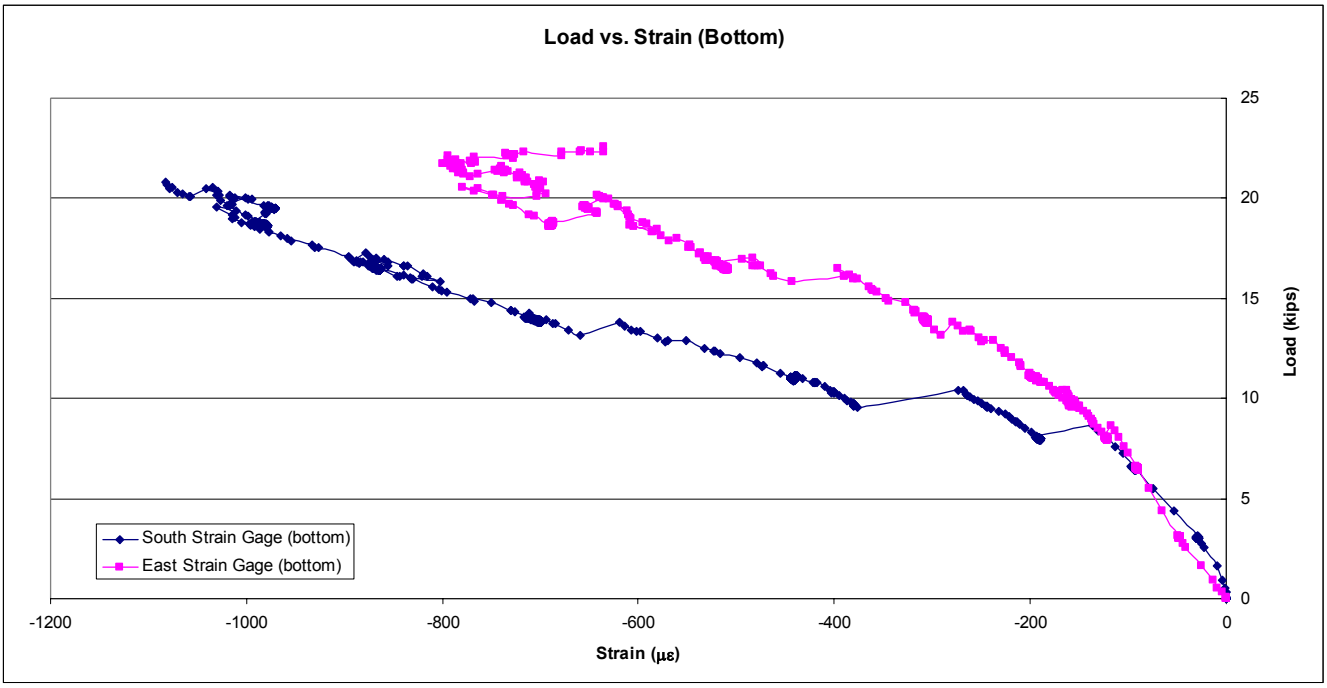

Figure B-27 - Load vs. Bottom Strain (2.0 in. slab – 2.0 in. plate)

Series 2

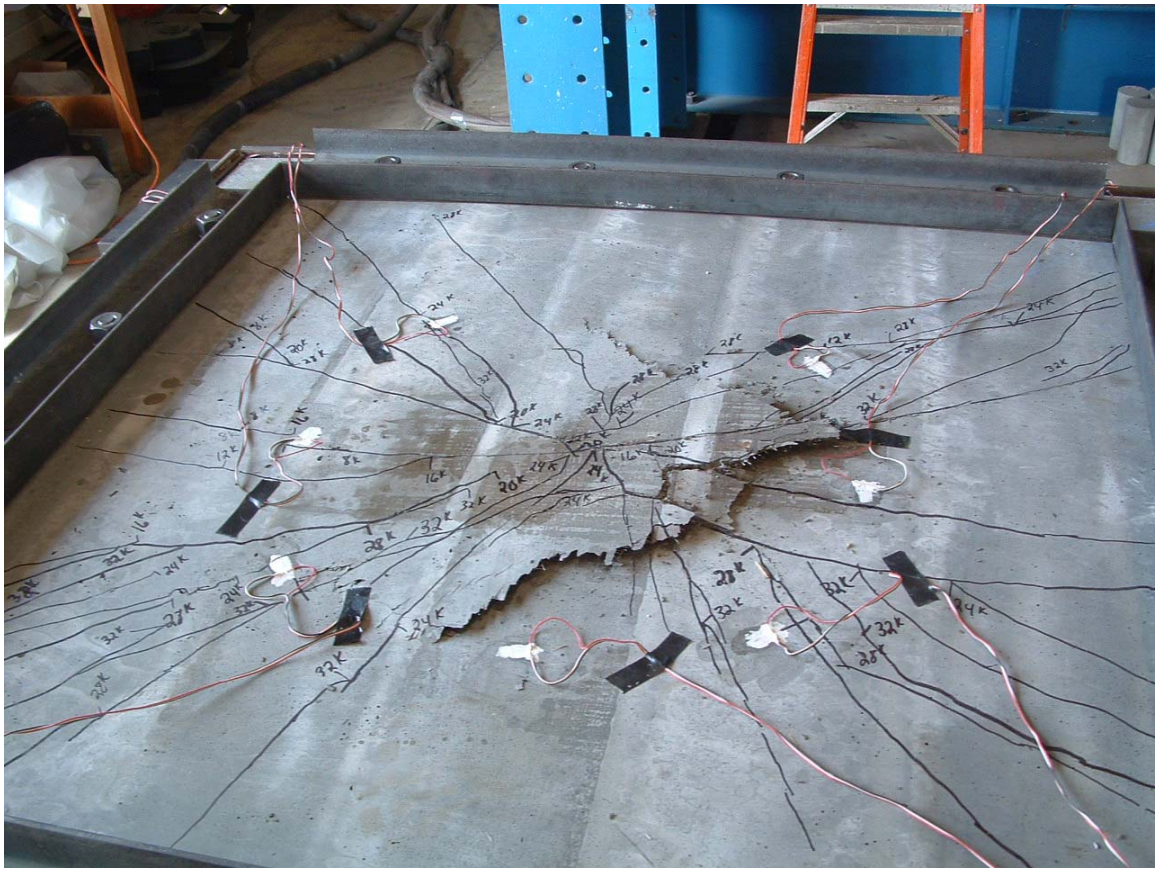

Figure B-28 – Failure Surface (2.5 in. slab – 2.0 in. plate)

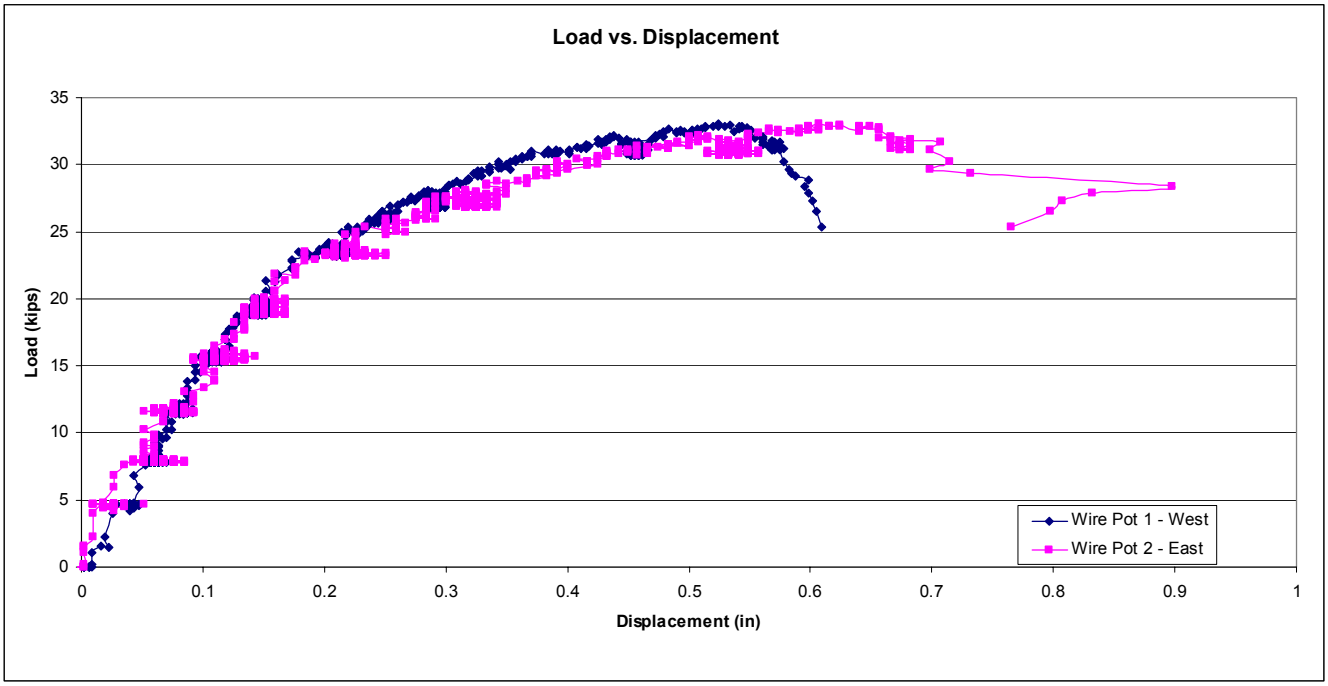

Figure B-29 - Load vs. Displacement (2.5 in. slab – 2.0 in. plate)

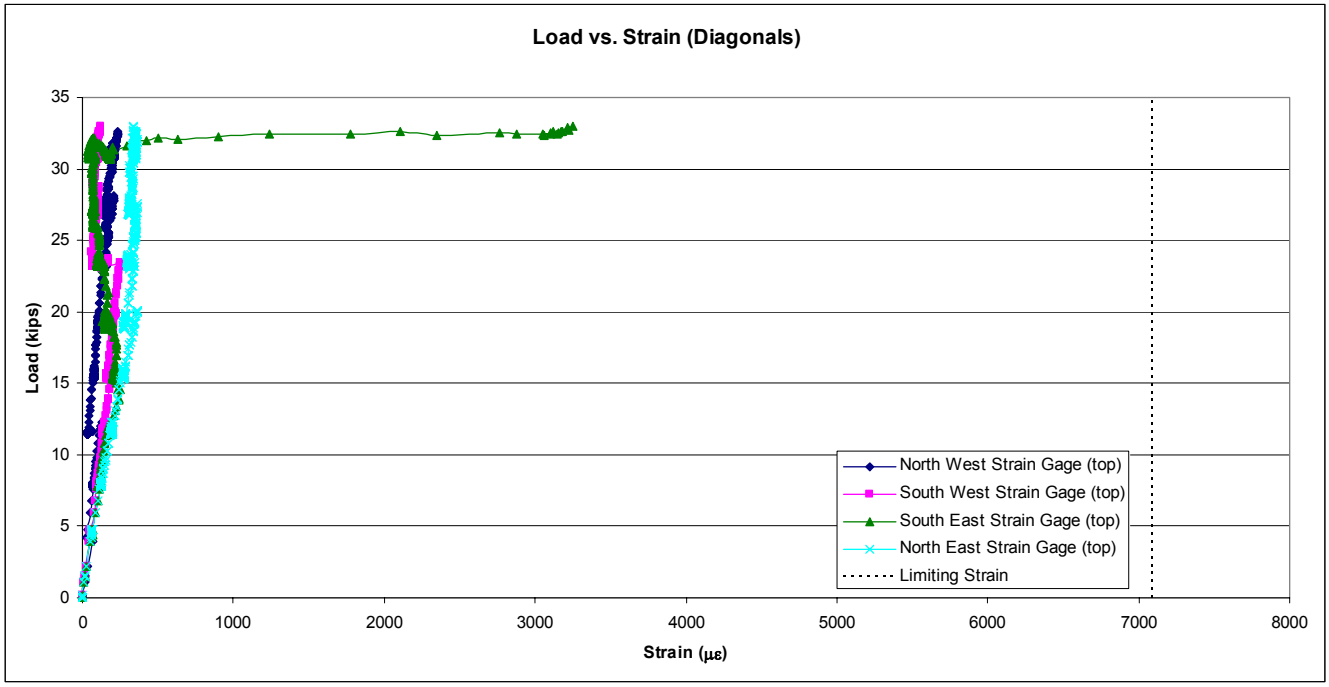

Figure B-30 - Load vs. Diagonal Strain (2.5 in. slab – 2.0 in. plate)

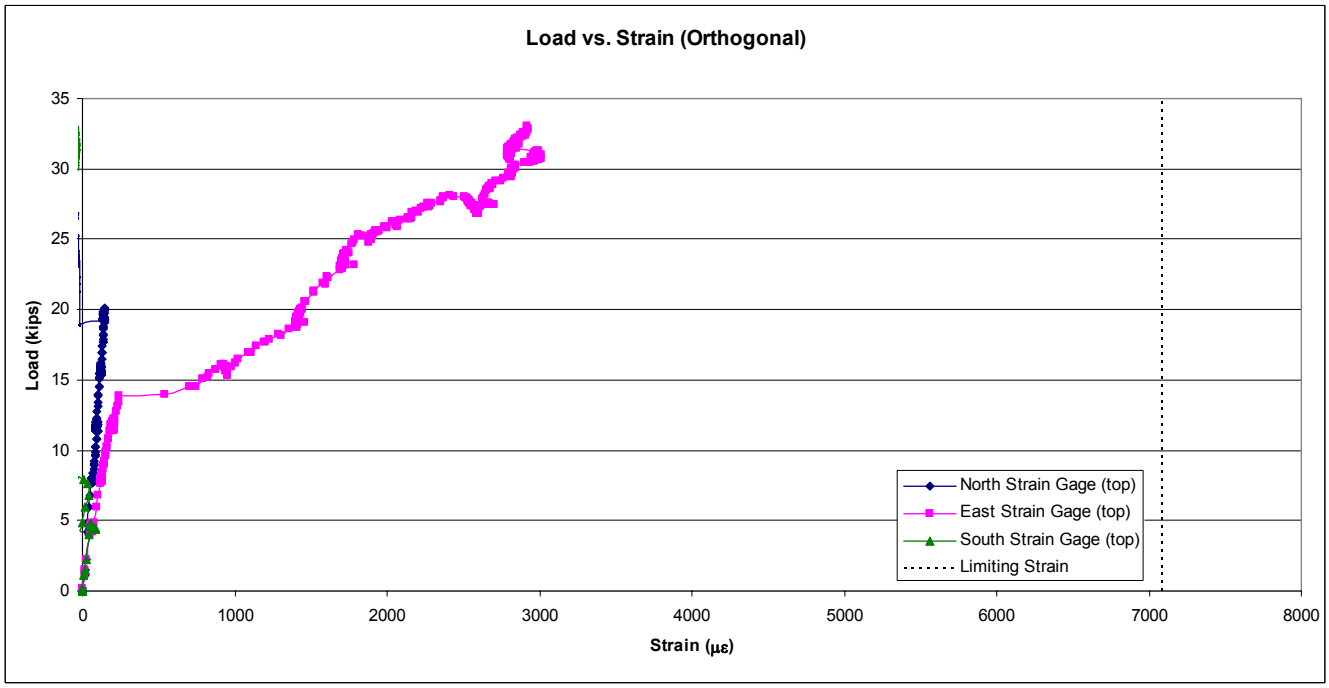

Figure B-31 - Load vs. Orthogonal Strain (2.5 in. slab – 2.0 in. plate)

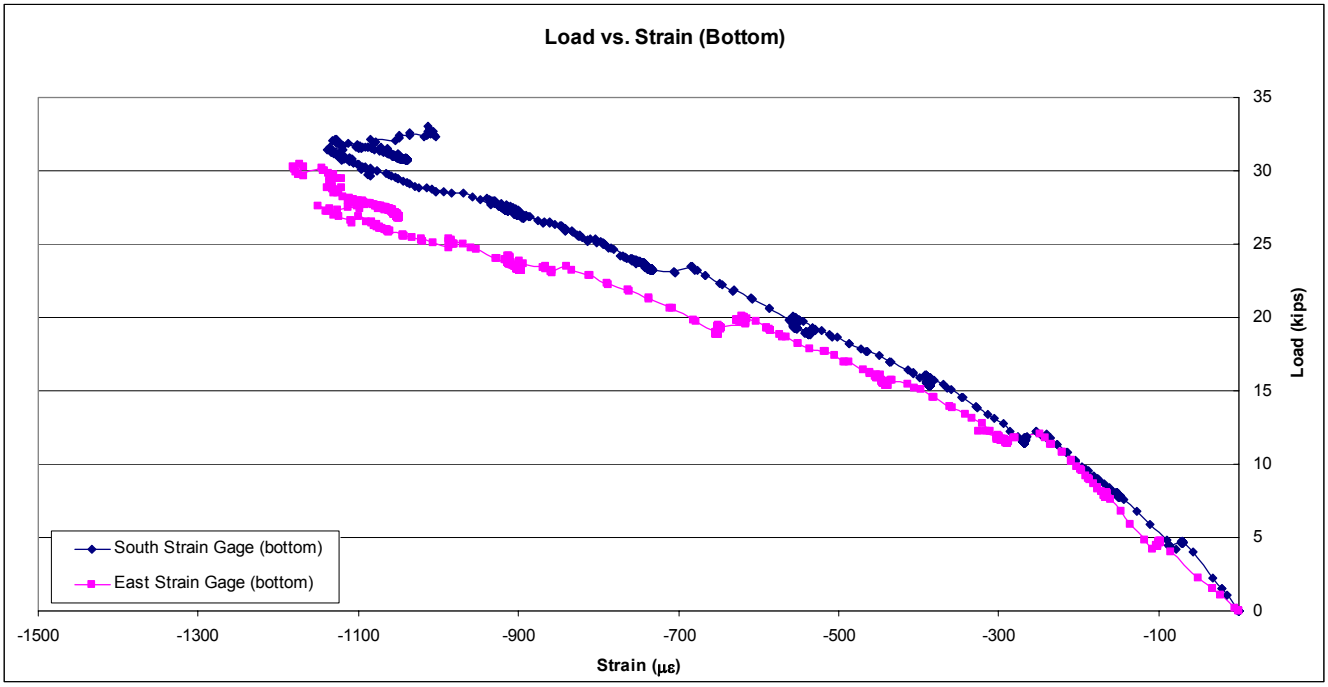

Figure B-32 - Load vs. Bottom Strain (2.5 in. slab – 2.0 in. plate)

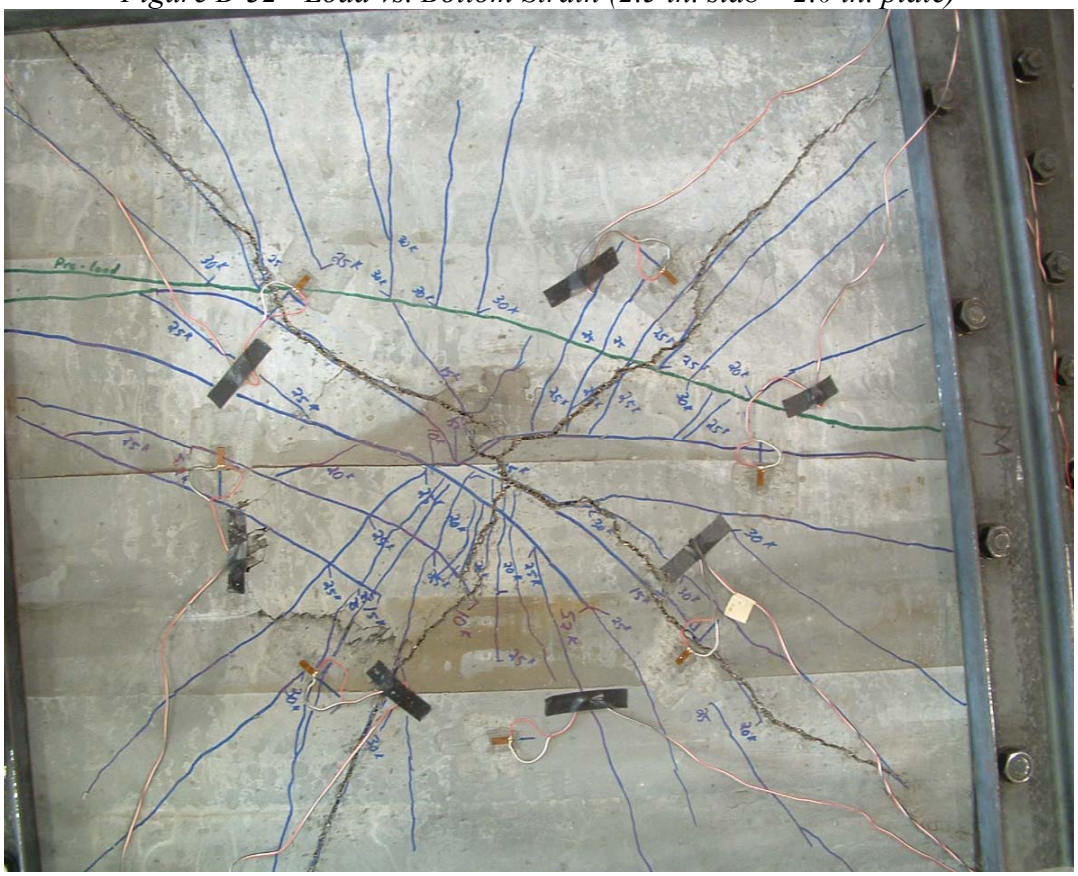

Figure B-33 – Failure Surface (2.5 in. slab – 3.0 in. plate)

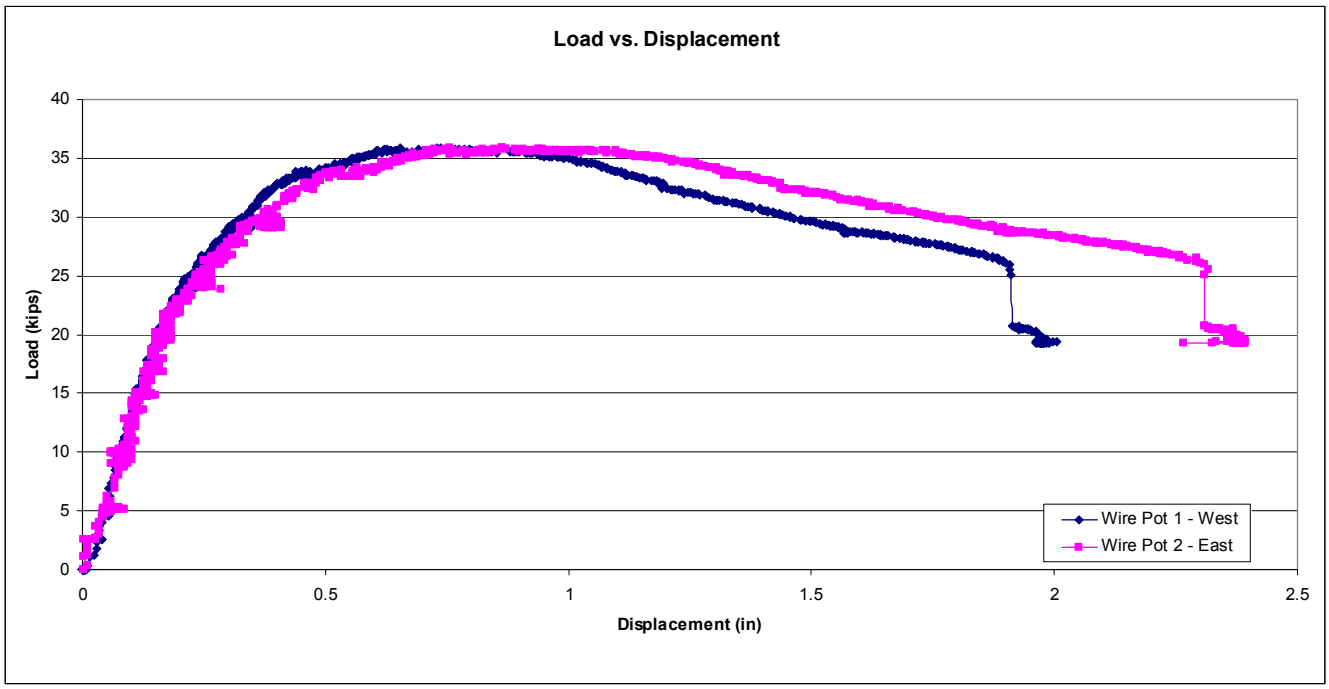

Figure B-34 - Load vs. Displacement (2.5 in. slab – 3.0 in. plate)

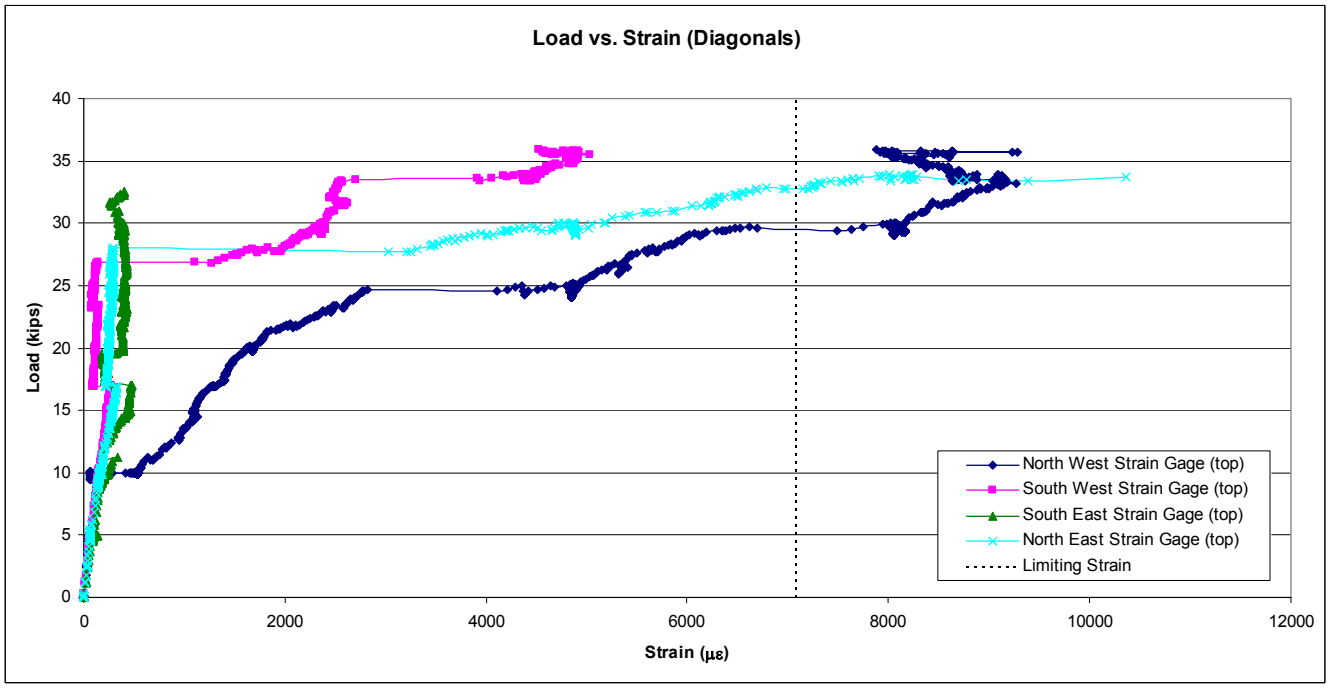

Figure B-35- Load vs. Diagonal Strain (2.5 in. slab – 3.0 in. plate)

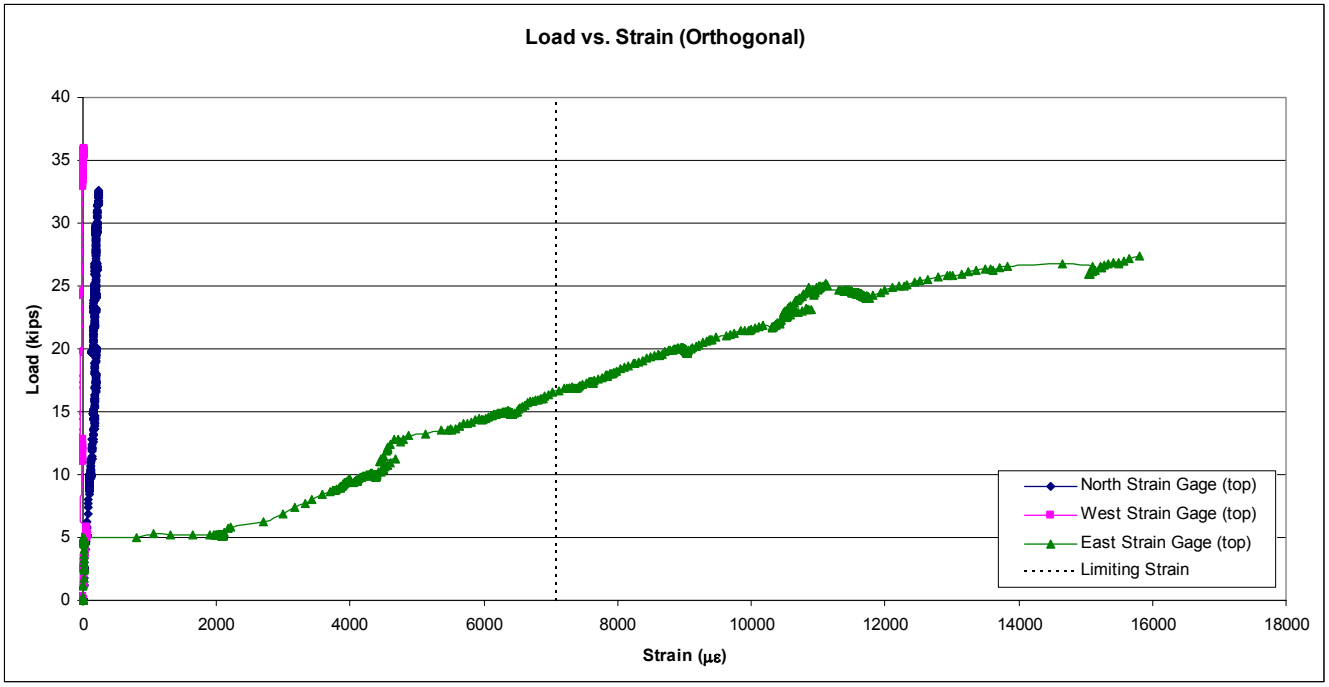

Figure B-36 - Load vs. Orthogonal Strain (2.5 in. slab – 3.0 in. plate)

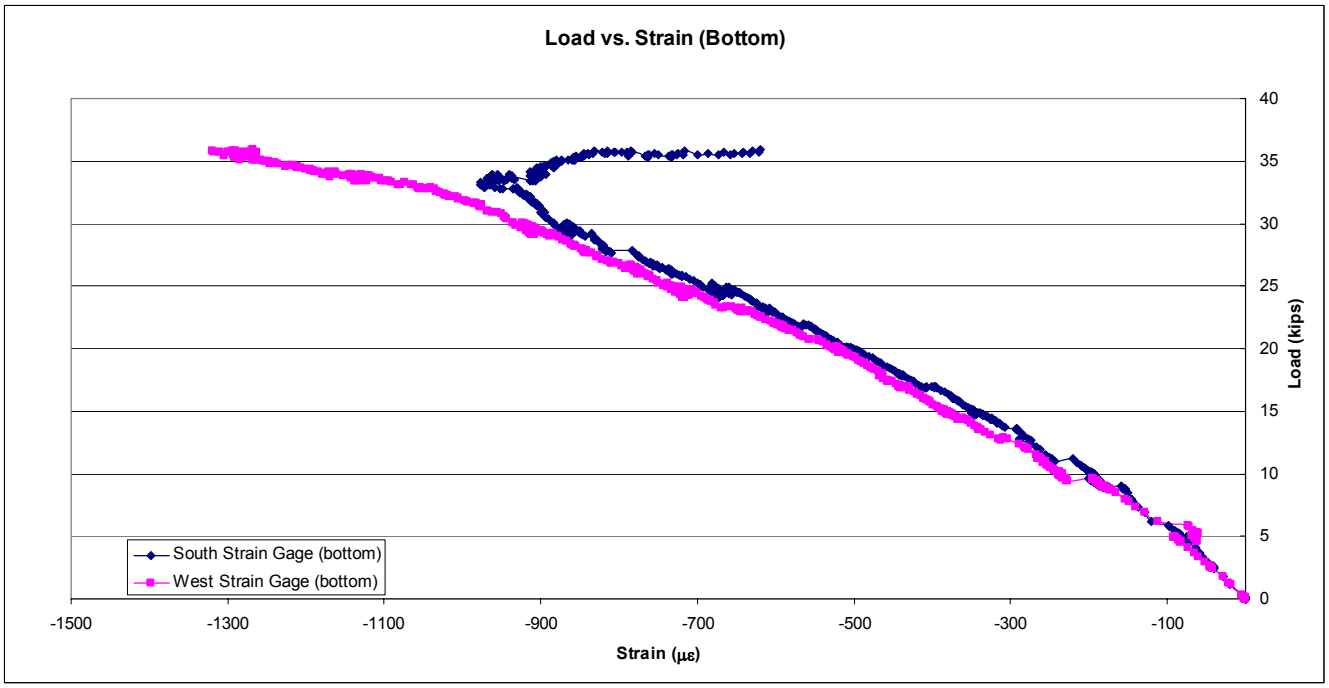

Figure B-37 - Load vs. Bottom Strain (2.5 in. slab – 3.0 in. plate)

Figure B-38 – Failure Surface (2.5 in. slab – 1.5 in. plate)

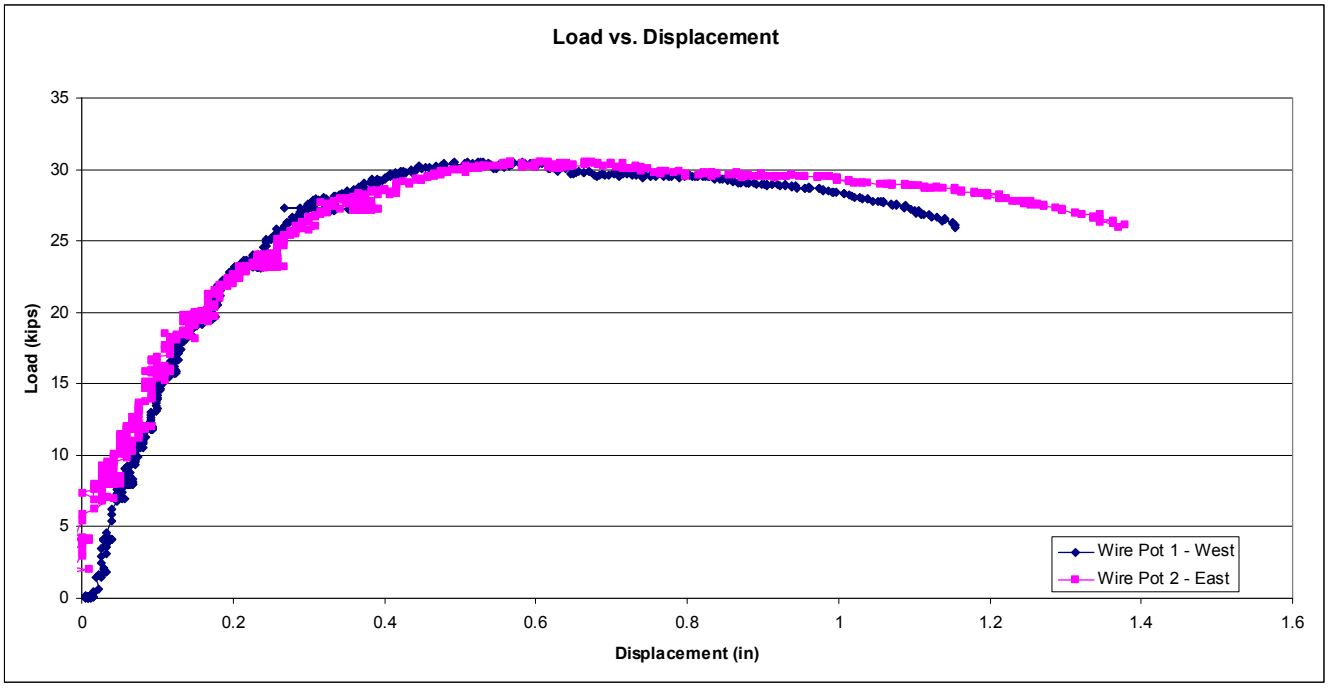

Figure B-39 - Load vs. Displacement (2.5 in. slab – 1.5 in. plate)

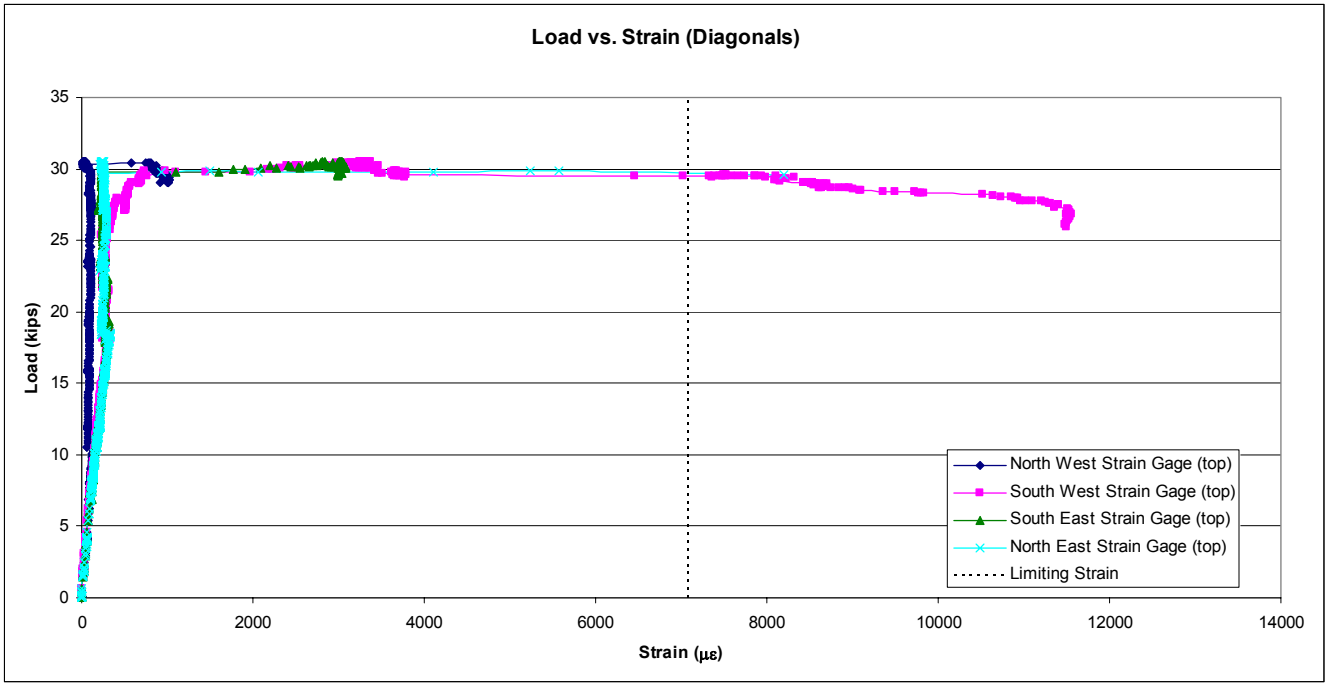

Figure B-40 - Load vs. Diagonal Strain (2.5 in. slab – 1.5 in. plate)

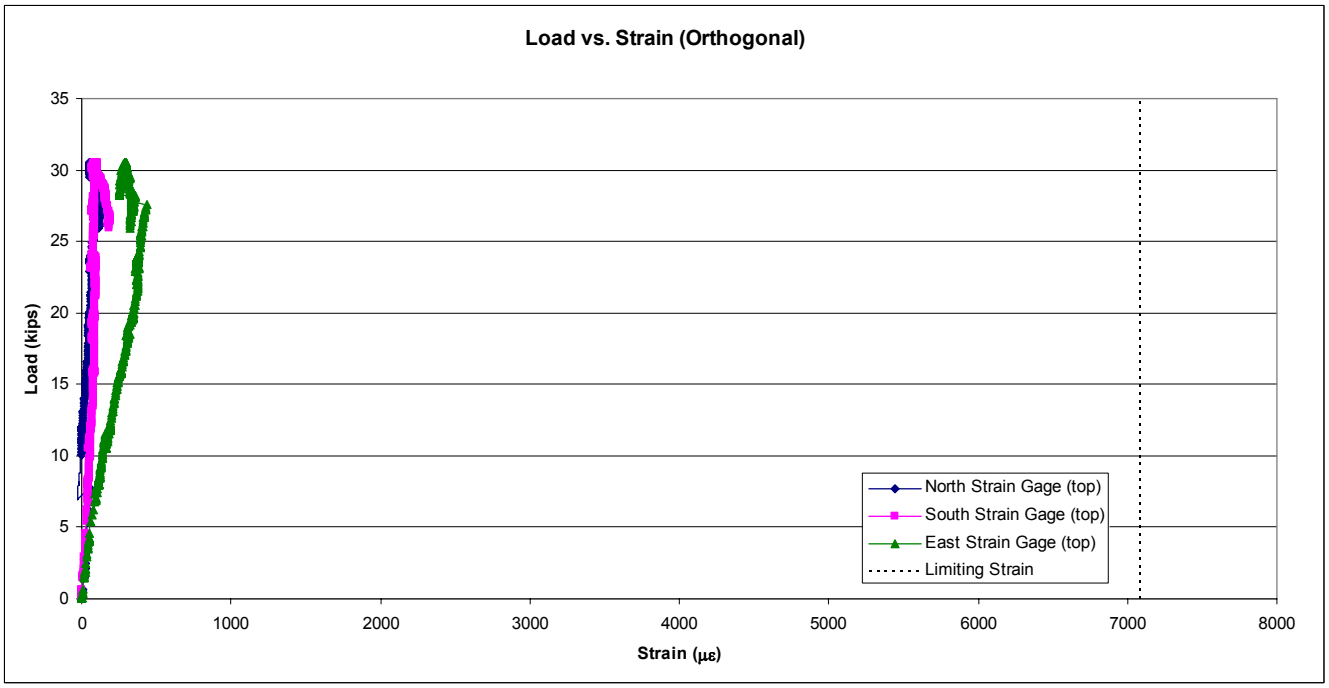

Figure B-41 - Load vs. Orthogonal Strain (2.5 in. slab – 1.5 in. plate)

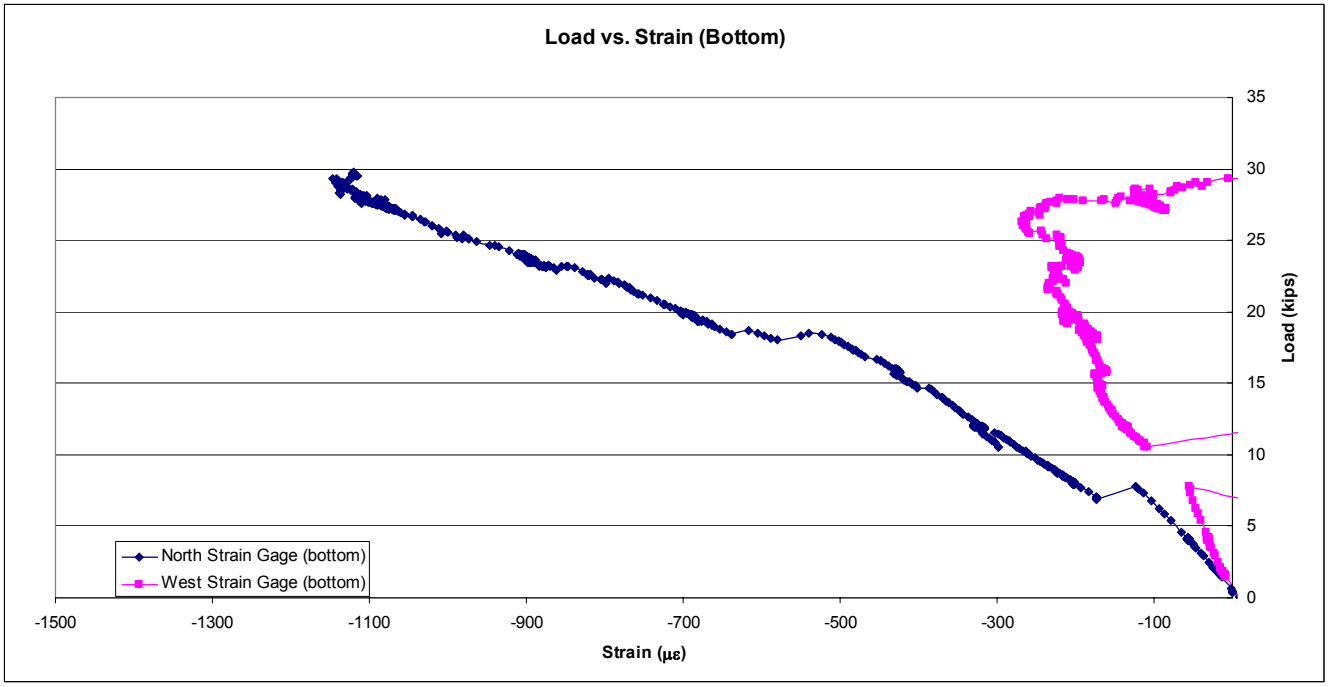

Figure B-42 - Load vs. Bottom Strain (2.5 in. slab – 1.5 in. plate)

Figure B-43 – Failure Surface (2.5 in. slab – 2.5 in. plate)

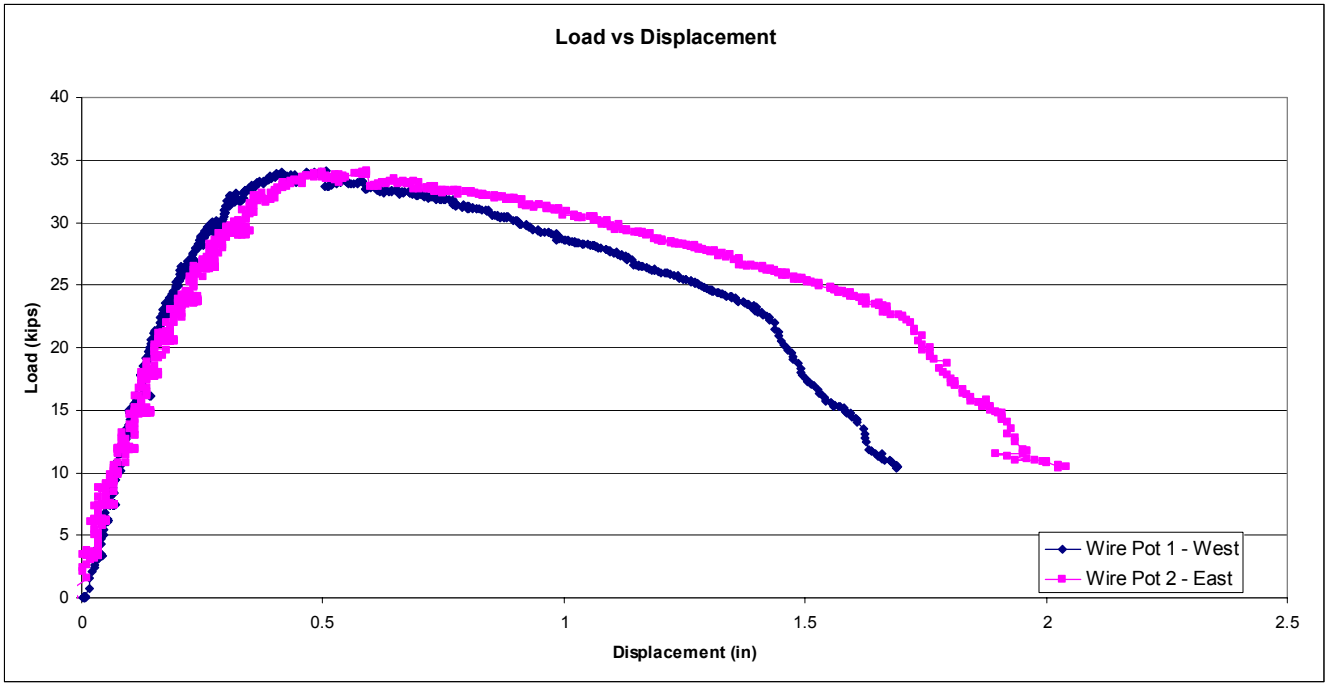

Figure B-44 - Load vs. Displacement (2.5 in. slab – 2.5 in. plate)

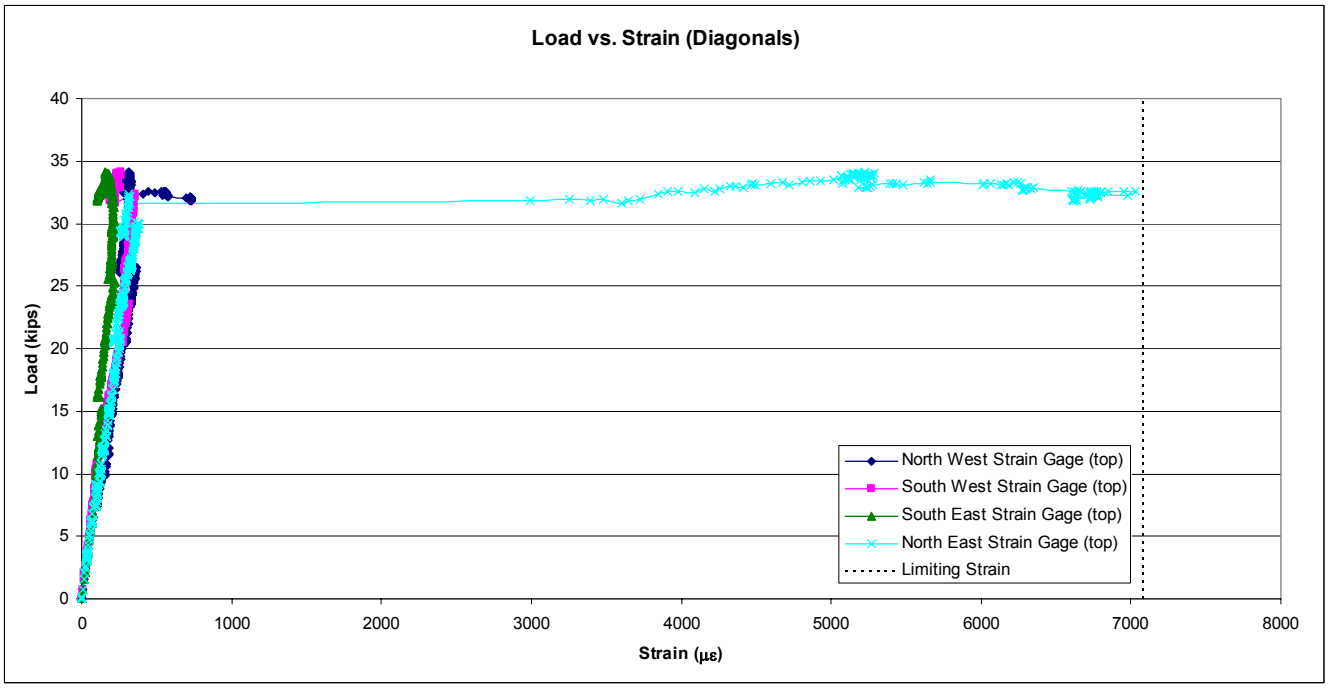

Figure B-45 - Load vs. Diagonal Strain (2.5 in. slab – 2.5 in. plate)

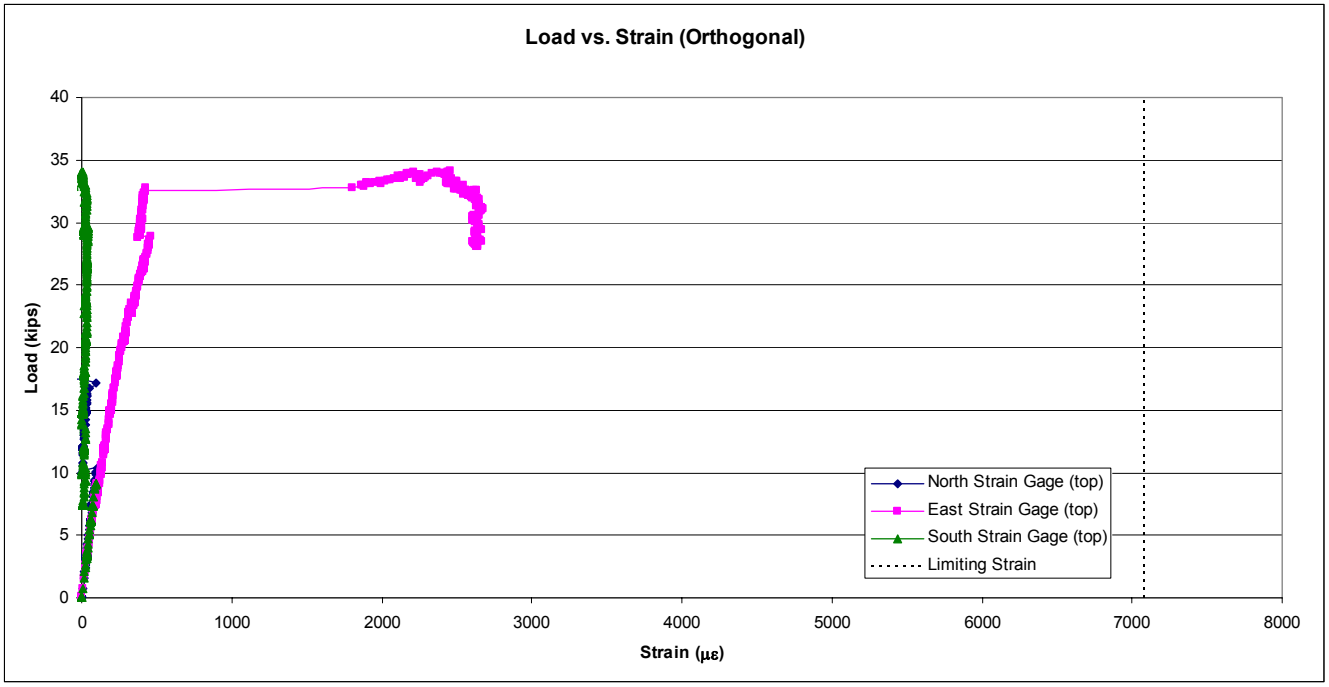

Figure B-46 - Load vs. Orthogonal Strain (2.5 in. slab – 2.5 in. plate)

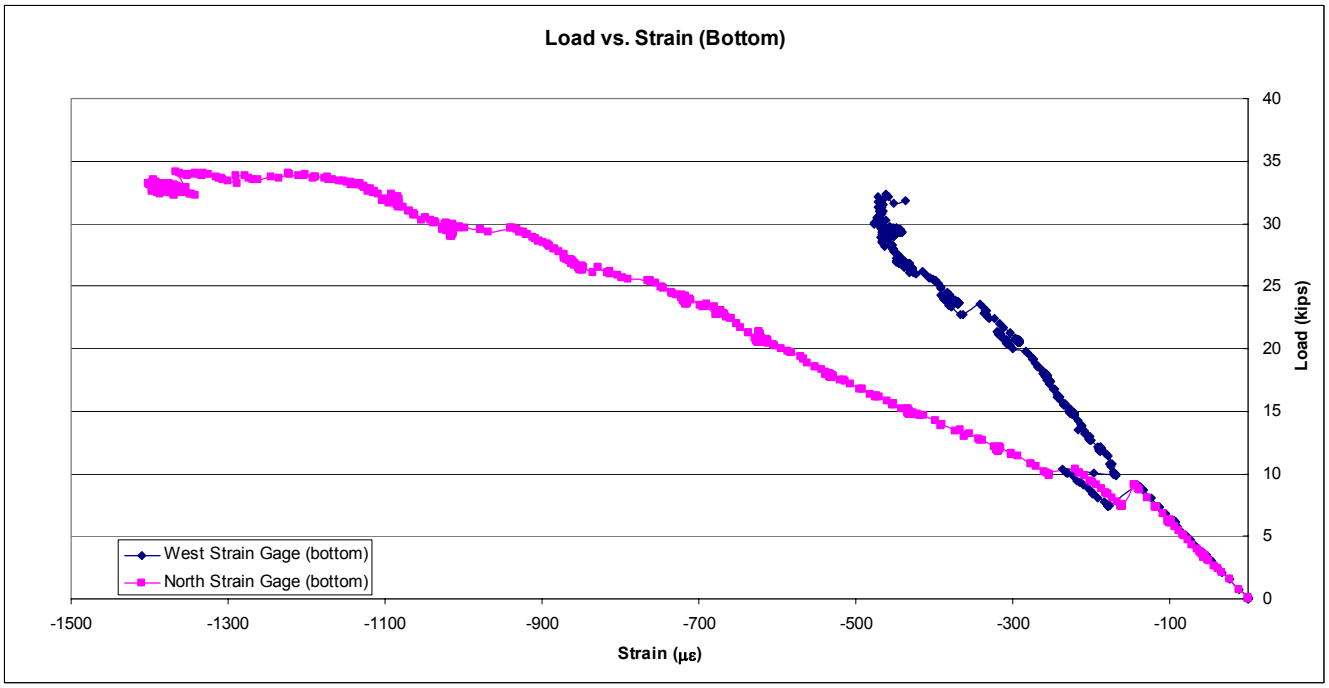

Figure B-47 - Load vs. Bottom Strain (2.5 in. slab – 2.5 in. plate)

Series 3

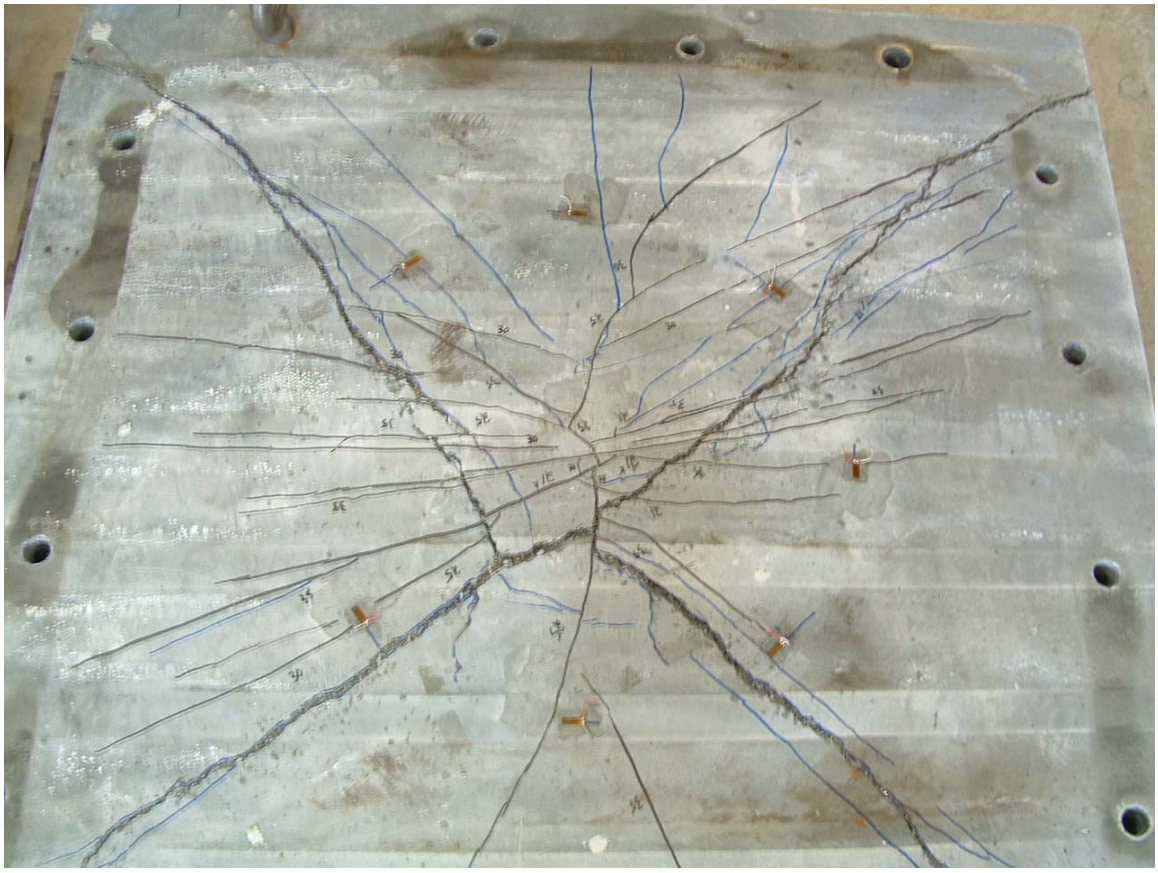

Figure B-48 – Failure Surface (3.0 in. slab – 2.5 in. plate)

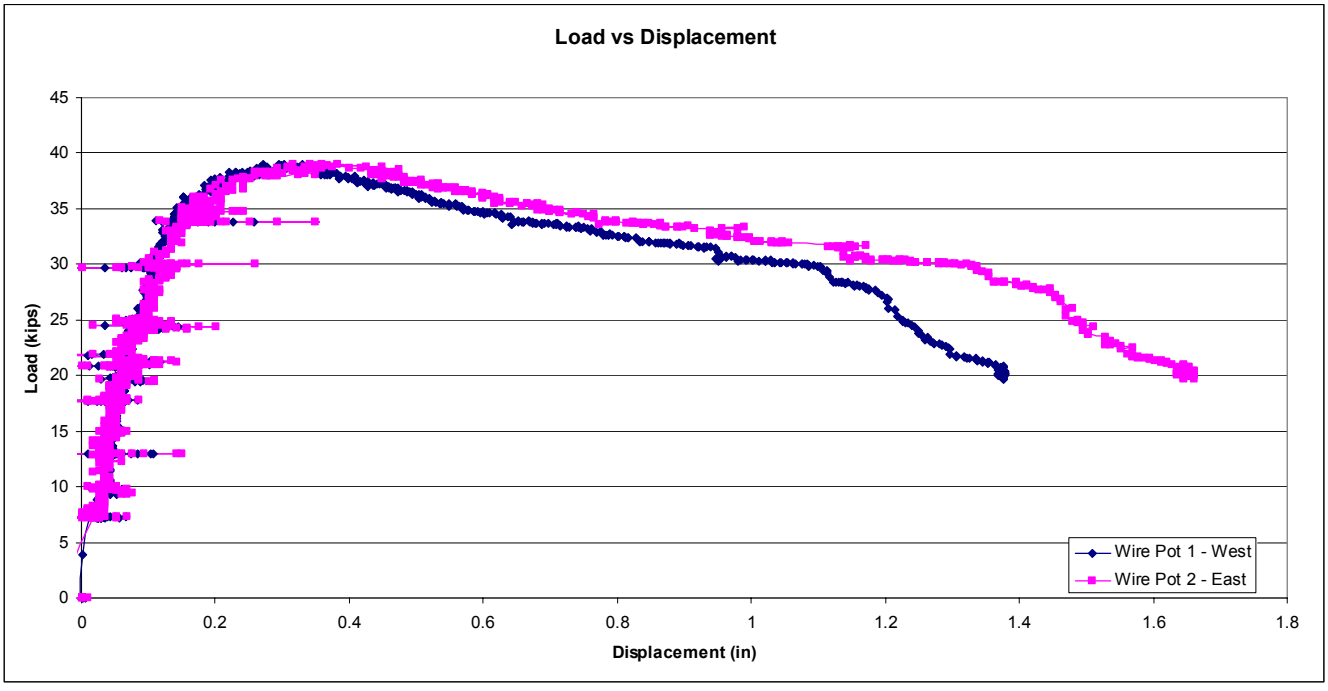

Figure B-49 - Load vs. Displacement (3.0 in. slab – 2.5 in. plate)

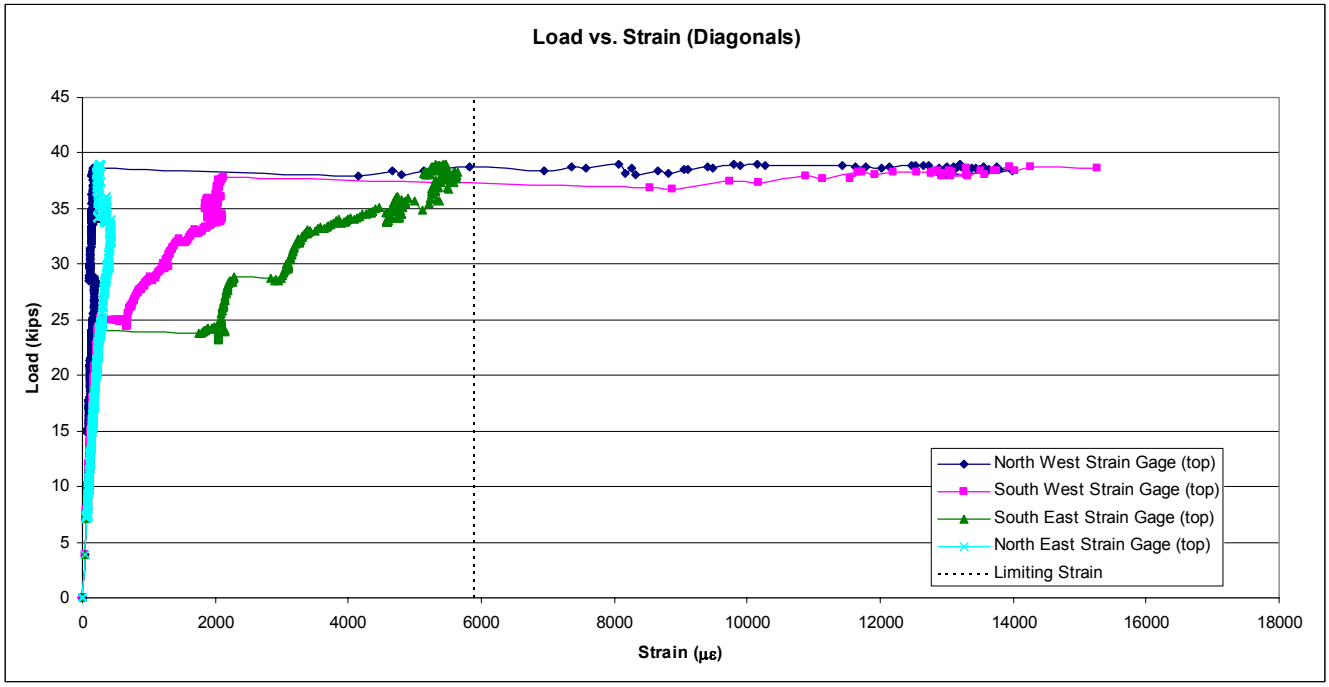

Figure B-50 - Load vs. Diagonal Strain (3.0 in. slab – 2.5 in. plate)

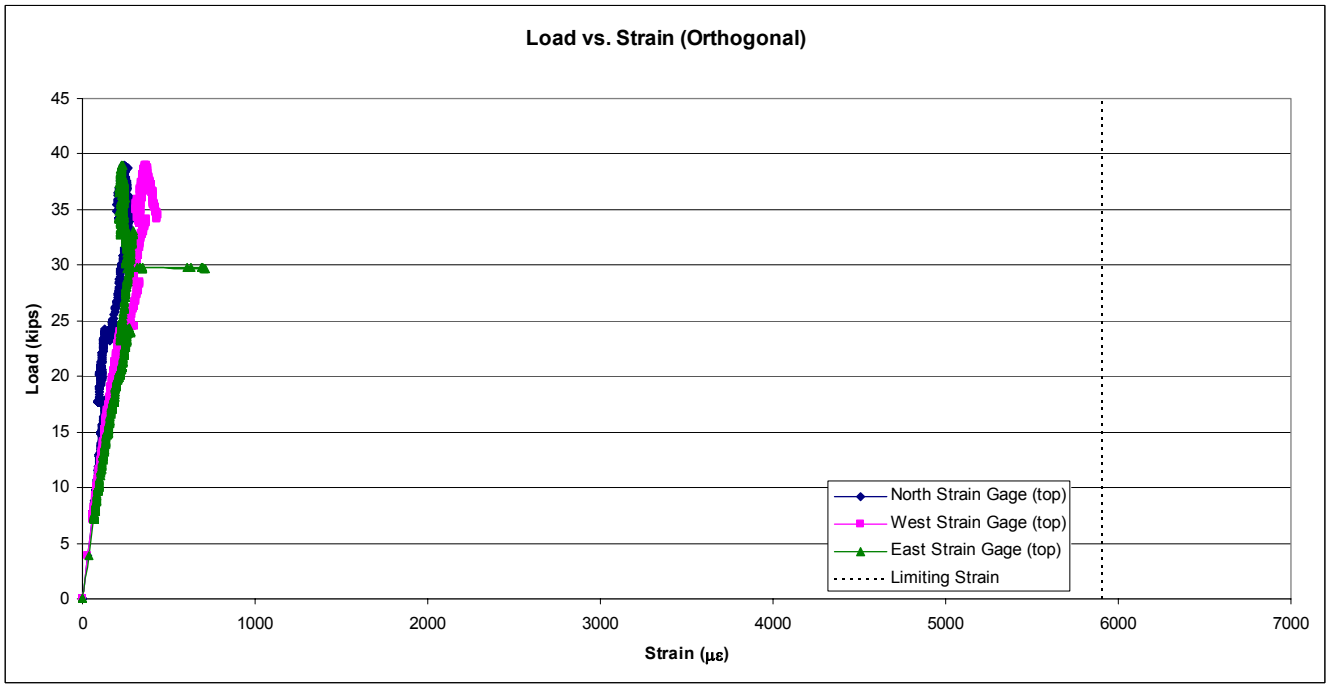

Figure B-51 - Load vs. Orthogonal Strain (3.0 in. slab – 2.5 in. plate)

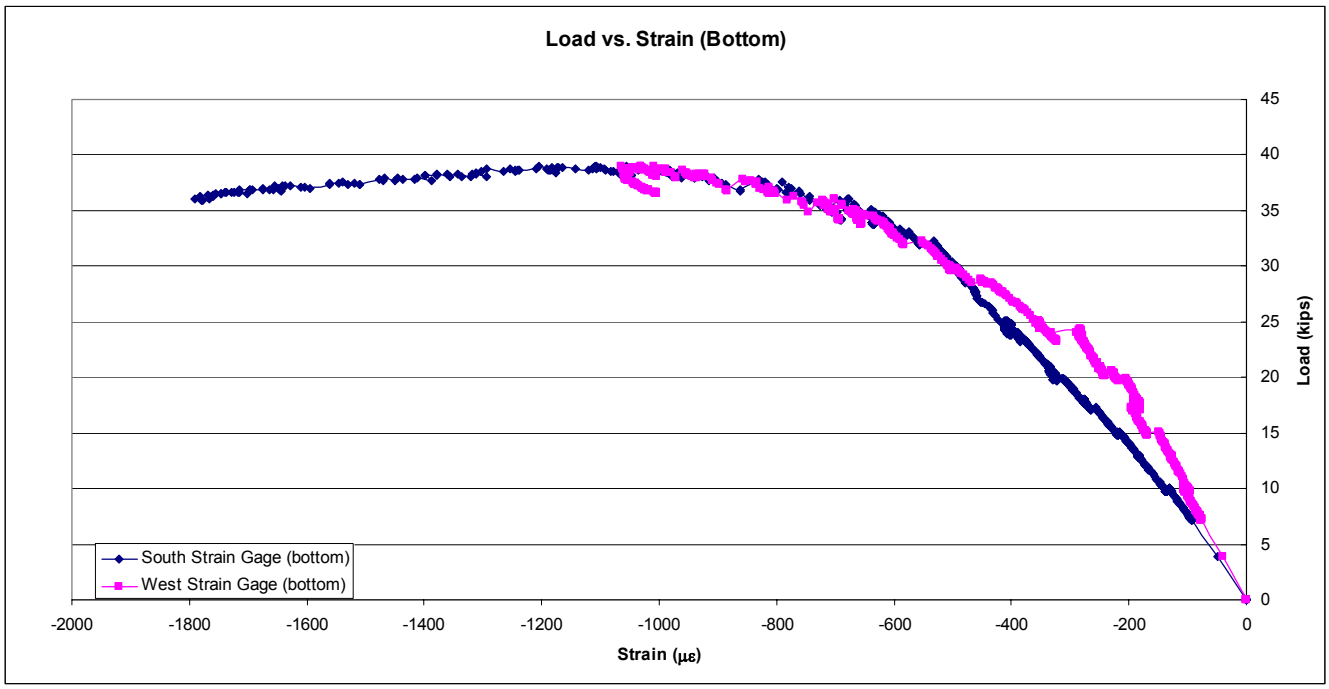

Figure B-52 - Load vs. Bottom Strain (3.0 in. slab – 2.5 in. plate)

Figure B-53 – Failure Surface (3.0 in. slab – 1.5 in. plate)

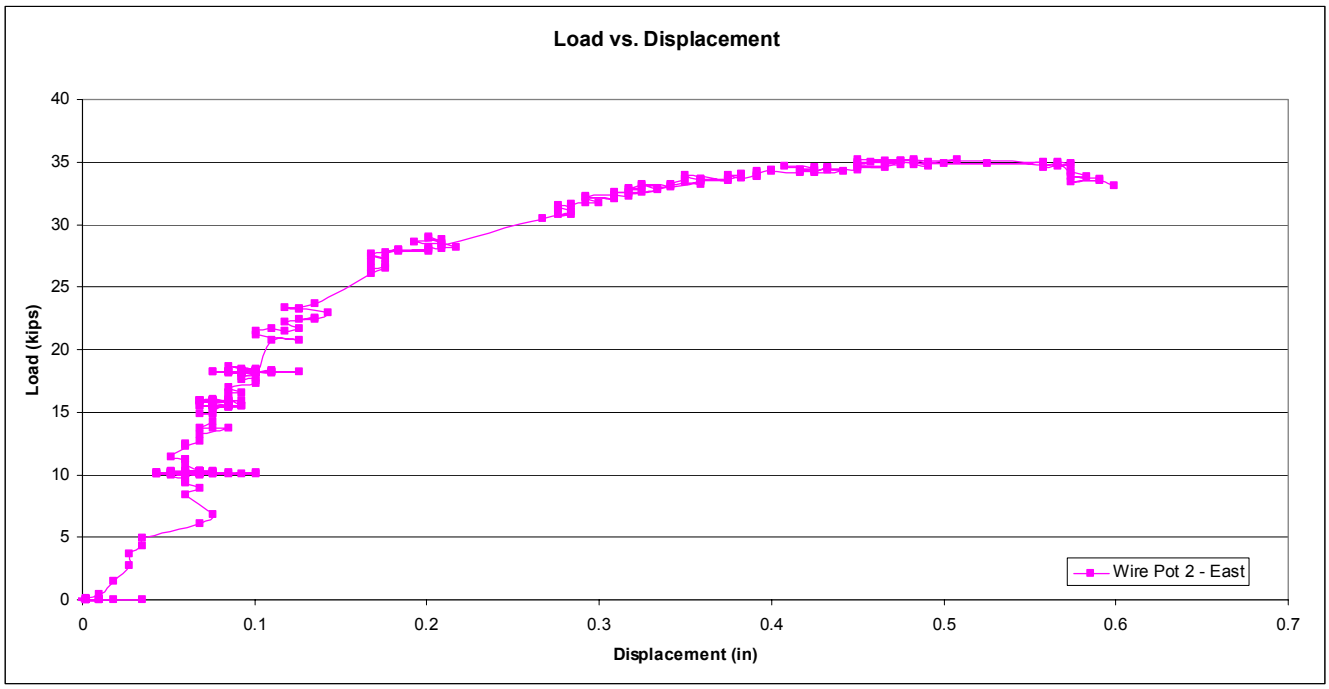

Figure B-54 - Load vs. Displacement (3.0 in. slab – 1.5 in. plate)

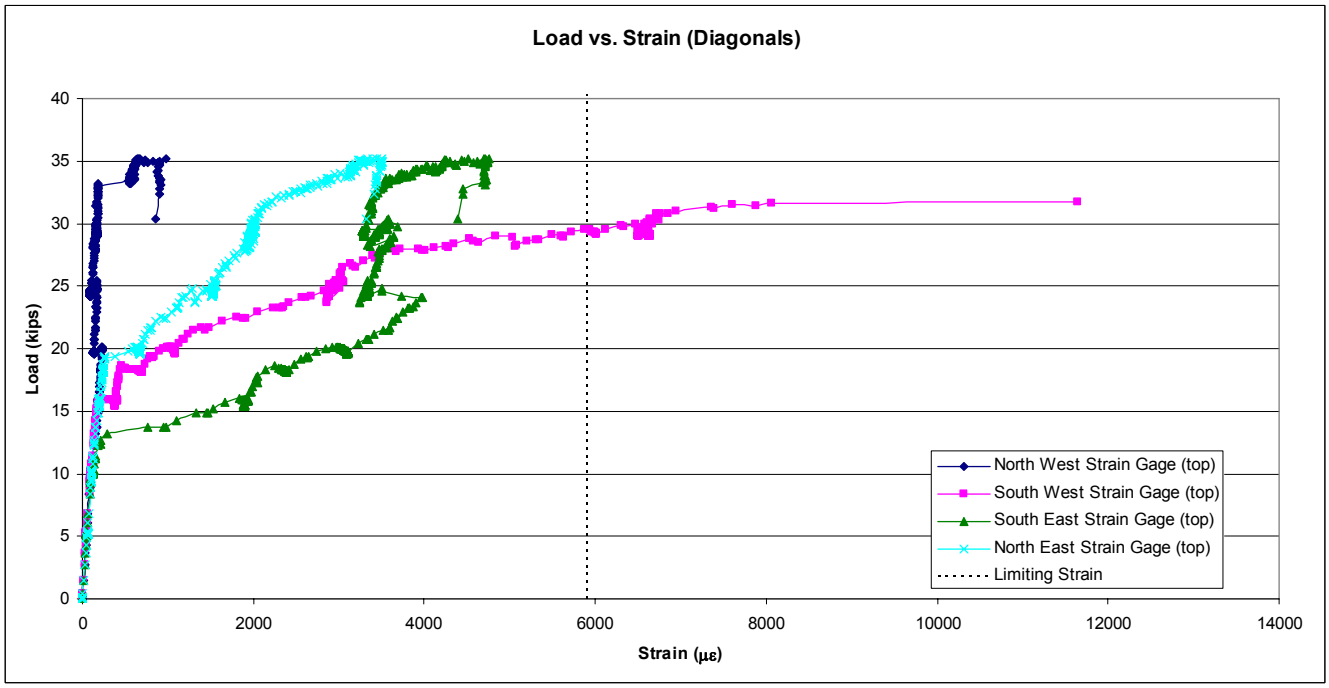

Figure B-55 - Load vs. Diagonal Strain (3.0 in. slab – 1.5 in. plate)

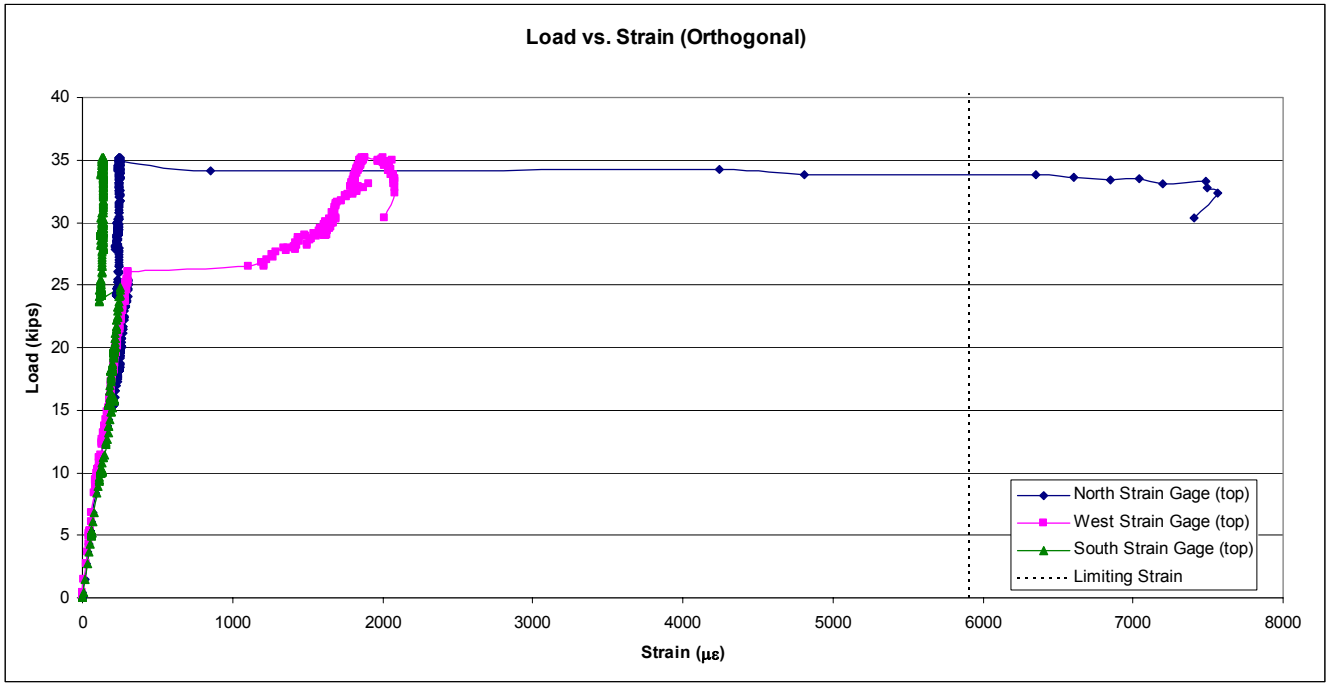

Figure B-56 - Load vs. Orthogonal Strain (3.0 in. slab – 1.5 in. plate)

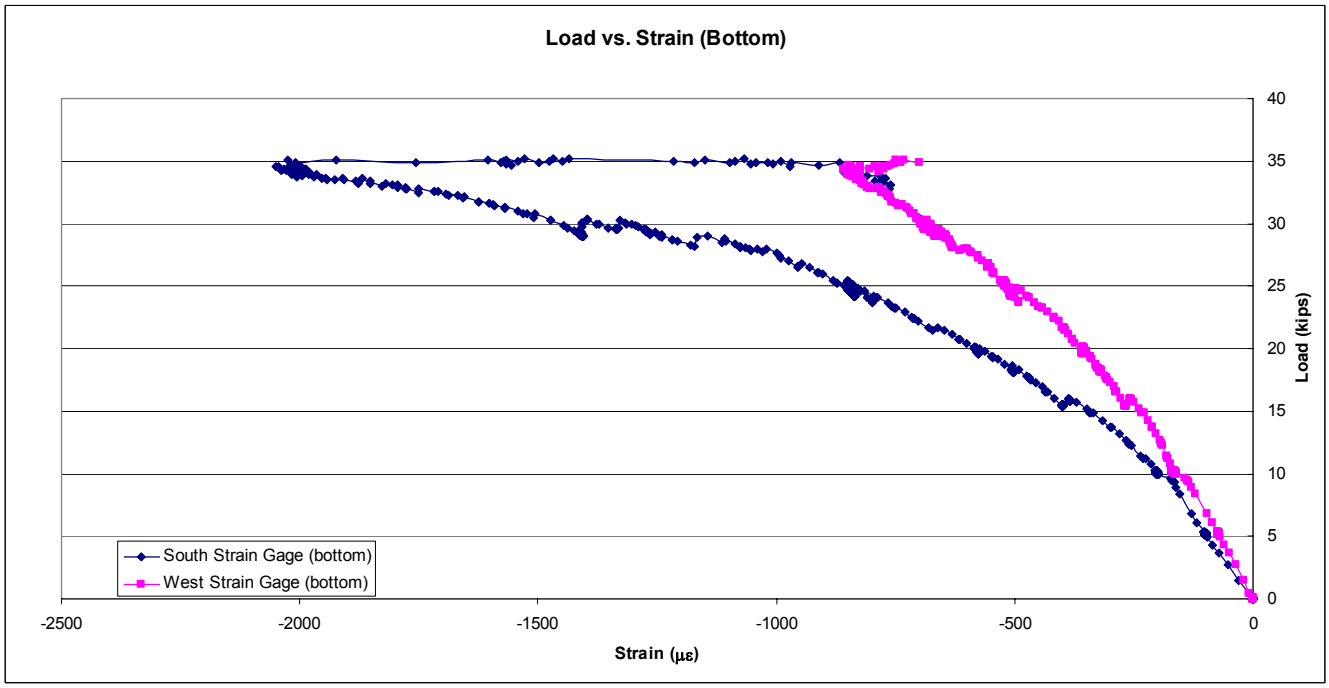

Figure B-57 - Load vs. Bottom Strain (3.0 in. slab – 1.5 in. plate)

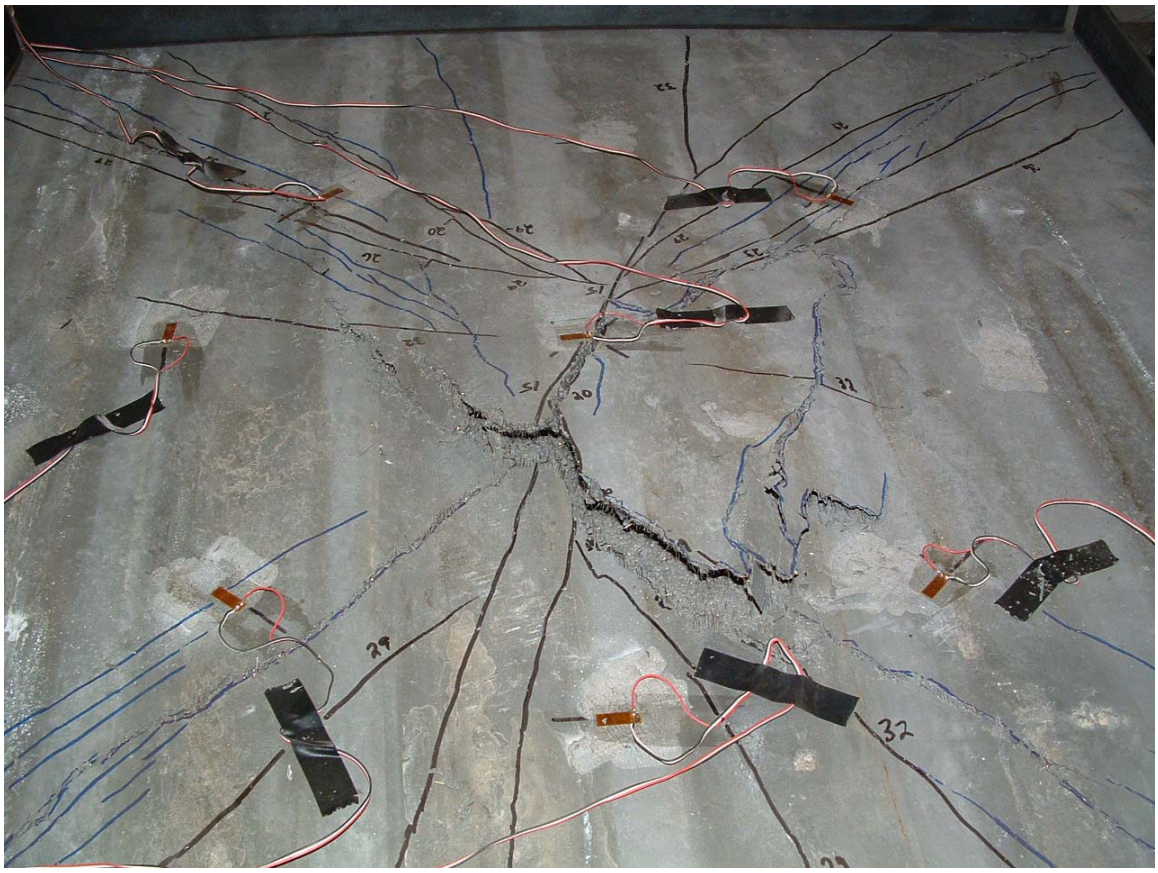

Figure B-58 – Failure Surface (3.0 in. slab – 1.0 in. plate)

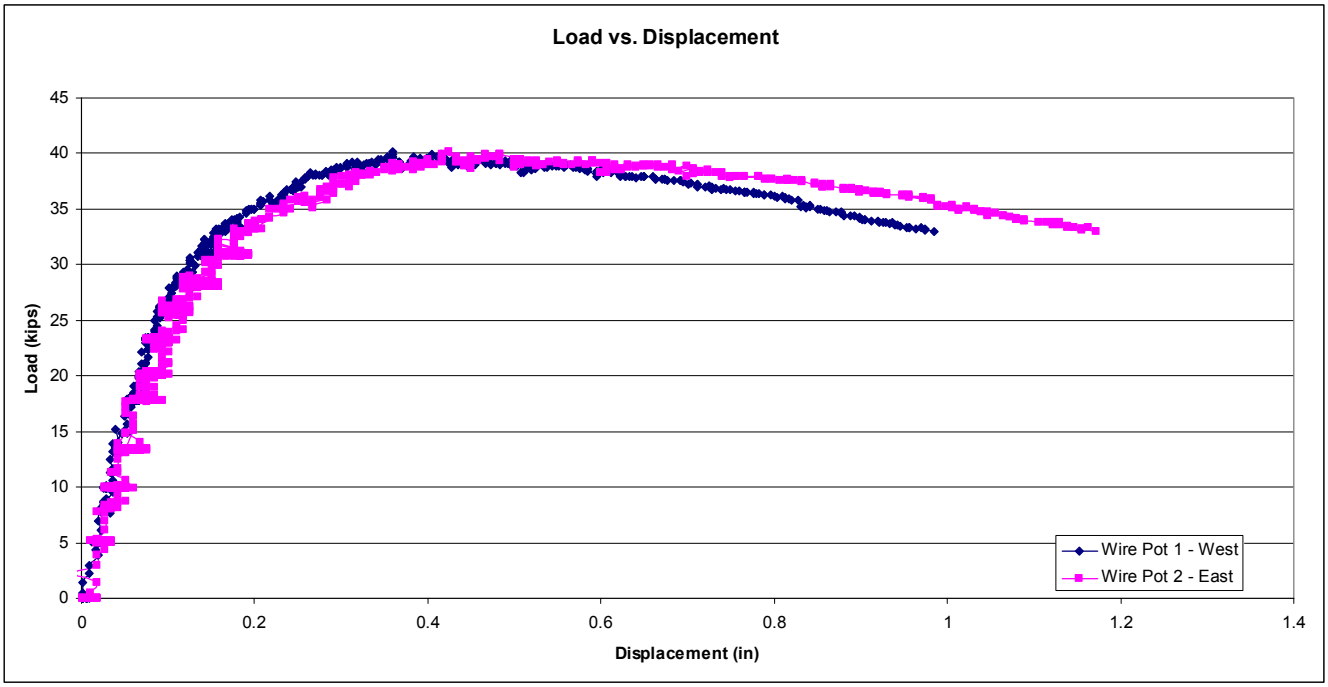

Figure B-59 - Load vs. Displacement (3.0 in. slab – 1.0 in. plate)

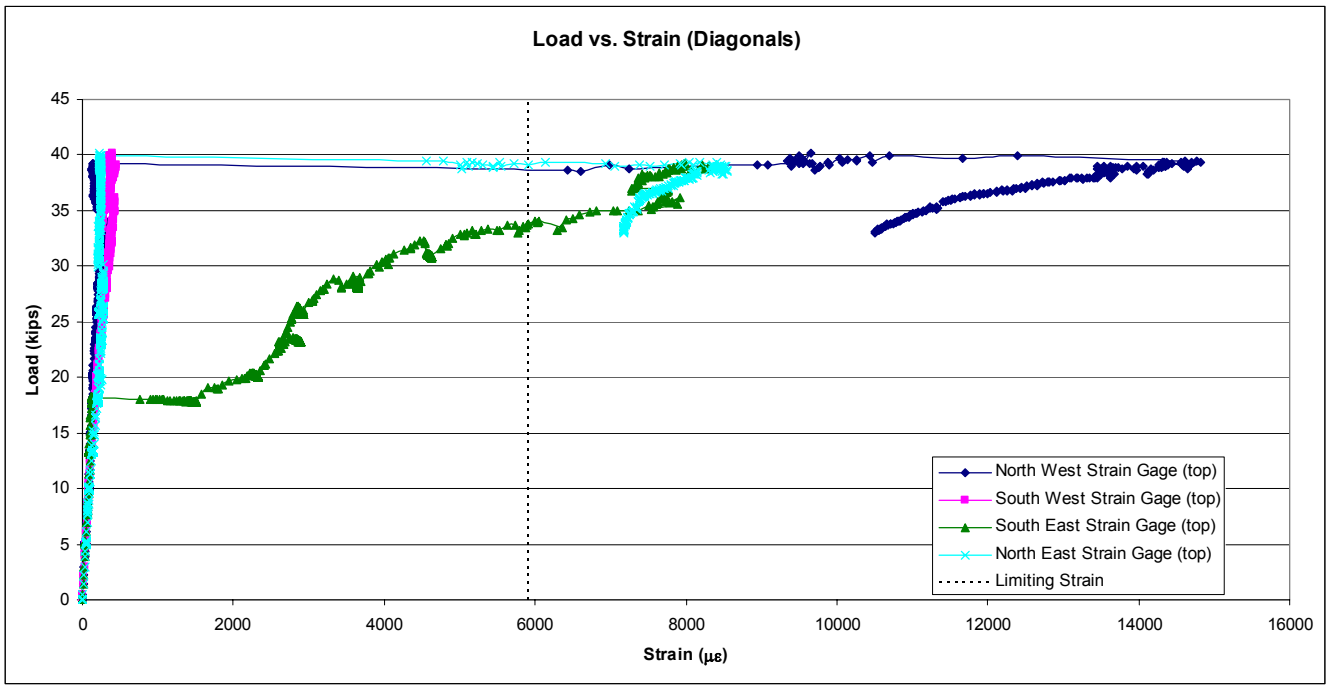

Figure B-60 - Load vs. Diagonal Strain (3.0 in. slab – 1.0 in. plate)

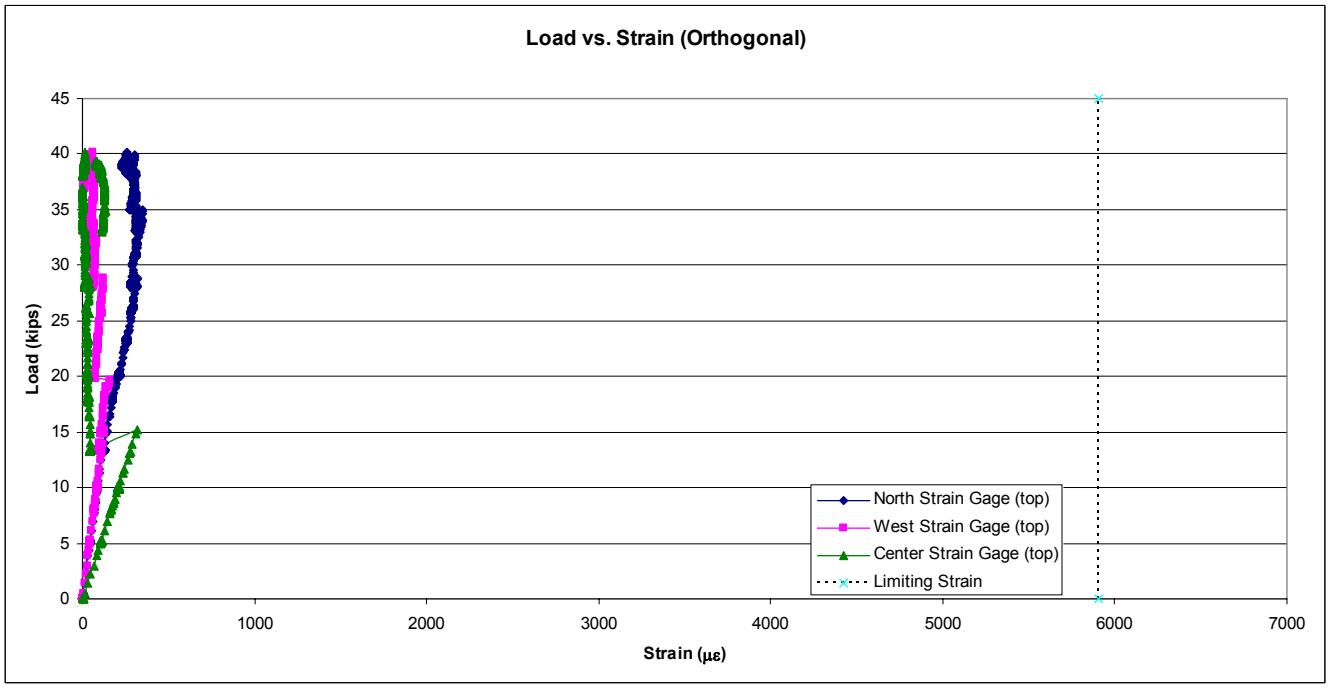

Figure B-61 - Load vs. Orthogonal Strain (3.0 in. slab – 1.0 in. plate)

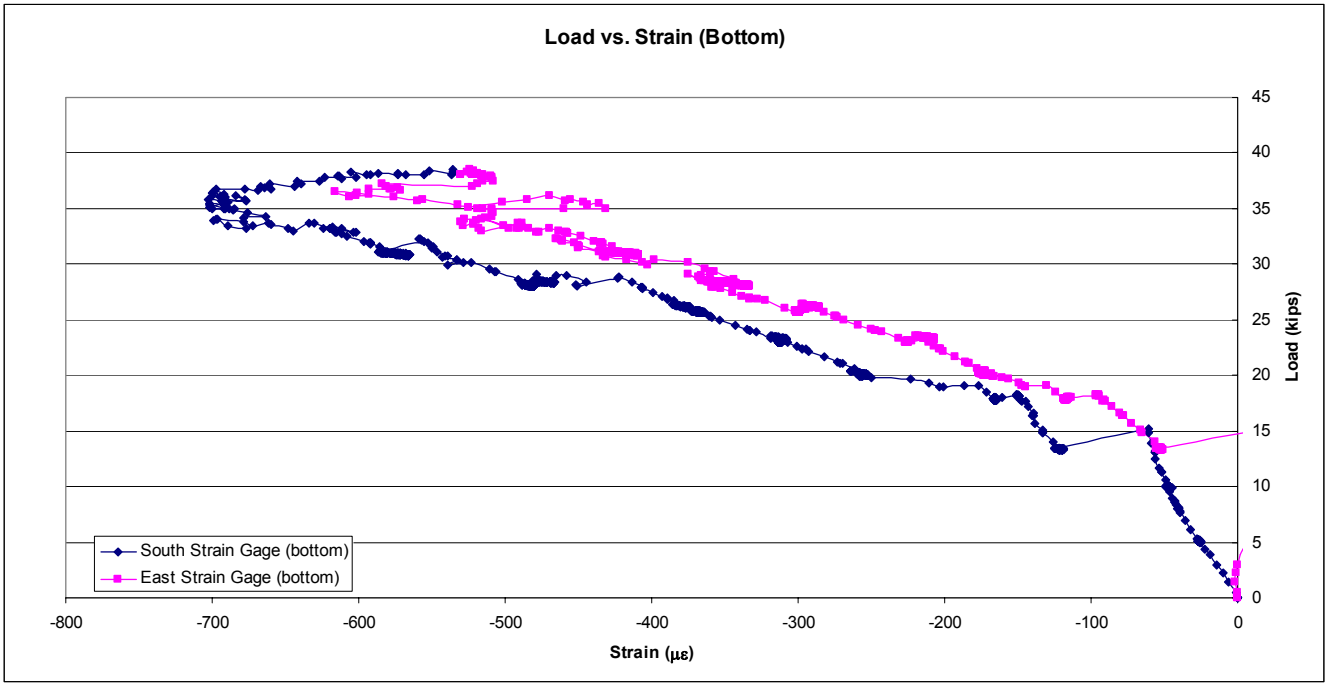

Figure B-62 - Load vs. Bottom Strain (3.0 in. slab – 1.0 in. plate)

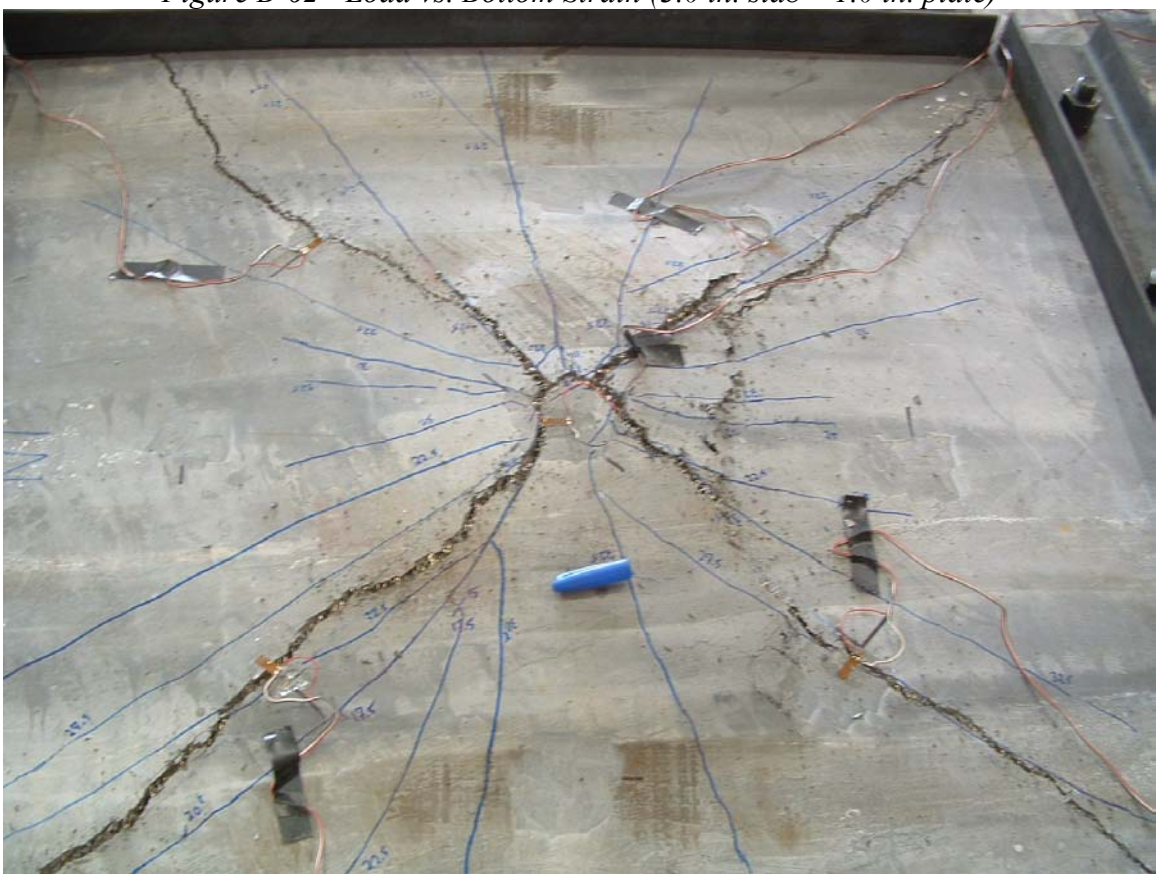

Figure B-63 – Failure Surface (3.0 in. slab – 2.0 in. plate)

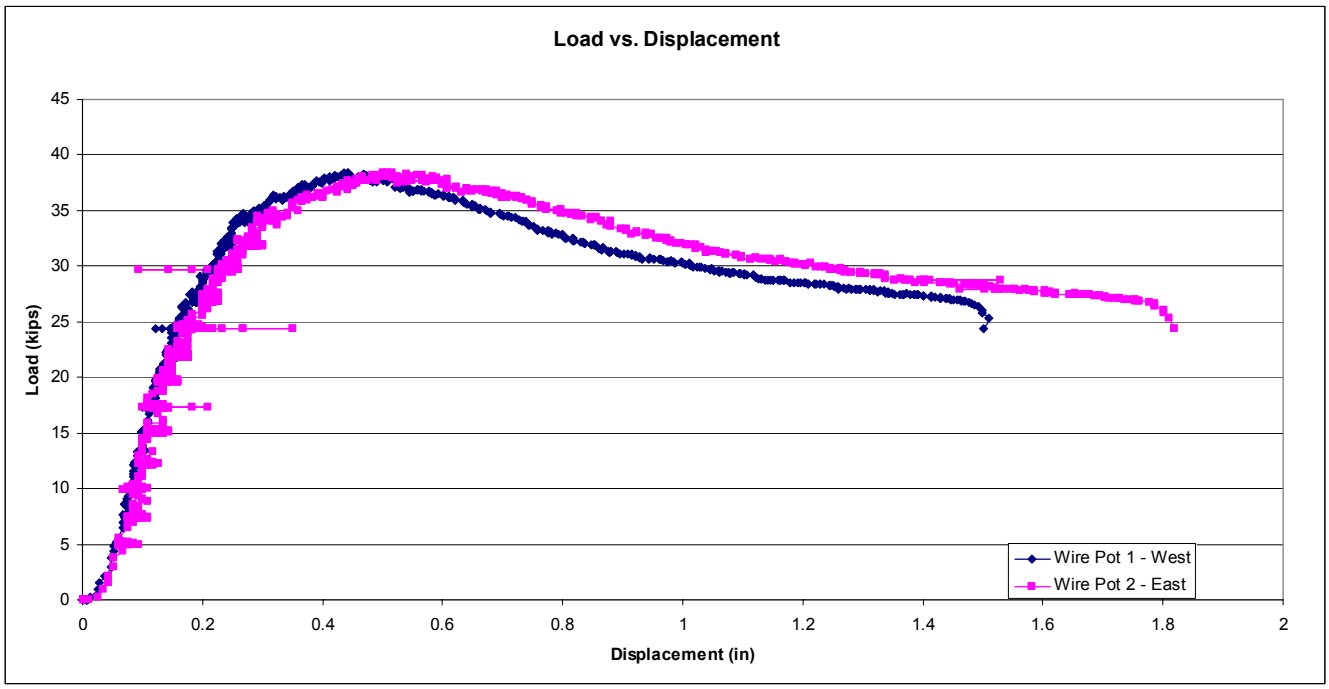

Figure B-64 - Load vs. Displacement (3.0 in. slab – 2.0 in. plate)

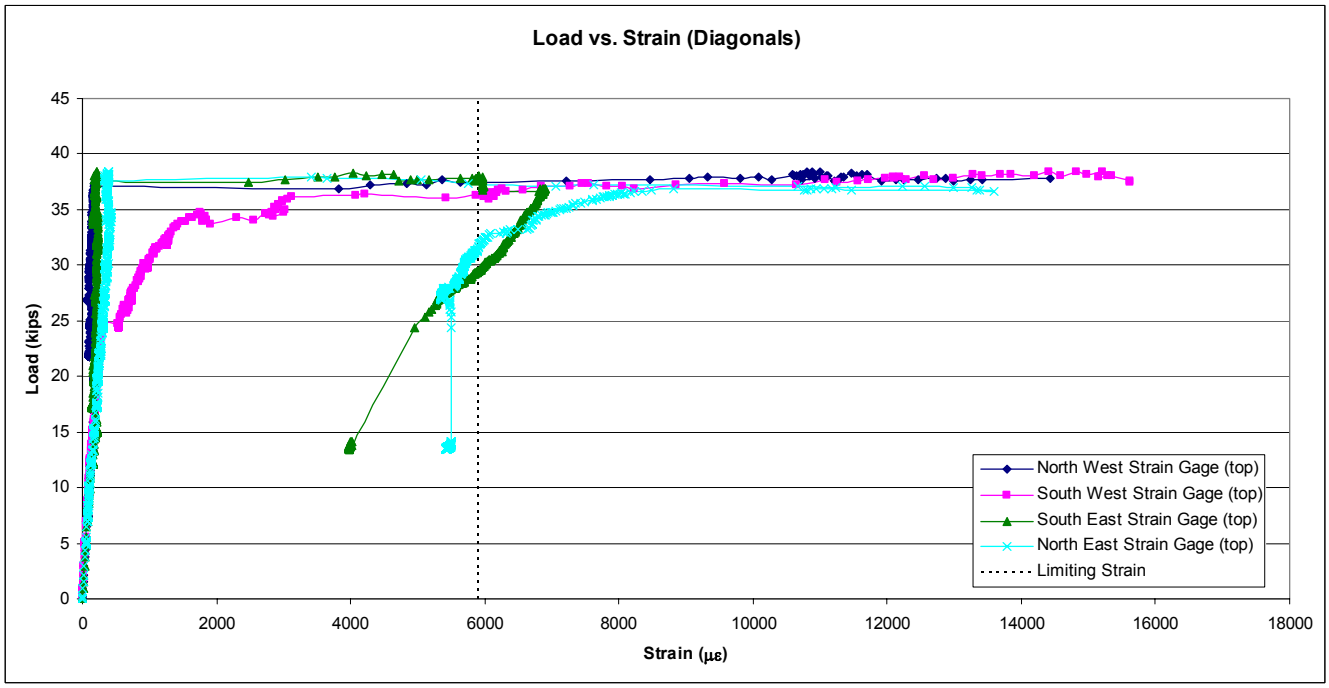

Figure B-65 - Load vs. Diagonal Strain (3.0 in. slab – 2.0 in. plate)

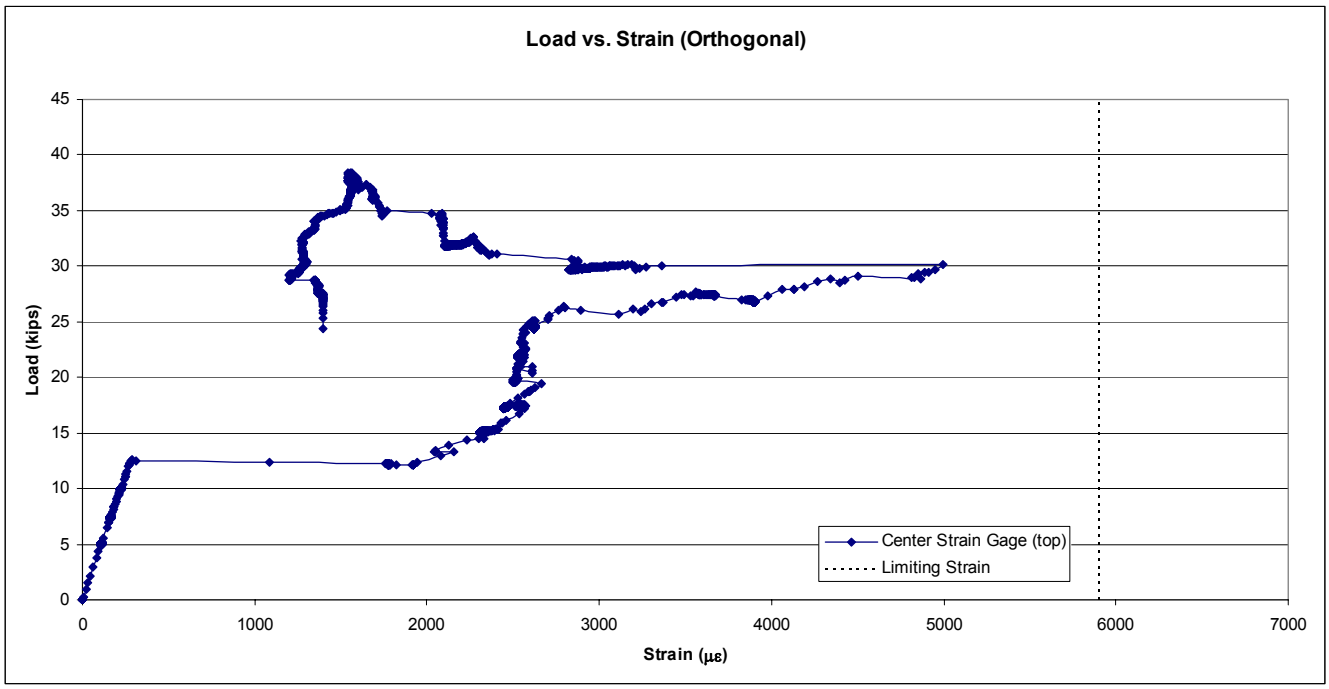

Figure B-66 - Load vs. Orthogonal Strain (3.0 in. slab – 2.0 in. plate)

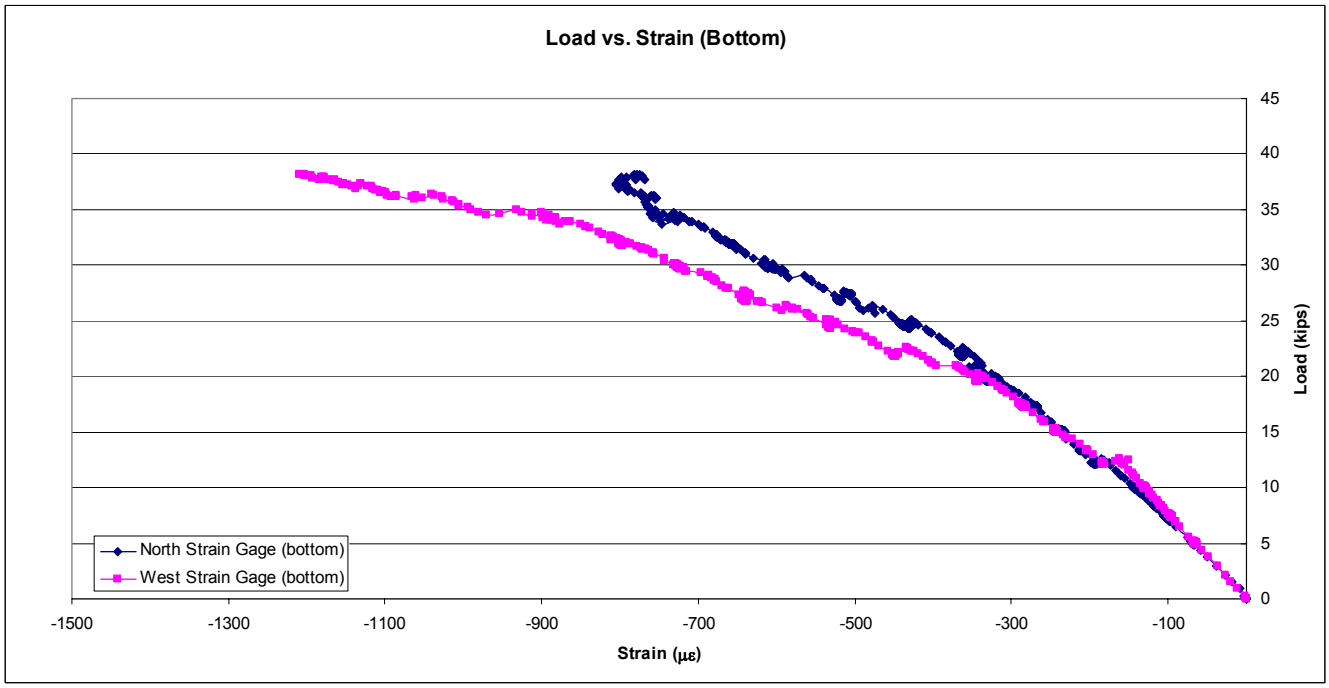

Figure B-67 - Load vs. Bottom Strain (3.0 in. slab – 2.0 in. plate)

Figure B-68 – Failure Surface (3.0 in. slab – 1.75 in. plate)

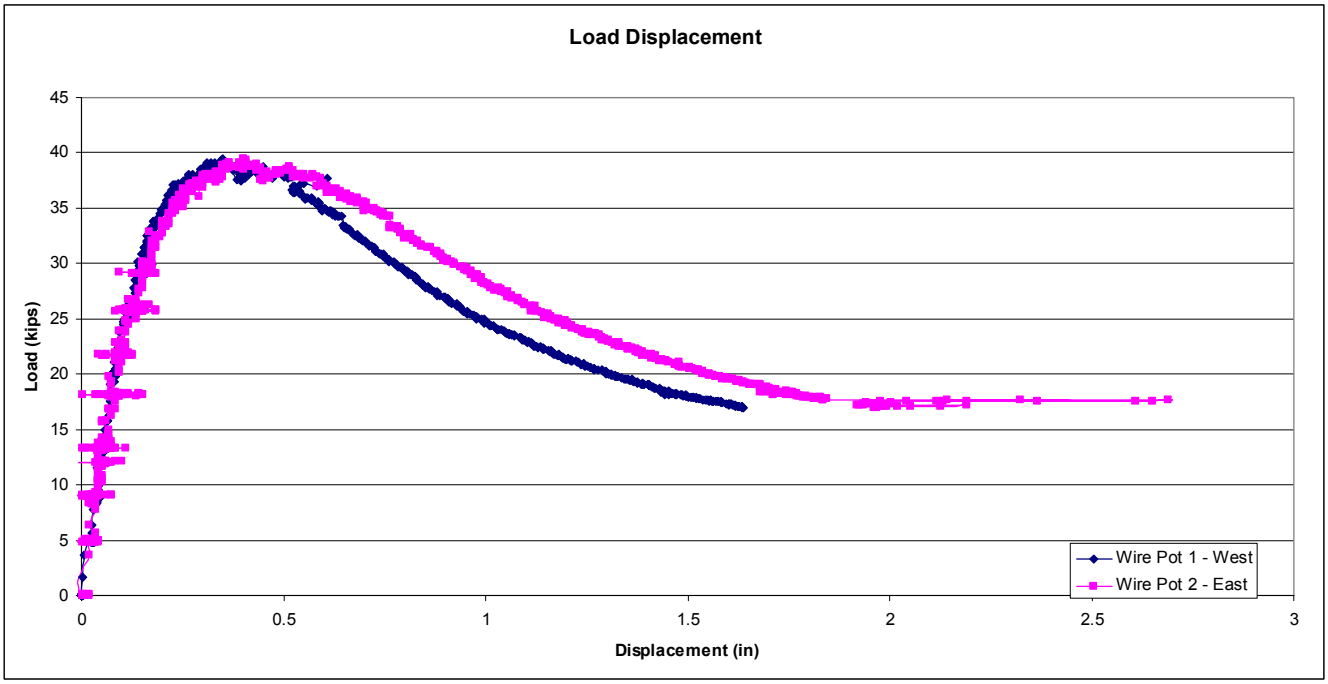

Figure B-69 - Load vs. Displacement (3.0 in. slab – 1.75 in. plate)

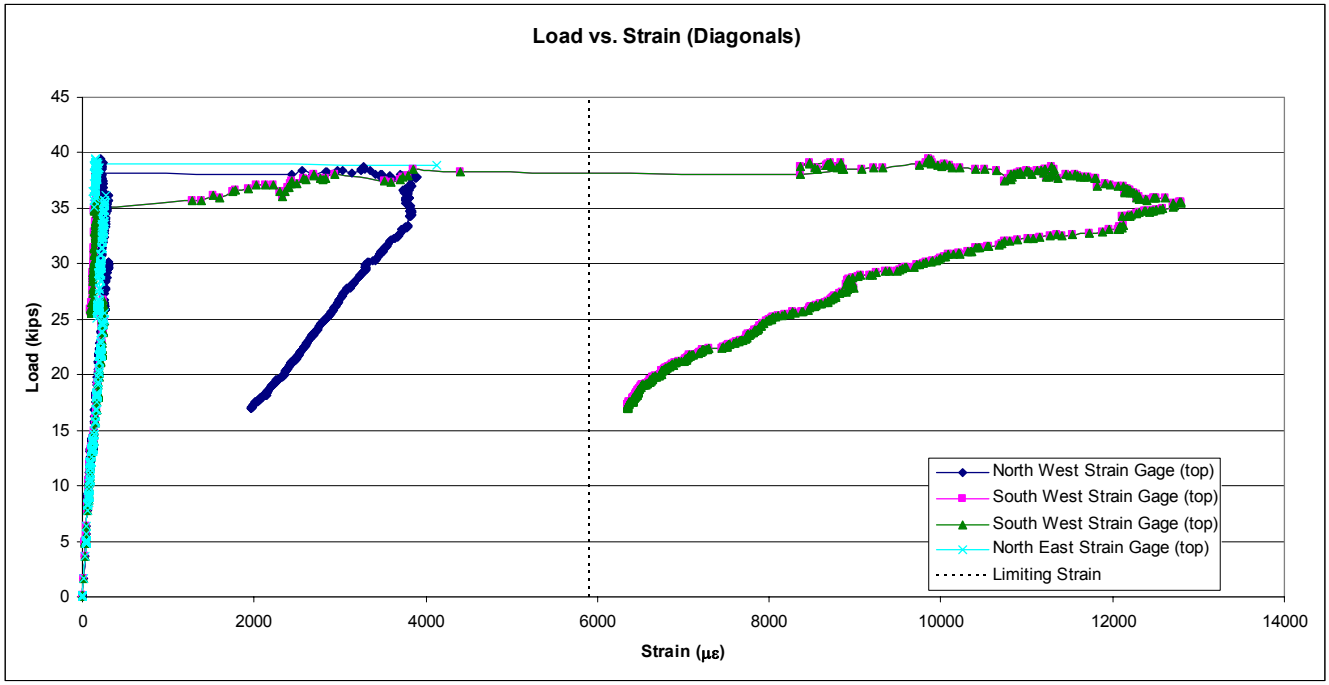

Figure B-70 - Load vs. Diagonal Strain (3.0 in. slab – 1.75 in. plate)

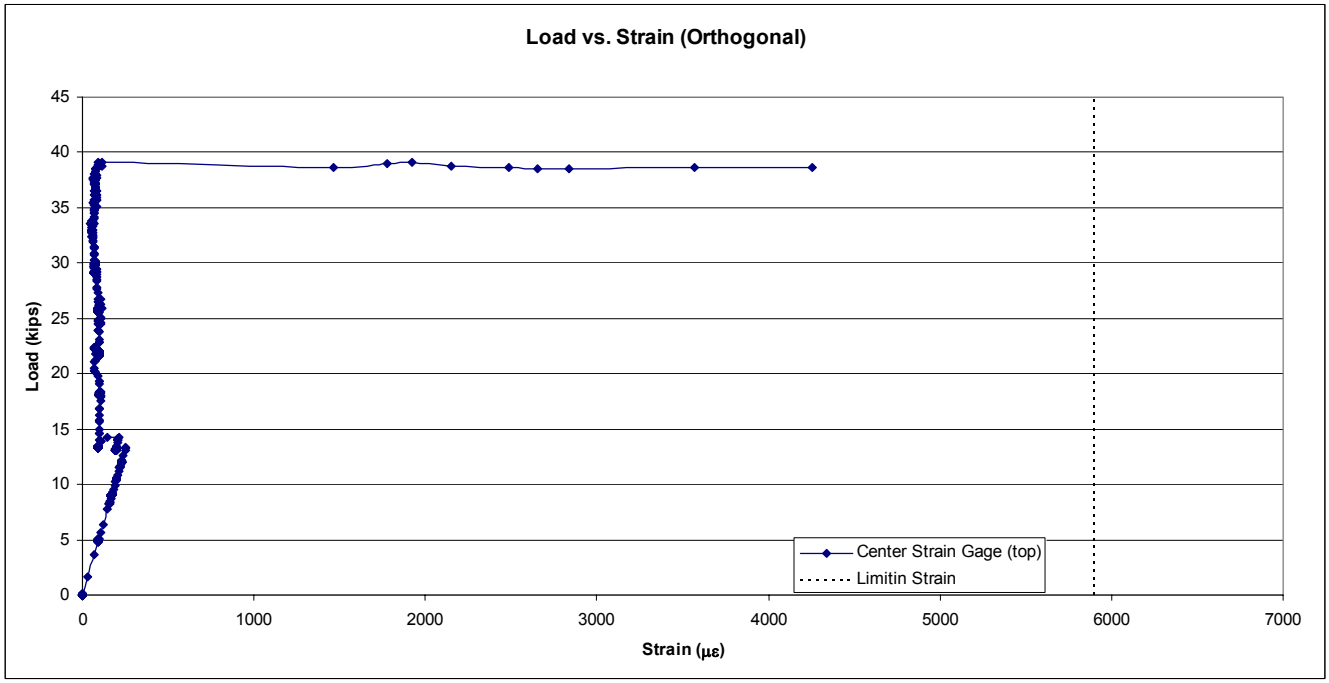

Figure B-71 - Load vs. Orthogonal Strain (3.0 in. slab – 1.75 in. plate)

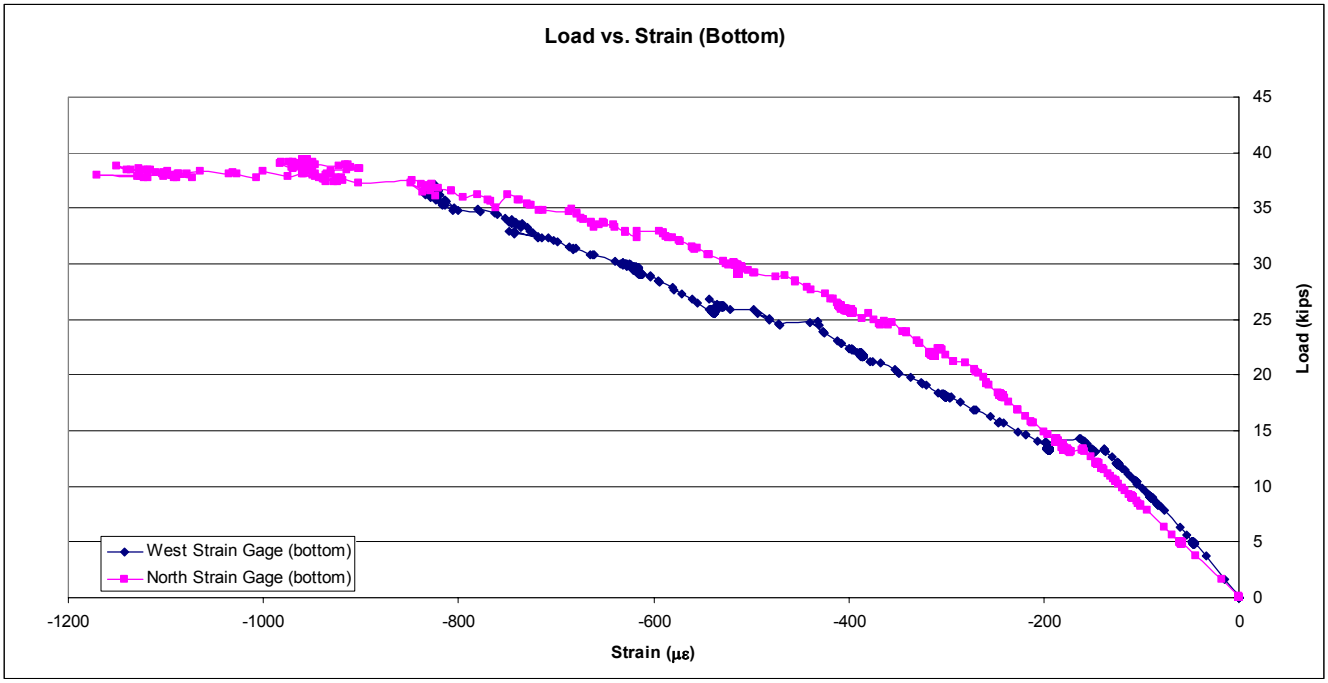

Figure B-72 - Load vs. Bottom Strain (3.0 in. slab – 1.75 in. plate)

VITA

Devin Harris was born on October 10, 1977 in Philadelphia, Pennsylvania to Jerome and Petra Harris. He spent his childhood in a number of locations in the United States and the Caribbean including: California, Puerto Rico, Jamaica, and Barbados. Devin attended Pine Crest Preparatory School as a boarding student in Ft. Lauderdale, Florida and graduated in 1995.

Devin enrolled as an undergraduate at the University of Florida in the fall of 1995. In June of 1999 he graduated with a Bachelor of Science degree in Civil Engineering. Upon graduation he began employment with ExxonMobil (formerly Exxon Company USA) in New Orleans, Louisiana as a drilling engineer.

After three and a half years of working for ExxonMobil, Devin enrolled at Virginia Polytechnic Institute and State University in the spring of 2003 to pursue graduate studies. Upon completion of his M.S. studies, Devin will begin his studies as a Ph.D. student at Virginia Polytechnic Institute and State University.